

University of Perugia  
Department of Civil and Environmental Engineering

**INTERNATIONAL  
DOCTORAL PROGRAM**  
IN CIVIL AND ENVIRONMENTAL ENGINEERING

PhD thesis  
XXXV cycle

**Transient response of water  
distribution networks: analysis of  
experimental and numerical tests.**

**PhD Candidate**  
Filomena Maietta

**Tutor**  
Professor Silvia Meniconi

**International Tutor**  
Professor Didia Covas

**Co - Tutor**  
Professor Bruno Brunone



A.D. 1308  
**unipg**

DIPARTIMENTO  
DI INGEGNERIA  
CIVILE E AMBIENTALE  
DIPARTIMENTO DI ECCELLENZA



**TÉCNICO  
LISBOA**



# International Faculty Board

## PhD Coordinator

Prof. Filippo Ubertini

## Italian members

Belardi Paolo  
Bianconi Fabio  
Brunone Bruno  
Brecolotti Marco  
Cavalagli Nicola  
Cerni Gianluca  
Cluni Federico  
Falcinelli Stefano  
Ferrante Marco  
Flammini Alessia  
Formisano Antonio  
Fornaciari Da Passano  
Gigliotti Giovanni  
Gioffrè Massimiliano  
Giorgi Giacomo  
Gusella Vittorio  
Kenny Jose Maria  
Manciola Piergiorgio  
Materazzi A. Luigi  
Meniconi Silvia  
Menchetelli Valeria  
Mochi Giovanni  
Morbidelli Renato  
Orlandi Fabio  
Pezzolla Daniela  
Puglia Debora  
Salciarini Diana  
Saltalippi Carla  
Terenzi Benedetta  
Torre Luigi  
Valentini Luca  
Venanzi Ilaria  
Ventura Flaminia

## **International members**

Arwade Sanjay  
Caracoglia Luca  
Covas Didia  
Denoël Vincent  
Glisic Branko  
Grigoriu Mircea  
Halevi Yoram  
Laflamme Simon  
Rodríguez-Tembleque Luis  
Saez Andres  
Sritharan Sri

### **International Review Board:**

David Ferras, IHE Delft.

Arris S Tijsseling, TU Eindhoven.

**Funding:** This research received no external funding.

**Data Availability Statement:** Some or all data, models, or code generated or used during the study are available in a repository online in accordance with funder data retention policies: Meniconi, Silvia, Brunone, Bruno, & Maietta, Filomena. (2021). Pressure signals acquired in a pipe network at the Water Engineering Laboratory of the University of Perugia, Italy [Data set]. Zenodo. URL: <https://doi.org/10.5281/zenodo.5535442>, accessed on 1 June 2022.

### **Design/research activity in national or int. programs:**

Member of the following research grants:

- 2021-2022 Commissario Straordinario per la sicurezza del sistema idrico del Gran Sasso, Italy, "Identification of the most suitable technique for verifying the functionality of the aqueduct infrastructure Ex Ferriera"
- 2021 A.S.S.M. S.p.A., Italy, "Research and development activities for the research study of the water losses of the Collattoni transmission main and for the optimization of Tolentino (MC) water distribution system supply for the minimization of energy consumption"
- 2021 Jindal, Italy, "Determination of the roughness parameter of the internal coating subjected to a lapping process in the ductile iron pipes produced by Jindal"
- 2019 NovaReti S.p.A. (Gruppo Dolomiti Energia), Rovereto, Italy "Check of the functionality of the DN500 transmission main between Galleria Serbatoio di Castel Dante and Solatrix reservoir"
- 2019. ASA S.p.A., Livorno, Italy "Survey of the DN400 pipe between Migliarino and Fiume Morto"
- 2019. CAP HOLDING S.p.A. - Milan, Italy "New technologies for leak detection and assessment of functioning performance of the transmission main Casc.Porro - HUB Comune di Aicurzio"

## Scientific production:

Peer-reviewed publications – Indexed journals:

- Capponi, C., Brunone, B., Maietta, F. et al. Hydraulic Diagnostic Kit for the Automatic Expeditious Survey of in-line Valve Sealing in Long, Large Diameter Transmission Mains. *Water Resour Manage* 37, 1931–1945 (2023). <https://doi.org/10.1007/s11269-023-03463-7>
- Brunone, B.; Maietta, F.; Capponi, C.; Duan, H.-F.; Meniconi, S. Detection of Partial Blockages in Pressurized Pipes by Transient Tests: A Review of the Physical Experiments. *Fluids* 2023, 8, 19. <https://doi.org/10.3390/fluids8010019>
- Meniconi, S., Maietta, F., Alvisi, S., Capponi, C., Marsili, V., Franchini, M., & Brunone, B. (2022). Consumption change-induced transients in a water distribution network: Laboratory tests in a looped system. *Water Resources Research*, 58, e2021WR031343. <https://doi.org/10.1029/2021WR031343>  
WOS:000863597100001
- Meniconi, S.; Maietta, F.; Alvisi, S.; Capponi, C.; Marsili, V.; Franchini, M.; Brunone, B. A Quick Survey of the Most Vulnerable Areas of a Water Distribution Network Due to Transients Generated in a Service Line: A Lagrangian Model Based on Laboratory Tests. *Water* 2022, 14, 2741. <https://doi.org/10.3390/w14172741>  
WOS:000851811800001
- Brunone, B., Maietta, F., Capponi, C., and Meniconi, S. (2022). Improvement of the Carrying Capacity of Cast Iron Pipes Due to the Coating Lapping Process, *Journal of Pipeline Systems Engineering and Practice*, 13(3), 06022001. [https://doi.org/10.1061/\(ASCE\)PS.1949-1204.0000659](https://doi.org/10.1061/(ASCE)PS.1949-1204.0000659)  
WOS:000811215600020
- Bruno Brunone, Filomena Maietta, Caterina Capponi, Alireza Keramat & Silvia Meniconi (2022) A review of physical experiments for leak detection in water pipes through transient tests for addressing future research, *Journal of Hydraulic Research*, 60:6, 894-906.  
DOI: 10.1080/00221686.2022.2067086  
WOS:000838597100001

Peer-reviewed publications:

- S. Meniconi, F. Maietta, C. Capponi, S. Alvisi, V. Marsili, M. Franchini, and B. Brunone Laboratory simulation of transients in looped water distribution network. The 7th IAHR Europe Congress (Atene, 7-9 Settembre 2022)
- Marsili V., Alvisi S., Maietta F., Capponi C., Meniconi S., Brunone B. and Franchini M. (2022) Characterizing the effects of water distribution system topology modifications on its dynamic behaviour through connectivity metrics. 2nd WDSA/CCWI Joint Conference. Valencia (Spain), 18-22 July 2022.
- Covas D.I., Maietta F., Cabral M., Meniconi S., Capponi C., Brunone B. (2022) Hydraulic Transient Solver Calibration in a Viscoelastic Pipe Network: Lessons Learnt. Proceedings of the 39th IAHR World Congress. Granada (Spain), 19-24 June 2022, doi:10.3850/IAHR-39WC2521711920221665 (ISBN: 978-90-832612-1-8).
- Marsili V., Mazzoni F., Alvisi S., Maietta F., Capponi C., Meniconi S., Brunone B. and Franchini M. (2022) Monitoring a Real Service Line Under Users' Activity. Proceedings of the 39th IAHR World Congress. Granada (Spain), 19-24 June 2022, doi:10.3850/IAHR-39WC2521711920221476 (ISBN: 978-90-832612-1-8).
- Maietta, F., Capponi, C., Brunone, B. and Meniconi, S. (2020). The effect of the functioning conditions on the transient behaviour of a water distribution system: laboratory tests. Proc., the 1st IAHR Young Professionals Congress- YPN (online, 17-18 Novembre 2020), 154-155 (ISBN: 978-90-82484-6-63).
- Capponi, C., Montoro, F., Chignola, M., Maietta, F., Brunone, B. and Meniconi, S. (2020). Chasing transients in a water transmission main in Milan, Italy. Proc., the 1st IAHR Young Professionals Congress- YPN (online, 17-18 Novembre 2020), 148-149 (ISBN: 978-90-82484-6-63).
- Rubin, A., Tirello, L., Capponi, C., Maietta, F., Favaro, S., Brunone B., and Meniconi, S. (2020). A preliminary low-frequency pressure analysis towards high-frequency transients monitoring in the Padua water distribution system. Proc., the 1st IAHR Young Professionals Congress- YPN (online, 17-18 Novembre 2020), 150-151 (ISBN: 978-90-82484-6-63).
- Maietta F., Meniconi S., Capponi C. & Brunone B. (2022). Sull'utilizzo di idranti per la diagnosi di reti di distribuzione mediante transitori. Prove preliminari di laboratorio. XXVIII Convegno Nazionale di Idraulica e Costruzioni Idrauliche - IDRA2022. Reggio Calabria, Settembre 2022, paper n. 174

- Capponi C., Meniconi S., Maietta F., Chignola M., Montoro F. & Brunone B. (2022). Una tecnica per la verifica della tenuta di valvole di sezionamento nelle adduttrici. Risultati preliminari. XXVIII Convegno Nazionale di Idraulica e Costruzioni Idrauliche - IDRA2022. Reggio Calabria, Settembre 2022, paper n. 121
- Brunone, B., Meniconi, S., Capponi, C., & Maietta, F. (2021) Una procedura orientata al gestore per la diagnosi dei sistemi di adduzione in pressione. Atti del XXXVII Convegno Nazionale di Idraulica e Costruzioni Idrauliche – IDRA2020, “Ingegneria delle Acque: cambiamenti globali e sostenibilità”, Reggio Calabria, paper n. 349, ISBN: 9788894379914.
- Meniconi, S., Falocci, D. Maietta, F., Capponi, C., and Brunone, B. (2022). Procedura per la caratterizzazione idraulica di una rottura “naturale” (crack) in una condotta in materiale polimerico, Servizi a Rete, 3, pp. 80-81.
- Brunone, B., Maietta, F., Capponi, C., and Meniconi, S. (2021). La lunga storia delle tubazioni in ghisa: da tubazioni “scabre” a tubazioni “idraulicamente lisce”, Servizi a Rete, 6, pp. 77-80.
- Meniconi, S., Maietta, F., Capponi, C., and Brunone, B. (2020). Transitori nelle reti di distribuzione idrica, Servizi a Rete, 2, pp. 31-34.
- Brunone, B., Meniconi, S., Capponi, C., and Maietta, F. (2020). Il Laboratorio di Ingegneria delle Acque dell’Università di Perugia, Servizi a Rete, 1, pp. 63-65.

Peer-reviewed publications (under review) – Indexed journals:

- Marsili V., Alvisi S., Maietta F., Capponi C., Meniconi S., Brunone B. and Franchini M., 2022. Extending the application of connectivity metrics within the framework of the dynamic behaviour of a WDS subjected to users’ activity. *Water Resources Research*.
- Marsili V., Mazzoni F., Alvisi S., Maietta F., Capponi C., Meniconi S., Brunone B. and Franchini M., 2022. Exploring the effects of transients induced by users’ activity on a real service line. *Water Resources Management*.

Data bases:

- Pressure signals acquired in a pipe network at the Water Engineering Laboratory of the University of Perugia, Italy [Data set]. Zenodo.

URL: <https://doi.org/10.5281/zenodo.5535442>, accessed on 1 June 2022.

### **Acknowledgments:**

The contribution of many people has been essential for the development of this research work, I would like to acknowledge them for it.

I would like to express my gratitude to Professor Bruno Brunone and Professor Silvia Meniconi for their constant trust, support and guidance, without them this research work would not have been possible. I owe to them my enthusiasm for research and everything I've learned during these years. To them goes my esteem.

I would like to special thank Professor Silvia Meniconi for her availability shown during the drafting of the thesis paper.

I would like to sincerely thank Professor Dída Covas and Dr Marta Cabral of the Instituto Superior Técnico – Lisbon (PT) for their important contribution to this research work.

I would also like to thank Professor Caterina Capponi for her support for this research work.

I would like to extend my thanks to Professor Marco Franchini, Professor Stefano Alvisi, and Dr Valentina Marsili of the University of Ferrara for constructive collaboration.

I would like to thank Claudio Del Principe of the Water Engineering Laboratory for his help in the execution of laboratory tests.

I am deeply grateful to Francesco, my Family, and my Friends for all the love they give me.

# Contents

<b>1</b>	<b>Introduction</b>	<b>1</b>
1.1	Hydraulic transients in water distribution network . . . . .	1
1.2	Objectives . . . . .	2
1.3	Thesis outline . . . . .	3
<b>2</b>	<b>State of the art</b>	<b>5</b>
2.1	Introduction . . . . .	5
2.2	Transients in water distribution network . . . . .	5
2.2.1	Introduction . . . . .	6
2.2.2	Numerical tests . . . . .	7
2.2.3	Laboratory and field tests . . . . .	7
2.2.4	Conclusions . . . . .	9
2.3	Transient Test-Based Techniques for leak detection . . . . .	11
2.3.1	Introduction . . . . .	11
2.3.2	Laboratory and field tests . . . . .	19
2.3.3	Conclusions . . . . .	30
2.4	Transient Test-Based Techniques for partial blockages detection	32
2.4.1	Introduction . . . . .	32
2.4.2	Interaction between pressure waves and partial blockage	38
2.4.3	Laboratory and field tests . . . . .	44
2.4.4	Conclusions . . . . .	48
<b>3</b>	<b>Transients modelling</b>	<b>50</b>
3.1	Introduction . . . . .	50
3.2	Classic waterhammer problem . . . . .	50
3.3	Unconventional waterhammer problems . . . . .	52
3.3.1	Unsteady friction losses . . . . .	52
3.3.2	Non-elastic and viscoelastic behaviour of the pipe material	53
3.4	Method of Characteristics . . . . .	55
3.4.1	Compatibility equations . . . . .	58
3.4.2	Boundary conditions . . . . .	60
3.5	The Lagrangian Model . . . . .	63
3.6	Conclusions . . . . .	65

<b>4</b>	<b>Experimental data collection programme</b>	<b>66</b>
4.1	Introduction . . . . .	66
4.2	The experimental set-up . . . . .	67
4.3	Preliminary tests for the end-user and service line characterization	73
4.4	Laboratory transient tests . . . . .	74
4.5	Key quantities characterizing the network transient response . .	76
<b>5</b>	<b>Consumption change-induced transients in a water distribution network</b>	<b>78</b>
5.1	Introduction . . . . .	78
5.2	Occurrence of cavitation in the service line . . . . .	79
5.3	Pressure signals for no-cavitating flows . . . . .	79
5.4	Effect of the end-user discharge change . . . . .	81
5.4.1	Transient response of the network during the first phases	81
5.4.2	Transient response along time . . . . .	82
5.5	Combined effect of simultaneous consumers . . . . .	84
5.5.1	Effect of deterministic water consumption variations . .	84
5.5.2	Effect of random water consumption variations . . . . .	86
5.6	Conclusions . . . . .	87
<b>6</b>	<b>The most vulnerable areas of a water distribution network due to transients generated in a service line</b>	<b>89</b>
6.1	Introduction . . . . .	89
6.2	The Effect of the Network Topology . . . . .	90
6.3	The Effect of the Transient Generation Point . . . . .	93
6.4	Maps of Vulnerability by the Lagrangian Model (LM) . . . . .	93
6.5	Conclusions . . . . .	96
<b>7</b>	<b>Hydraulic transient solver calibration in a water distribution network</b>	<b>100</b>
7.1	Introduction . . . . .	100
7.2	Forward and inverse solvers . . . . .	102
7.3	Hydraulic model construction and calibration . . . . .	103
7.3.1	Main steps . . . . .	103
7.3.2	Definition of the pipe-system layout . . . . .	104
7.3.3	Calibration of the valve initial opening and the valve manoeuvre . . . . .	104
7.3.4	Calculation of the elastic wave speed . . . . .	106
7.3.5	Calibration of the viscoelastic pipe behaviour and model validationd . . . . .	106
7.4	Hydraulic model calibration and validation for test series #6 . .	108
7.5	Hydraulic model validation for test series #8 . . . . .	110
7.6	Hydraulic model validation for test series #1 . . . . .	111

## Contents

7.7	Conclusions . . . . .	112
<b>8</b>	<b>Conclusions</b>	<b>114</b>
8.1	Research overview . . . . .	114
8.2	Main scientific contributions . . . . .	115
8.3	Research perspectives . . . . .	116
	<b>References</b>	<b>117</b>

# 1. Introduction

## 1.1. Hydraulic transients in water distribution network

Water distribution Networks (WDNs) are complex, usually highly looped, systems with thousands of elements such as pipes, pumps, and valves. Most of them in Europe – and in Italy – are really aged, and their structural integrity and the actual degree of deterioration is often poorly known (Misiunas et al., 2005). Aging infrastructures and their poor maintenance, corrosion, and excessive pressure resulting from operating errors are the main causes of water losses (Yusop et al., 2019; Puust et al., 2010), which lead to a reduction in the energy efficiency of the system, as well as losses from an economic and social point of view (Puust et al., 2010; Colombo et al., 2009). Moreover, hydraulic transients occur frequently in WDNs and they are not only due to flow and pressure control operations, but also to the almost continuous water consumption variations. Traditionally, the effects of transients in WDNs are often underestimated, in the belief that the generated pressure waves would exit through the active consumers. Consequently, pipe breaks in WDNs are attributed to the large mean pressure or, in case the pressure regime is considered appropriate, the inaccurate installation of pipes, additional loads due to traffic, and a large number of connections.

However, in many cases, it is arduous to identify the actual cause of faults occurring in only some parts of the WDN that exhibit no clear differences with respect to other ones in terms of pipe material, maintenance practices, external loads, as well as operating pressures, usually monitored at a low frequency. A possible explanation of such a feature could derive from proper identification of the nature of the actually dangerous transients and the different exposure to them of individual parts of the considered WDN.

Nevertheless, in the few available papers based on physical experiments, transients are generated by maneuvers in the supply lines (e.g., pump trip-off), and their effects are analyzed in the main pipes. Such a phenomenon is very different with respect to the transients generated within the network (i.e., in the service

## Chapter 1. Introduction

lines) due to water consumption variations, and very few papers experimentally analyze in detail their effects. These papers do not highlight the role of the network topology or the location of the transient generation point, as well as of the entity and the simultaneity of water consumption changes, for a given layout.

In recent years, hydraulic transients have been used for fault detection (e.g., leaks, partial blockages, wall deteriorations), and several techniques – the so-called “Transient Test-Based Techniques” (TTBTs)–, have been developed for detecting system defects by monitoring the pressure waves. A pressure wave travelling along a pipeline changes its characteristics when it crosses a singularity, i.e. a hydraulic device, a geometric variation, a partial blockage, a wall deterioration, an air pocket, and a leak. In fact, part of the incident wave can be reflected or transmitted by the singularity (Brunone, 1999, Brunone and Ferrante, 2001, Colombo et al., 2009, Covas and Ramos, 1999, Ferrante et al., 2007, Ferrante et al., 2009a, Wang et al., 2001). The analysis of the measured pressure signal can give useful information regarding the characteristics of the faults. However much of the research carried out has involved very simple pipelines or simplified systems (Brunone et al., 2022; Ayati et al., 2019; Capponi et al., 2020), and has little investigated the real leaks.

Moreover, an effective numerical model simulating the transient behaviour of a WDN is very challenging. In particular, the implementation of a transient solver for pressurized water pipe networks incorporating unsteady friction and pipe wall viscoelasticity is important to better understand the behaviour of a system, and to provide for unusual pressure variations under different operational conditions (Carrico et al., 2016; Covas and Ramos, 2010; Soares et al., 2011).

### 1.2.Objectives

The research project aims to analyze the transient response of a polymeric looped water distribution network, when transients are due to deterministic or stochastic consumption variations. Both intact and damaged pipe networks are considered.

Specifically, this work aims to give a contribution to the analysis of the mechanism of propagation of a pressure wave in a looped network (two  $100 \times 100$  m square loops) with one or more active service lines in different locations. These experiments have been carried out at the Water Engineering Laboratory (WEL) of the University of Perugia, Italy. The experimental results have been examined by means of a Lagrangian model (LM), to point out the most excited part of the system, both in the main pipe and in the service line, according to the different locations of the transient generation point. The effect of the

## Chapter 1. Introduction

topology of the network, the location of the transient generation point, and the entity of the water consumption variation, as well as the combined effect of simultaneous active users have been highlighted.

Furthermore, numerical simulations of pressurized pipe systems in unsteady state conditions have been carried out, incorporating both unsteady friction and viscoelasticity. The viscoelastic parameters have been calibrated and the effect of the service line and a leak has been analysed. An excellent fitting has been observed.

In summary, the thesis objectives are:

- to develop an extensive literature review for identifying the gaps of the knowledge in the WDN transient behaviour analysis;
- to perform an extensive experimental programme in a complex WDN composed of two loops;
- to identify the most excited part of the system, both in the main pipe and in the service line;
- to understand the effect of the topology of the network, the location of the transient generation point, and the entity of the water consumption variation, as well as the combined effect of simultaneous active users;
- to identify the reasons for the high occurrence and severity of faults in some portions of WDNs;
- to calibrate the main parameters in hydraulic transient solvers in viscoelastic pipes also in the case of damaged WDN.

### 1.3. Thesis outline

The present thesis is organized into eight chapters.

In addition to this Chapter, [Chapter 2](#) presents an extensive review of the articles that numerically and experimentally analyze the transient behavior of a WDN. Moreover, the state of the art of TTBTs for leak and blockage detection is introduced. The main gaps of knowledge in the literature review are highlighted.

In [Chapter 3](#), the governing equations for one-dimensional, transient flow within a closed conduit are exposed.

[Chapter 4](#) introduces a description of the experimental set-up, a breakdown of the laboratory transient tests, and it introduces the key quantities that characterize the network transient response.

## Chapter 1. Introduction

Chapters 5, 6, and 7 show the main research carried out on the transient response of the laboratory WDN, with numerical and laboratory tests, and some important results that could help the water utility companies in understanding the occurrence of faults in some parts of the network will be obtained.

In more detail, in [Chapter 5](#) and [Chapter 6](#), the occurrence of cavitation in the service line, the effect of the end-user discharge variations during the first phases of the transients and in time, the combined effect of simultaneous consumers, the effect of the network topology and the transient generation point are highlighted.

Moreover, [Chapter 7](#) aims at the analysis of the transient behaviour of the network also in the presence of a leak and at the calibration of main parameters in hydraulic transient solvers in viscoelastic pipes. A transient solver developed for pressurized water pipe networks incorporating both unsteady friction and pipe wall viscoelasticity is also used, and the main associated uncertainties are discussed.

In [Chapter 8](#), an overview of the developed work is illustrated and the main achievements of this research are outlined. Moreover, the research areas that need further investigations are identified.

## 2. State of the art

### 2.1. Introduction

In order to understand the dynamic behavior of WDNs an extensive literature review has been executed.

Specifically, the literature review relates to papers dealing with transients caused by variations in the functioning conditions (i.e., due to flow and pressure control operations and the almost continuous water consumption variations). Moreover, in order to get a comprehensive perspective, the review is also extended to papers dealing with controlled transients for fault detection, generated deliberately with Transient Test-Based Techniques (TTBTs).

It is worth noting that the review focuses mainly on physical experiments (laboratory and field tests), and that it has given priority to journal articles, since conference articles, research reports and doctoral theses, in most cases, include preliminary results of data published in subsequent journal articles.

All the works considered belong to the Scopus and/or Web of Science databases. The background review was essential to evaluate the state of the art in the research area and to identify further investigations to carry out. This chapter includes contributions given in four already published papers.

### 2.2. Transients in water distribution network

This section partially corresponds to:

Meniconi, S., **Maietta F.**, Alvisi, S., Capponi, C., Marsili, V., Franchini, M., Brunone, B. (2022). Consumption change-induced transients in a water distribution network: Laboratory tests in a looped system. *Water Resources Research*, 58, e2021WR031343. DOI: 10.1029/2021WR031343.

Meniconi, S.; **Maietta F.**; Alvisi, S.; Capponi, C.; Marsili, V.; Franchini, M.; Brunone, B. (2022). A Quick Survey of the Most Vulnerable Areas of a Water Distribution Network Due to Transients Generated in a Service Line: A Lagrangian Model Based on Laboratory Tests. *Water* 2022, 14, 2741. DOI: 10.3390/w14172741.

### 2.2.1. Introduction

In pipe networks, pressure plays a key role and, in particular, pressure variations due to transients can induce additional stresses not only on pipes but also on the other components, such as junctions and devices.

Traditionally, in transmission mains, attention is focused on the effects of a valve maneuver, carried out to set an appropriate discharge, or pump trip that can give rise to severe overpressure (Liou and Wylie, 2016, Meniconi et al., 2021a, Meniconi et al., 2018). Very different is the approach with respect to transients in Water Distribution Networks (WDNs) which are the topic of this work. Precisely, the effects of the transients in WDNs are often underestimated in the belief that such systems are always intrinsically self-protected against them. Such a conviction is based on the assumption that a large part of the generated pressure waves would exit through the consumers that, when active, behave as pressure relief valves. Thus, pipe breaks in WDNs are attributed to the large value of the steady-state pressure regime and/or to large, even if infrequent, overpressures caused by, as an example, pump switch-off. As an example, in Martínez García et al. (2020) the role of the high pressure values is shown to be correlated to the frequency of pipe breaks. In accordance with such assumptions, in most cases, the only preventive action is the installation of pressure-reducing valves (e.g., Prescott and Ulanicki, 2008; Meniconi et al., 2017). In case the pressure regime is considered appropriate, the inaccurate installation of pipes, additional loads due to traffic, and the large number of connections that undermine the integrity of the system.

Posed the question in these terms, in many cases it is arduous identifying the actual cause of the large leakage that characterizes only some parts of a WDN that exhibit no clear differences with respect to other ones in terms of pipe material, maintenance, external loads, as well as the pressure values, usually monitored at a low frequency. A possible explanation of such a feature could derive from proper identification of the nature of the actually dangerous transients and the different exposure to them of individual parts of the considered WDN. It is quite arduous for the water utility companies to suppress all leaks or prevent all pressure variations in WDNs. They usually install conventional surge protection devices (e.g., air vessels) in the main pipes to damp the more extreme pressure variations (e.g., the ones due to pump failure). However, the sources may be within the plumbing systems of the end-users and out of the

## Chapter 2. State of the art

regulatory control of the water utilities (Gong et al., 2018b). In fact, transients generated by users' consumption variations may be dangerous because of their very high frequency (Marsili et al., 2020): such small, but incessant, pressure changes can, in fact, increase the failure rate (Kwon and Lee, 2008; Rezaei et al., 2015). Furthermore, the frequent occurrences of transients due to the daily pump operation for system management can result in the deterioration of infrastructure safety and life cycles in the long term (Xing and Sela, 2020). With the aim of explaining the results achieved by this work and pointing out the open questions and urgent matters to address, a literature review is offered below.

### 2.2.2. Numerical tests

Numerous papers analyze numerically the transient behaviour of a WDN. More in details, the numerical papers deal with four main aspects: (i) the use of transients for detecting an anomaly (Vítkovský et al., 2000b; Vítkovský et al., 2003; Misiunas et al., 2006; Haghghi and Ramos, 2012; Shi et al., 2020; Che et al., 2022) or treating biofilm (Zeidan and Ostfeld, 2022), (ii) the performance of different numerical models (Axworthy and Karney, 1997, 2000; Filion and Karney, 2002; Wood et al., 2005; Vítkovský et al., 2011; Zecchin et al., 2014; Nault and Karney, 2016; Creaco et al., 2017; Nault et al., 2018; Pal et al., 2021; Ulanicki and Beaujean, 2021) with particular regard to the effect of the layout simplification – skeletonization – (Jung et al., 2007; Huang et al., 2017,0; Meniconi et al., 2021b), and uncertainties in the pipe properties and actual state of the system (Kazemi and Collins, 2018a; Kazemi and Collins, 2018b; Edwards and Collins, 2014); (iii) the effect of boundaries, and control devices (Karney and McInnis, 1992; Jung and Karney, 2006); and (iv) the identification of the most severe scenarios in terms of pressure variations: e.g., water consumption fluctuations (Haghghi, 2015), pump trip (Huang et al., 2020a) or transients generated in the supply line (Bohorquez et al., 2020b) for a real-time control (Prescott and Ulanicki, 2008; Creaco et al., 2019), by evaluating the optimal sensor location for capturing fast pressure variations (Zecchin et al., 2022).

### 2.2.3. Laboratory and field tests

The lack of space and a large number of possible combinations of loops (e.g., number, diameter distribution, and layout) make more attractive, also from an economic point of view, numerical experiments with respect to the laboratory ones. The need of monitoring a large number of sections in terms of not only pressure but also discharge – to control the users' random water consumption and all boundary conditions – makes the execution of significant tests in real WDNs very arduous. Then, very few papers deal with transient laboratory and

field tests.

With regard to the laboratory tests, the most active research group is the one at the University of Adelaide, Australia. However, the overwhelming part of such experiments concerns a single, quite short (with a length of about 40 m), and small diameter (about 20 mm) copper pipe. Such a circumstance makes these papers out of topic for the analysis provided in this thesis work. The only exception is the paper by Zeng et al. (2021) in which the mentioned copper pipe – with two artificial leaks – is connected to the Adelaide water main through a polymer hose and a copper pipe at each side for anomaly detection. However, the transients carried out in the real WDN are not of interest for the present analysis as they fall within what the Authors call “background noise”, a feature that must be reduced to better localize the leaks. A further contribution is offered by the research group at the University of Sheffield, UK, in the conference paper by Hampson et al. (2014), where the transient source location has been detected in a 25 mm MDPE pipe network with a single 20x20 m square loop and two branches by comparing the experimental arrival time of transient pressure primary wave fronts and those estimated by the graph theory.

The literature is slightly more extensive for field tests. Specifically, the usefulness of acquiring the pressure signals at a low frequency (15 minutes) or higher frequencies is discussed in Mounce et al. (2012); Machell et al. (2014); Mounce et al. (2015). Furthermore, an example of the application of the transient test-based techniques for a leak survey in a WDN is offered in Meniconi et al. (2015), where transients are generated by a pump trip. In addition, Stephens et al. (2011) check the performance of unsteady models for transients generated by the closure of a small valve, installed at two separate locations, with pressure measured only at three sections. The considered system is a small-town WDN – with 2 loops and several branches supplied by a tank – comprising 4 km of pipe of homogeneous material (asbestos cement, with a diameter ranging from 96 mm to 231 mm). However, also these tests are of limited relevance in the light of the present paper: transient tests are carried out during the night, just to reduce the impact of water consumption (see below). The analysis of two transient tests carried out in a real WDN with three loops of pipes of different material and diameter (cast iron pipes with a diameter from DN80 to DN250, and PVC pipes with a diameter from DN100 to DN200) is reported in Gong et al. (2018b) to verify the damping effect of a plastic pipe replacing an old metallic one in a relay program. The transients are generated by the opening and closing of a solenoid valve installed in the plastic pipe, and then characterized by a lower impedance with respect to the other WDN pipes, and pressure is measured only in four measurement sections at the main pipes. In the conference papers by Starczewska et al. (2014), Starczewska et al. (2015a), and Starczewska et al. (2015b), the transient behavior of WDNs is analyzed. Specifically, in Starczewska et al. (2014) transient tests, due to pump trip, show no decrease in the transient upsurges amplitude despite progression from

trunk to distribution pipes. The Authors notice that the pressure waves do not damp because of the presence of several contractions and dead ends. In Starczewska et al. (2015a) tests are carried out in two areas of a WDN dominated by industrial user and pump activity, respectively. The data are used to demonstrate the validity of a methodology that quantifies the pressure changes experienced by pipes and evaluate the fingerprint in terms of pressure gradient. In Starczewska et al. (2015b), a high frequency pressure monitoring is carried out for two weeks in two sections of five differently supplied sites of WDNs. These have been chosen to represent the complexity of the water network with looped and branched connections included. The aim is to correlate the severity of transients to pipe material, diameter, age, WDNs complexity, and types of users. A conclusive result has not been achieved, with only the percentage of plastic pipes, and the source of the transient (e.g., pumps, commercial users) proven to be significant. The Authors highlight the need to better understand the widespread occurrence of transients within complex WDNs. Such a conclusion reinforces what explicitly pointed out in the pioneering paper by McInnis and Karney (1995), where the results of a single field test are reported. Precisely, it is stated that “the results are not sufficient to generalize about the transient behavior of pipe networks. On the contrary, experience gained from this field test indicates that more rigorous field-testing programs are necessary if we are to isolate and understand the nature of transient flow in complex pipe systems.” In fact, in most cases, in real WDNs, very few tests (or just a single test) are carried out for several reasons, with the main being the evident non-repeatability of the tests. This circumstance makes very hard to generalize the obtained results. In complex systems, as WDNs, the cause-and-effect link is not clear: a given measured overpressure could be due to several causes also because several are the possible paths of the pressure waves. More successful is the correlation between the varying pressure and the main failure highlighted in Rezaei et al. (2015) for data acquired in forty-eight District Metered Areas (DMAs) feeding a total population of approximately 100,000 people in UK.

### 2.2.4. Conclusions

From the above literature review it emerges that in the few available papers based on physical experiments, transients are generated by maneuvers in the supply lines (e.g., pump trip) and their effects are analyzed in the main pipes. Such a phenomenon is very different with respect to the transients generated within the network (i.e., in the service lines) due to water consumption variations. Indeed, such transients are very frequent, one could say “almost continuous”, and very few papers analyze in details their effects experimentally (Marsili et al., 2020; Marsili et al., 2022; Lee et al., 2012; Lee, 2015).

As a premise to properly analyze the characteristics of transients in WDNs, it is

important to make a distinction between the main pipes and service lines, that usually meet at a junction. The former are the municipal pipes and form the distribution network, whereas the latter connect the main pipes to the internal plumbing systems of individual users. Such a distinction is motivated in two respects. The first respect is of an administrative nature: the municipal pipes and service lines (up to the curb stop or water meter) are maintained by the utility company, whereas the remaining part of the service lines is under the user's responsibility. The second respect concerns the characteristics of these two components, with the diameter of the main pipes being significantly larger than the one of the service lines. In Marsili et al. (2020,0), the pressure signals acquired in a real WDN in ordinary operational conditions (i.e., with no maneuvers on pumps or valves in the main pipes) indicate that the short term pressure variations occurring in the main pipes are due to the water consumption changes. In Lee et al. (2012), laboratory experiments concern a limited (i.e., six) number of tests on a tree layout system. Transients from both outside (i.e., generated in the main pipe), and inside (i.e., within the plumbing system) are considered. The main goal of these tests is to point out the possible occurrence of negative pressures, and related back-flow phenomena, in the plumbing system. Accordingly, pressure traces are not acquired in the main pipes. In Lee (2015), the main aims are to check whether transients generated in the main pipes are responsible for the failure in the service lines and a leak in the service line may attenuate pressure waves. However, the few carried out tests do not allow drawing general conclusions and highlighting the role of the location of the transient source, as well as of the entity and the simultaneity of water consumption changes, for a given layout.

Because of the lack of experimental data and their often poor quality, a reliable criterion on the actual behavior of transients in WDNs is strongly desired by water companies.

### 2.3. Transient Test-Based Techniques for leak detection

This section corresponds to the following research paper:

Brunone B., **Maietta F.**, Capponi C., Keramat A., Meniconi S. (2022) A review of physical experiments for leak detection in water pipes through transient tests for addressing future research, *Journal of Hydraulic Research*, 60:6, 894-906, DOI: 10.1080/00221686.2022.2067086.

#### 2.3.1. Introduction

In recent years there has been increasing attention on the maintenance of adequate water resources and the condition of pressurized pipe systems. Water distribution networks (WDNs) and transmission mains (TMs) play an essential role in the delivery of water resources to the population. However, in many cases, pipe systems are degraded infrastructures since they often have been in service for many years, far beyond their life-cycle (Filion et al., 2004). The aging of pipe systems reflects in several aspects. A first example is the increase of frictional resistance – due to processes as internal corrosion, bio-film formation, and tuberculation – must be mentioned (Sharp and Walski, 1988). Such a feature increases the electricity consumption in pumping systems, reduces the carrying capacity of gravity pipelines, and efficiency of hydro-power plants (Abbasi and Abbasi, 2011). Furthermore, deteriorating pipe systems experience the temporal increase of leakage that implies not only the wastage of a precious resource but also other important downsides. These are the risk of compromising water quality – because of the possible back-flow phenomena – and undermining roadways and building foundations – because of the erosion of the underlying soil (Colombo and Karney, 2002). Finally, energy costs increase more than proportionately with leakage (Nogueira Vilanova and Perrella Balestrieri, 2015; Ghorbanian et al., 2017). The economic impact of the efficiency from the energy point of view is given by the fact that the 2-3 % of the worldwide electricity consumption is used for pumping in water systems (Nogueira Vilanova and Perrella Balestrieri, 2014).

For the above reasons, leakage management is a clear priority of water system managers because of the evident crucial importance of the drinkable water from both the social and economic point of view.

The suitability of leak detection techniques depends on the characteristics of the test pipe systems. WDNs and TMs are different in their layout and number of users. WDNs have much more complex layout; they are organized in loops to increase the system resilience without making construction unaffordable. The number of users is much smaller for TMs than for WDNs, as they convey the resource from the production area to a reservoir. These differences are reflected

in the accessibility of the system, with almost every user of a WDN being a possible access point. Due to the greater accessibility of WDNs there has been more progress in recent years in leak detection for these systems than for TMs. In the last two decades, transient test-based techniques (TTBTs) have been investigated because the pressure waves generated during transient tests allow TMs to be studied despite their poor accessibility.

A discussion about the proper procedure to follow within TTBTs for an effective leak detection as well as the most appropriate techniques for the analysis of the acquired pressure traces is beyond the scope of this paper. In these regards, existing literature may help the interested reader (Colombo et al., 2009; Liu and Kleiner, 2013; Abdulshaheed et al., 2017; Xu and Karney, 2017; Ayati et al., 2019; Duan et al., 2020; Che et al., 2021). The aims of this paper are instead different, and very focused ones. Firstly, it wants to give a picture, as complete as possible, of the available experimental data concerning the use of transient tests for locating and sizing leaks. Then it wants to make a contribution for orienting future research by indicating “categories” – e.g., pipe system layout, materials, diameters, flow conditions and leak characteristics – that need further experiments. In this light, this paper must be considered as a service paper.

To achieve these tasks, it was very important identifying rational criteria for selecting the papers, and related experimental results, from literature. The reasons for excluding the papers from such a review are six. (1) Studies of acoustic waves are not included as their mechanisms of dissipation are very different from those of pressure waves. (2) Studies of burst formation are not included as the pressure wave is not caused by a dedicated manoeuvre but leak formation itself generates the transient; this implies a completely different experimental approach. (3) If the frequency acquisition is smaller than some tens of Hz the study is excluded, as some important features of the transient response are not captured properly. (4) When the pipe break is due to fatigue phenomena the study is not included. In this case, as for bursts, transients are not used for detecting an existing leak, but they are the cause of the leak, and a different experimental approach is followed. (5) Studies investigating back-flow phenomena are excluded, as attention is focused not on the pipe system’s response to a dedicated transient but on the mechanisms of interaction with the surrounding environment through the leak. As a consequence, collected data are not appropriate for leak detection. (6) Finally, the exclusion of conference papers, research reports and PhD theses is due to the fact that, in most cases, they include preliminary results with the complete series of data published in successive journal papers. As a result, 49 papers have been selected, published between 1994 and 2020. In this review, tests executed by Joukowsky at the sunset of the 19th century have been deliberately excluded since they merit a separate analysis within an appropriate historical framework.

A timeline of the published papers is reported in Fig. 2.1. Such a figure indicates a constant behavior – about two/three papers per year – with few exceptions

## Chapter 2. State of the art

when more papers have been published (2007 and 2011, 2012, and 2019 with 5 and 4 papers, respectively). For the sake of clearness and to not weight the text with many citations per section, in Table 2.2 all the selected papers are listed with their main characteristics indicated according to the categories below identified.

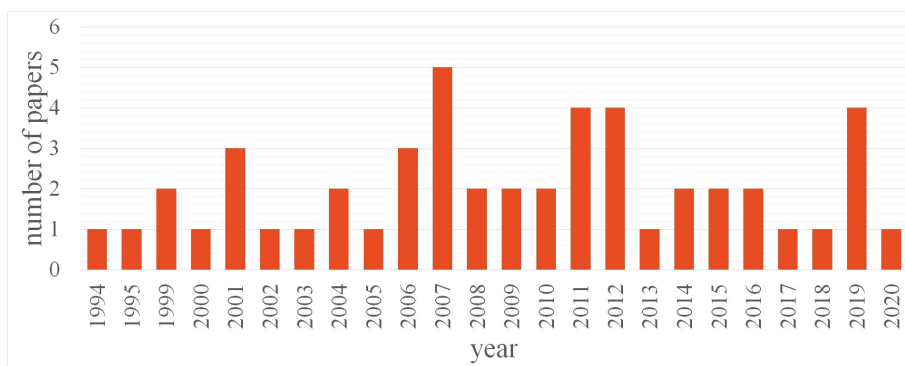


**Fig. 2.1:** Number of papers per year with experiments on leak detection by transient tests.

**Table 2.1:** Categories identified for the analysis of the experimental tests.

Category (#)	Title
1	complexity of the test system
2	modality of transient generation
3	pipe material
4	pipe diameter
5	pre-transient pressure regime
6	inserted pressure wave
7	pre-transient flow regime
8	leak simulation

## Chapter 2. State of the art

**Table 2.2:** Selected papers with the main characteristics of the executed experimental tests.

Paper number	Type	Lay.	Mod.	Mat.	$D$	$h$	$\Delta h$	Re	no.	Leak leaks	size
Al-Khomairi (2008)	L	SP	MV	Cu	$D_2$	–	–	$Re_3$	1		$L_5,$ $L_6,$ $L_7$
Amin et al. (2014)	L	SP	MV	PE	$D_2$	$h_2,$ $h_3$	–	$Re_3$	1		$L_{10}$
Asada et al. (2020)	L	SP	MV	Fe	$D_2$	–	$\Delta h_1$	$Re_1$	1		$L_1$
Beck et al. (2005)	L	BS	MV	Cu	$D_6$	–	–	–	1		$L_{11}$
	L	N	MV	Cu	$D_8$	–	–	–	1		$L_{11}$
Beck et al. (2006)	L	BS	HD	Cu	$D_6$	–	–	–	1		$L_{11}$
Brunone (1999)	L	SP	HD	PE	$D_3$	$h_1$	$\Delta h_2$	$Re_1$	1,2		$L_3$
Brunone and Ferrante (2001)	L	SP	MV	PE	$D_3$	$h_1,$ $h_2$	$\Delta h_2,$ $\Delta h_3$	$Re_3$	1		$L_3,$ $L_4$
Brunone and Ferrante (2004)	L	SP	MV	PE	$D_3$	$h_2$	$\Delta h_4$	$Re_3$	1		$L_3,$ $L_4$
Brunone et al. (2008b)	L	SP	OD	PE	$D_3$	$h_2$	$\Delta h_1$	$Re_2$	1		$L_{10}$
Brunone et al. (2015)	L	SP	MV	PE	$D_3$	$h_2,$ $h_3$	$\Delta h_2$	$Re_3$	1		$L_3,$ $L_4$
Capponi et al. (2017)	L	BS	MV	PE	$D_7$	$h_3$	$\Delta h_1,$ $\Delta h_3$	$Re_3$	1		$L_4$
Covas et al. (2004a)	L	SP	MV	PE	$D_3$	$h_4$	$\Delta h_3$	$Re_3$	1		$L_2$
	F	SP	MV	PE	$D_4$	$h_1$	$\Delta h_3$	$Re_3$	1		$L_{13}$
Covas and Ramos (2010)	L	SP	MV	PE	$D_3$	$h_4$	$\Delta h_3$	$Re_2,$ $Re_3$	1,2		$L_3$
	F	SP	MV	PE	$D_4$	$h_1$	$\Delta h_3$	$Re_3$	1		$L_{13}$
Ferrante and Brunone (2003)	L	SP	MV	PE	$D_3$	$h_2$	$\Delta h_3$	$Re_3$	1		$L_{10}$
Ferrante et al. (2007)	L	SP	MV	PE	$D_3$	$h_2,$ $h_3$	$\Delta h_3,$ $\Delta h_5$	$Re_3$	1		$L_{10}$
Ferrante et al. (2009a)	L	BS	HD	PE	$D_7$	$h_3$	$\Delta h_1,$ $\Delta h_3$	$Re_2,$ $Re_3$	1		$L_{10}$
	F	BS	HD	Fe	$D_7$	$h_2$	$\Delta h_4$	$Re_3$	1		–
Ferrante et al. (2009b)	L	SP	MV	PE	$D_3$	$h_1,$ $h_2$	$\Delta h_4$	$Re_3$	1		$L_7,$ $L_8$
Ferrante et al. (2014)	L	SP	MV	PE	$D_3$	$h_1,$ $h_2,$ $h_3,$ $h_4$	$\Delta h_3$	$Re_3$	1		$L_3,$ $L_4$
Ghazali et al. (2011)	L	SP	HD	PE	$D_3$	$h_3$	–	$Re_3$	1		$L_{10}$
Ghazali et al. (2012)	F	N	HD	Fe	$D_9$	–	–	–	1		$L_{15}$
Gong et al. (2016)	L	SP	HD	Cu	$D_2$	–	$\Delta h_3$	$Re_2$	1		$L_{10}$

## Chapter 2. State of the art

Guo et al. (2012)	L	SP	MV	Fe	$D_5$	$h_1$	$\Delta h_1, \Delta h_2$	$Re_3$	1	$L_5$
Haghighi et al. (2012)	F	SP	HD	Fe	$D_5$	$h_5$	$\Delta h_1, \Delta h_3$	$Re_3$	1	$L_{16}$
Jönsson (1994)	L	SP	MV	Cu	$D_1$	$h_2$	$\Delta h_4, \Delta h_5$	$Re_2$	1	$L_5, L_6$
Jönsson (1999)	L	SP	MV	Fe	$D_3$	$h_5$	$\Delta h_5$	$Re_3$	1	$L_7$
Jönsson (2001a)	L	SP	MV	Fe	$D_3$	$h_4$	$\Delta h_5$	$Re_2, Re_3$	1	$L_5, L_6, L_7$
Jönsson (2001b)	L	SP	MV	Fe	$D_3$	$h_4$	$\Delta h_4, \Delta h_5$	$Re_2, Re_3$	1	$L_6, L_7$
Keramat et al. (2019)	L	SP	MV	PE	$D_3$	$h_2$	$\Delta h_4$	$Re_3$	1	$L_8$
Lee et al. (2006)	L	SP	MV	Cu	$D_2$	–	$\Delta h_4$	$Re_3$	1	$L_2$
Lee et al. (2007a)	L	SP	MV	Cu	$D_2$	$h_3, h_4$	$\Delta h_1, \Delta h_2, \Delta h_3$	$Re_3$	1	$L_2$
Lee et al. (2007b)	L	SP	MV	Cu	$D_2$	–	$\Delta h_1$	$Re_3$	1	$L_2$
Liou and Tian (1995)	F	SP	PO	Fe	$D_5$	–	–	$Re_1$	1	–
Meniconi et al. (2011c)	L	SP	HD	PE	$D_3$	$h_2, h_3$	$\Delta h_1$	$Re_2$	1	$L_4$
Meniconi et al. (2013a)	L	SP	MV	PE	$D_3$	$h_2, h_3$	$\Delta h_2, \Delta h_3, \Delta h_4$	$Re_3$	1	$L_{10}$
Meniconi et al. (2015)	F	N	PO	Fe	$D_{10}$	$h_8, h_9$	$\Delta h_8$	$Re_3$	1	–
Meniconi et al. (2018)	F	N	PO	Fe	$D_{10}$	$h_8$	$\Delta h_8$	$Re_3$	1	–
Shucksmith et al. (2012)	F	SP	HD	PVC	$D_3$	$h_5$	–	–	1	–
	F	SP	HD	Fe	$D_3, D_4$	$h_3, h_4, h_5$	–	–	1	$L_{14}, L_{15}$
	F	SP	HD	AC	$D_4$	$h_5$	–	–	1	$L_{15}$
Soares et al. (2011)	L	N	MV	PVC	$D_8$	$h_6, h_7$	$\Delta h_6, \Delta h_7$	$Re_3$	1	$L_9$
Souza et al. (2000)	L	SP	PO	PVC	$D_1$	$h_1$	$\Delta h_4$	$Re_2, Re_3$	1	$L_7, L_9$
Stephens et al. (2011)	F	N	HD	AC	$D_9$	$h_8, h_9$	$\Delta h_6, \Delta h_7$	$Re_1, Re_2, Re_3$	1	$L_{15}$
Sun et al. (2016)	L	SP	MV	Fe	$D_2$	$h_2$	$\Delta h_5$	$Re_3$	2	$L_{10}$
Taghvaei et al. (2006)	L	BS	HD	Cu	$D_6$	–	–	–	1	$L_{10}, L_{12}$
Taghvaei et al. (2007)	L	BS	HD	Cu	$D_6$	–	–	–	1	$L_{10}, L_{11}, L_{12}$

## Chapter 2. State of the art

Taghvaei et al. (2010)	L	SP	HD	PE	$D_3$	–	–	$Re_3$	1	$L_8,$ $L_9$
Vítkovský et al. (2007)	L	SP	MV	Cu	$D_2$	$h_2,$ $h_3$	$\Delta h_1$	$Re_2,$ $Re_3$	1,2	$L_1,$ $L_2$
Wang et al. (2002)	L	SP	MV	Cu	$D_2$	$h_3$	–	$Re_3$	1	$L_2$
Wang et al. (2019a)	L	SP	MV	PE	$D_3$	$h_4$	$\Delta h_1$	$Re_2$	2,3	$L_3$
Wang et al. (2019b)	L	SP	MV	PE	$D_3$	$h_2,$ $h_4$	$\Delta h_1,$ $\Delta h_4$	$Re_3$	1	$L_8,$ $L_{10}$
Yusop et al. (2019)	L	SP	MV	PE	$D_2$	–	–	–	1	–
	L	SP	HD	PE	$D_2$	–	–	–	1	–

**Table 2.3:** Meaning of the abbreviations used in Tab. 2.2

<b>Category #1: complexity of the test system</b>		
<b>Complexity of the system layout</b>	<b>Symbol</b>	
Single pipe	SP	
Branched system	BS	
Network	N	
<b>Complexity of the functioning condition</b>	<b>Symbol</b>	
Laboratory tests	L	
Field tests	F	
<b>Category #2: modality of transient generation</b>		
Maneuver valve	MV	
Pump operation	PO	
ad hoc device	HD	
<b>Category #3: pipe material</b>		
<b>Material</b>	<b>Symbol</b>	
Polyethilene	PE	
Copper	Cu	
Steel, iron, cast iron	Fe	
Polyvinyl chloride	PVC	
Asbestos cement	AC	
<b>Category #4: pipe diameter, <math>D</math></b>		
<b>Complexity of the test system</b>	<b>Symbol</b>	<b><math>D</math> Range [mm]</b>
SP	$D_1$	$D < 20$
SP	$D_2$	$20 \leq D < 50$
SP	$D_3$	$50 \leq D < 100$
SP	$D_4$	$100 \leq D < 200$
SP	$D_5$	$D \geq 200$
BS	$D_6$	$D < 20$
BS	$D_7$	$D \geq 20$

## Chapter 2. State of the art

N	$D_8$	$D < 100$
N	$D_9$	$100 \leq D < 300$
N	$D_{10}$	$D \geq 300$
<b>Category #5: pre-transient pressure regime, <math>h</math></b>		
Complexity of the test system	Symbol	$h$ Range [m]
SP - BS	$h_1$	$h < 10$
SP - BS	$h_2$	$10 \leq h < 20$
SP - BS	$h_3$	$20 \leq h < 40$
SP - BS	$h_4$	$40 \leq h < 60$
SP - BS	$h_5$	$h \geq 60$
N	$h_6$	$h < 20$
N	$h_7$	$20 \leq h < 40$
N	$h_8$	$40 \leq h < 60$
N	$h_9$	$h \geq 60$
<b>Category #6: inserted pressure wave, <math>\Delta h</math></b>		
Complexity of the test system	Symbol	$\Delta h$ Range [m]
SP - BS	$\Delta h_1$	$\Delta h < 5$
SP - BS	$\Delta h_2$	$5 \leq \Delta h < 10$
SP - BS	$\Delta h_3$	$10 \leq \Delta h < 20$
SP - BS	$\Delta h_4$	$20 \leq \Delta h < 30$
SP - BS	$\Delta h_5$	$\Delta h \geq 30$
N	$\Delta h_6$	$\Delta h < 10$
N	$\Delta h_7$	$10 \leq \Delta h < 30$
N	$\Delta h_8$	$\Delta h \geq 30$
<b>Category #7: pre-transient flow regime, <math>Re</math></b>		
Complexity of the test system	Symbol	$Re$ Range [-]
SP - BS - N	$Re_1$	$Re < 2000$
SP - BS - N	$Re_2$	$2000 \leq Re < 8000$
SP - BS - N	$Re_3$	$Re \geq 8000$
<b>Category #8: leak simulation</b>		
Complexity of the functioning condition	Symbol	Range [ $m^2$ ]
L	$L_1$	$C_{sv}A_L < 5 \cdot 10^{-7}$
L	$L_2$	$5 \cdot 10^{-7} \leq C_{sv}A_L < 5 \cdot 10^{-6}$
L	$L_3$	$5 \cdot 10^{-6} \leq C_{sv}A_L < 5 \cdot 10^{-5}$
L	$L_4$	$C_{sv}A_L \geq 5 \cdot 10^{-5}$
Complexity of the functioning condition	Symbol	$q/Q_{in}$ and $A_L/A$ Range [%]
L	$L_5$	$q/Q_{in} < 5$
L	$L_6$	$5 \leq q/Q_{in} < 10$
L	$L_7$	$10 \leq q/Q_{in} < 20$
L	$L_8$	$20 \leq q/Q_{in} < 30$
L	$L_9$	$q/Q_{in} \geq 30$
L	$L_{10}$	$A_L/A < 5$
L	$L_{11}$	$5 \leq A_L/A < 10$
L	$L_{12}$	$A_L/A \geq 10$

Complexity of the functioning condition	Symbol	Range [ $m^2$ ]
F	$L_{13}$	$C_{sv}A_L \leq 1 \cdot 10^{-4}$
Complexity of the functioning condition	Symbol	Range [L/s]
F	$L_{14}$	$q < 0.5$
F	$L_{15}$	$q \geq 0.5$
Complexity of the functioning condition	Symbol	Range [%]
F	$L_{16}$	$A_L/A = 40$

Selected papers have been grouped into eight categories, each of them labelled by a progressive number; precisely: # 1 - complexity (layout) of the test system (abbreviated in Table 2.2 to “Lay.”); # 2 - modality of transient generation (abbreviated in Table 2.2 to “Mod.”); # 3 - pipe material (abbreviated in Table 2.2 to “Mat.”); # 4 - pipe diameter ( $D$ ); # 5 - pre-transient pressure regime (abbreviated in Table 2.2 to “ $h$ ”); # 6 - inserted pressure wave (abbreviated in Table 2.2 to “ $\Delta h$ ”); # 7 - pre-transient flow regime (abbreviated in Table 2.2 to “Re”), and # 8 - leak simulation (with in Table 2.2 indicated the number and size of the leaks). Moreover, as illustrated below, an acronym is used to indicate the sub-categories, identified for each category. As an example, with regard to category # 1 (complexity of the test system), three sub-categories have been identified: single pipe (indicated with the acronym “SP”), branched system (BS), and network (N); the meaning of the abbreviations used in this table is reported in Table 2.3. If in the experiments both a single pipe and a network have been investigated, the paper is included in both the SP and N sub-categories. As a further example, if in a given paper two different pipe materials have been used, the paper is included in both the related two sub-categories. Moreover, in the choice of the categories, both dimensional and dimensionless quantities have been considered. The reason is that a dimensional quantity, when incorporated in a dimensionless parameter, influences an aspect of the transient, whereas, if taken individually, it highlights other critical issues of the physical experiments. As an example, the pre-transient Reynolds number, pipe diameter, and the inserted pressure wave, even if linked together, have been considered separately. The reasons of such a choice are several. Firstly, the pre-transient Reynolds number influences remarkably the unsteady-state mechanisms of the energy dissipation. For its part, the value of the pipe diameter, and then the cross-sectional area, compared to leak size, is important for evaluating the relative relevance of the leak. Finally, the value of the inserted pressure wave – linked to the pre-transient mean velocity and then Reynolds number if a closure maneuver is executed – is a measure of the potential of the method. In fact, for all given quantities, the larger the inserted pressure wave, the smallest the detectable leak. As a further example, a category has been devoted to the pre-transient pressure regime that, in a given system, is linked to the flow regime. The reason is that, beyond leak size and inserted pressure

wave, the detectability of a given leak increases with decreasing the pressure at the leak (Liou, 1998). For each category, the explored range of variability is divided into an appropriate number of ranges. As an example, with regard to the diameter,  $D$ , the experiments executed in the laboratories have been divided (see the below # 4) in the following five ranges: i)  $D_1$ :  $D < 20$  mm; ii)  $D_2$ :  $20 \text{ mm} \leq D < 50$  mm; iii)  $D_3$ :  $50 \text{ mm} \leq D < 100$  mm; iv)  $D_4$ :  $100 \text{ mm} \leq D < 200$  mm; and v)  $D_5$ :  $D \geq 200$  mm.

Differently from the other critical points that will be highlighted in the below sections, two points merit special attention with the aim of allowing the scientific community to use the acquired data for other purposes. The first point to be mentioned concerns the need of including dimensional plots of the measured quantities. In fact, particularly when the analysis of the experimental results is executed in the frequency domain, often only the more *elegant* dimensionless plots are presented. From such plots it can be quite difficult to “extract” the measured quantities. The second point relates to the importance of indicating very precisely all the characteristics of the experimental set-up and possibly including a sketch.

As mentioned, each section of this chapter section is devoted to one of the mentioned categories. For each category, a description of the executed tests is given by pointing out main features, critical issues, and possible objectives for future research. In the Gaps of knowledge, some of the possible issues to address by means of further experimental tests are synthesized, as well as the need for a more efficient sharing of the existing data is pointed out, with a possible solution.

### 2.3.2. Laboratory and field tests

The available physical experiments are analysed referring to the categories reported in Table 2.1.

#### Category #1: complexity of the test system (layout)

The complexity of the system concerns two important features: the layout and functioning conditions. In terms of layout complexity, three sub-categories have been identified: single pipe (SP), branched system (BS), and network (N), with the latter type being characterized by at least one loop. Fig. 2.2 shows that in the vast majority of papers (n. 38, i.e., about 76 %), tests have been executed on single pipes, whereas almost the same number of papers concerns branched systems and networks (n. 6, i.e., about 12 %). For the sake of clarity, as much as possible, in the successive plots data concerning single pipes are depicted in green, whereas those of branched systems and networks are in purple and grey, respectively.

An evident reason for such a feature is the lack of space in most of laboratories.

However, it cannot be ruled out that a large number of possible combinations of branches (e.g., location, and size with respect to the main pipe) and loops (e.g., number, and layout) makes more attractive, also from the economical point of view, numerical experiments with respect to laboratory ones. As an example, in Meniconi et al. (2021b) a comprehensive analysis of the transient response of a branched system has been executed by means of numerical experiments by changing all the characteristics of the branch in such an extensively way that it would have been impractical in a lab even for a small part of the considered layout changes.

In terms of the complexity of the functioning conditions, two sub-categories clearly emerge: laboratory (L) and field (F) tests. In fact, in the former the functioning conditions are absolutely controlled and known during the experiments, whereas in the latter they depend on the behavior of the users in a quite uncontrollable way. Fig. 2.2 points out clearly that most of the experiments (n. 43, i.e., about 81%) have been executed in the lab. Again, for the sake of clarity, as much as possible, in the successive plots data concerning laboratory tests are depicted in blue, whereas those of field tests are in orange.

With the aim of investigating the role of the system complexity, in the future two issues could be addressed by research groups: to increase the number of the physical experiments in branched and looped systems and those in real systems. In the writers' opinion, these issues are justified by several clear reasons. The first reason is the fact that in branched/looped systems the overlapping of the pressure waves coming from different sections may complicate the procedures for leak identification. In fact, the dynamics of the pressure wave interaction has direct consequences on the uniqueness of the solution unless an adequate number of measurement sections is arranged. The second reason is that the choice of the section where the transient is generated – the so called *pressure wave insertion point* – plays a more important role than in a single pipe. In fact, the effectiveness of a given pressure wave in terms of the smallest detectable leak depends remarkably on the number of the singularities (e.g., changes of diameter and/or material, branches) placed between the pressure wave insertion point and the leak. In other words, the transient response of the leak can be obscured by other features interacting with the pressure waves generated by the transient. Finally, the changes in the boundary conditions, that in real systems may happen during transient tests, can be a hard testing for all methodologies used for the analysis of the pressure signals (Meniconi et al., 2021a).

### Category #2: modality of transient generation

In TTBTs a pressure wave is inserted into the test system. The pressure wave can be generated by changing the mean velocity or pressure head. The first modality is the most frequent one since the idea itself of the water hammer waves is inextricably linked to the closure of a valve and then an abrupt change

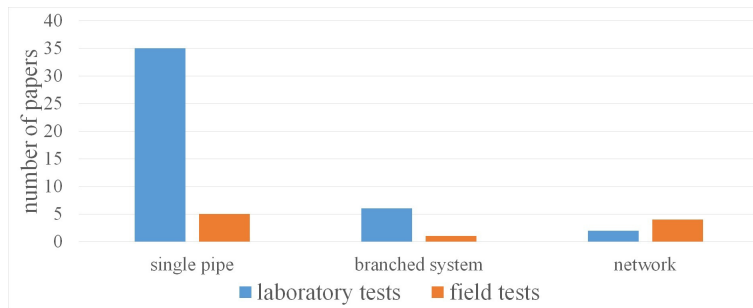


**Fig. 2.2:** Category #1: test system complexity. Number of papers in terms of layout complexity – single pipe (SP), branched system (BS), and network (N) – and functioning condition complexity – laboratory (L) and field (F) tests.

of the mean velocity.

Fig. 2.3 classifies papers by the modality used for generating transients in the experiments. In most of cases (n. 35, i.e., about 64 %), transients have been generated by maneuvering a valve (VM). Precisely, valve closure and impulse maneuver in the 86 % and 14 %, respectively, whereas in very few cases (n. 4, i.e., about 7 %) through pump operation (PO). In a conspicuous number of experiments (n. 16, i.e., about 29 %), an *ad hoc* device (HD) has been used. The latter is, as an example, the case of the connection of the Portable Pressure Wave Maker (PPWM) to the test pipe (Brunone et al., 2008b, Brunone et al., 2021).

The large number of cases in which transients have been generated by closing a valve is due to the extreme simplicity of such a maneuver. In 77 % (12 %) of the cases, the maneuver valve is placed at the pipe downstream (upstream) end section; in 11 % of tests, transients have been generated by closing a side discharge valve. On the contrary, the cause of the fact that in a real system the valve impulse has never been used is that such a maneuver is considered with *suspicion* – maybe unjustified – by water company technicians. As far as the writers are concerned, unspecified *resonance phenomena* are usually worried. Moreover, a bit unexpected is the limited use of pump operation for generating transients. However, a reason could be the usual long period of time required by the pump shutting off. Such a feature implies that the generated pressure wave is not sharp enough for an accurate leak location in a large part of the test system.

As the valves installed in real systems are usually too large to be closed quickly, a prescription for the future research activity is to refine alternative devices for generating controlled sharp pressure waves. In this regard, the spark generator developed at the University of Adelaide looks promising (Gong et al., 2018a). On the contrary, it seems appropriate to discourage the use of hydrants as pres-

## Chapter 2. State of the art

sure wave insertion points. In fact, the quality of the pressure wave generated at a hydrant may be poor because of the interaction between the conduit connecting the hydrant to the main pipe and the main pipe itself. Such an interaction happens very close to the pressure wave insertion point, the generated pressure wave is corrupted very soon. The use of hydrants within TTBTs is an example of the wrong extension to very different flow conditions of a device that gives positive results in another hydrodynamic context (i.e., within steady-state measurements).

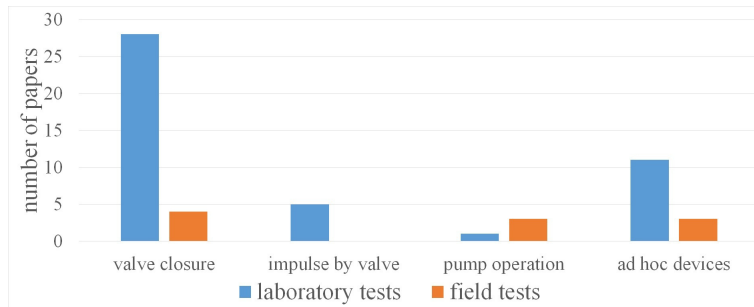


**Fig. 2.3:** Category #2: modality of transient generation. Number of the papers for each modality – valve closure and valve impulse (VM), pump operation (PO), and *ad hoc* device (HD) – and functioning condition complexity – laboratory (L) and field (F) tests).

### Category #3: pipe material

The effect of the pipe material reflects in two main features: i) the value of the pressure wave speed – that, in turn, influences the inserted pressure wave – and ii) the stress-strain relationship. Such features are strongly linked since the retarded strain component characterizing polymeric pipes is one of the causes of the smaller value of the pressure wave speed with respect to elastic (e.g., metallic and cement) pipes.

Fig. 2.4, where the percentage of papers for each pipe material is shown, indicates that most of the tests have been executed in polyethylene (PE) (43 %) and copper (23 %) pipes. As pointed out in Fig. 2.5, polyethylene pipes are used both in laboratory and field tests whereas copper (Cu) pipes – always with a small diameter (see the below category # 4) – are installed only in labs. Moreover, in very few tests cement (C) and polyvinyl chloride (PVC) pipes have been used.

Some of the plausible reasons of this situation are reported below. About the large use of copper pipes in the labs, tradition plays an important role. Precisely, it can be traced back to the times when the first tests were executed for the analysis of water-hammer phenomena (Contractor, 1965; Holmboe and

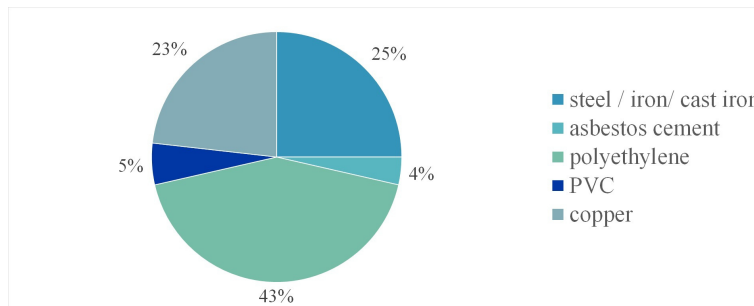


**Fig. 2.4:** Category #3: pipe material. Percentage of the papers in terms of pipe material: steel/iron/cast iron (Fe), cement (C), polyethylene (PE), polyvinil chloride (PVC), and copper (Cu).

Rouleau, 1967). Since small diameter copper pipes can be arranged easily around a drum, long pipes take up little space. Moreover, the fact that copper pipes are mostly used in heating systems explains why no tests on copper pipes have been carried out in real water pipe systems. The wide use of polyethylene pipes has at least three main reasons. The first is their low weight and high flexibility, making these pipes easy to carry and adaptable to small labs; the second positive element is their quite small cost. Moreover, it is easy to cut polyethylene pipes to install short devices simulating a leak at any section along the pipe. In the face of such positive aspects, the use of polymeric pipes may make more difficult leak detection and sizing when a procedure based on the Inverse Transient Analysis is followed. In fact, for polymeric pipes the number of parameters to be calibrated for simulating properly the transient response is much larger than for elastic pipes. Precisely, beyond the pressure wave speed and unsteady friction decay coefficient, the parameters describing the viscoelastic behavior of the pipe material must be evaluated in the preliminary calibration phase (Pezzinga et al., 2016). Finally, it can be hypothesized that the rigidity of PVC, iron/cast and cement pipes – for the last two also the heavy weight – discouraged their use in the lab.

According to the above discussion, in terms of pipe material, a fruitful integration of the existing experimental data would be given by further tests in steel/iron (Fe), cement (C), and polyvinyl chloride (PVC) pipes.

#### Category #4: pipe diameter

For practical reasons, the diameters,  $D$ , used in laboratory tests on a single pipe (SP) have been divided in five ranges: i)  $D_1$ :  $D < 20$  mm; ii)  $D_2$ :  $20$  mm  $\leq D < 50$  mm; iii)  $D_3$ :  $50$  mm  $\leq D < 100$  mm; iv)  $D_4$ :  $100$  mm  $\leq D < 200$  mm; and v)  $D_5$ :  $D \geq 200$  mm. Such an analysis points out that the most used diameter range (n. 24, i.e., about 53 %) is the third one ( $D_3$ :  $50$  mm  $\leq D <$

## Chapter 2. State of the art

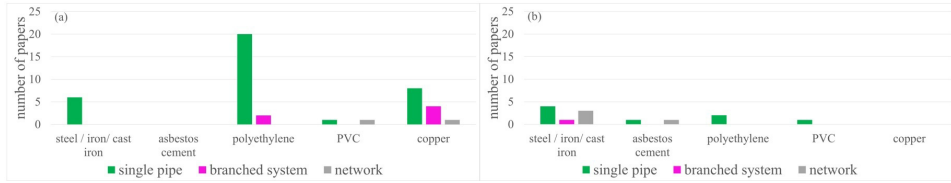


**Fig. 2.5:** Category #3: pipe material. Number of the papers for each pipe material and system layout – single pipe (SP), branched system (BS), and network (N) – for: (a) laboratory (L); and (b) field (F) tests.

100 mm). Another another range used quite frequently is the second one  $D_2$ :  $20 \text{ mm} \leq D < 50 \text{ mm}$  (n.11, i.e., about 24 %). On the contrary, the diameter ranges rarely used are:  $D_1$ :  $D < 20 \text{ mm}$ ,  $D_4$ :  $100 \text{ mm} \leq D < 200 \text{ mm}$ , and  $D_5$ :  $D \geq 200 \text{ mm}$ , with a percentage equal to 5 % (i.e., n. 2), 11 % (i.e., n. 5) and 7 % (i.e., n. 3), respectively. In terms of the number of papers (Fig. 2.6), such a result is confirmed for tests executed in the labs whereas for those executed in real systems (not shown), the most considered diameter range is the fourth one ( $D_4$ :  $100 \text{ mm} \leq D < 200 \text{ mm}$ ).

Because of the smaller number of papers, for tests executed in branched systems (BS) and networks (N), less diameter ranges have been considered. Precisely, two for the branched systems: i)  $D_6$ :  $D < 20 \text{ mm}$ , and ii)  $D_7$ :  $D \geq 20 \text{ mm}$ , and three for the networks: i)  $D_8$ :  $D < 100 \text{ mm}$ ,  $D_9$ : ii)  $100 \text{ mm} \leq D < 300 \text{ mm}$ , and iii)  $D_{10}$ :  $D \geq 300 \text{ mm}$ . For the tests executed in branched systems, the most frequent diameter range is  $D_7$ :  $D \geq 20 \text{ mm}$  (n. 4, i.e., about 57 %), whereas for those in the networks, it is  $D_9$ :  $100 \text{ mm} \leq D < 300 \text{ mm}$  (n. 3, i.e., about 43 %). The other diameter ranges for the networks have a percentage equal to about 28 % (n.2, for  $D_8$ :  $D < 100 \text{ mm}$ ) and 29 % (n. 2 for  $D_{10}$ :  $D \geq 300 \text{ mm}$ ).

The fact that in the labs small diameter pipes have been used much more frequently can be ascribed to the already mentioned lack of space. Moreover, for a given supply head, large diameters allow large values of the discharge. This implies a more powerful pumping group and a larger recycling system. For obvious reasons, experiments in the field have concerned larger diameter pipes. An option to take into account for further research is to increase the number of tests in large diameter pipes. This would allow evaluating the possible effect of the ratio between the leak effective area and the pipe cross-sectional area in the range of small values (i.e., a small leak in a large pipe, see also the below category # 8).

### Category #5: pre-transient pressure regime

Notwithstanding the mentioned problems of “extracting” pressure data when only non-dimensional graphs are presented, some useful information about the

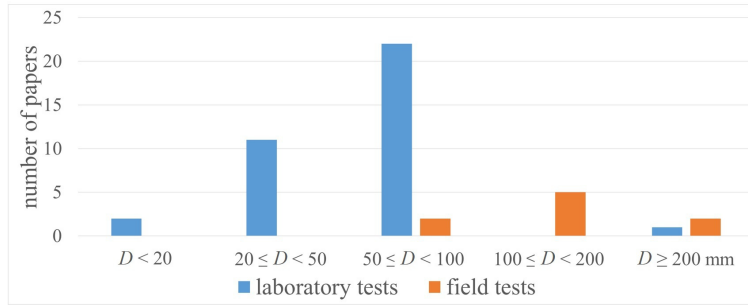


**Fig. 2.6:** Category #4: pipe diameter, laboratory and field tests executed in a single pipe (SP). Number of the papers for the five diameter ranges.

explored pre-transient pressure regimes are available in literature.

In this context, data have been divided in two groups: the single pipe and branched system data and the network ones. The reason of such a different choice is that in networks the value of the pressure may change significantly from one zone to another. This implies that in some cases a single value, representative of the whole system, is difficult to define. As a consequence, pre-transient pressure data for networks must be considered as purely indicative. For tests executed in single pipes and branched systems, five pressure ranges have been considered: i)  $h_1: h < 10$  m; ii)  $h_2: 10 \text{ m} \leq h < 20$  m; iii)  $h_3: 20 \text{ m} \leq h < 40$  m; iv)  $h_4: 40 \text{ m} \leq h < 60$  m; and v)  $h_5: h \geq 60$  m, with  $h$  being the pre-transient pressure head. As shown in Fig. 2.7a, in most cases (n. 36, i.e., about 35 %),  $h$  ranges between 10 m and 20 m ( $h_2$ ); only for few tests (n. 19, i.e., about 18 %) it is smaller than 10 m ( $h_1$ ). The other pressure ranges have a percentage equal to 20 % (n. 21 for  $h_3: 20 \text{ m} \leq h < 40$  m and  $h_4: 40 \text{ m} \leq h < 60$  m) and 7 % (n. 7 for  $h_5: h \geq 60$  m).

For tests executed in networks, four pressure ranges have been considered: i)  $h_6: h < 20$  m (n. 2, i.e., about 12 %); ii)  $h_7: 20 \text{ m} \leq h < 40$  m (n. 8, i.e., about 50 %); iii)  $h_8: 40 \text{ m} \leq h < 60$  m (n. 3, i.e., about 19 %); and iv)  $h_9: h \geq 60$  m (n. 3, i.e., about 19 %). Fig. 2.7b indicates that for most of the tests (i.e., about 50 %), the pre-transient pressure ranges between 20 m and 40 m ( $h_7$ ).

From the above description of the available data, the need for executing tests with *extreme* pre-transient pressure emerges. Precisely, it would be of interest to check the transient response for both  $h_1: h < 10$  m and  $h > 60$  m. In fact, these further experiments would allow examining in detail the role of the pre-transient pressure at the leak that, according to Liou (1998), influences the value of the leak reflection coefficient. It is worth noting that the mentioned large values of  $h$  are not typical of WDNs but they may occur in TMs, according to the orography of the area crossed by the pipeline.

## Chapter 2. State of the art

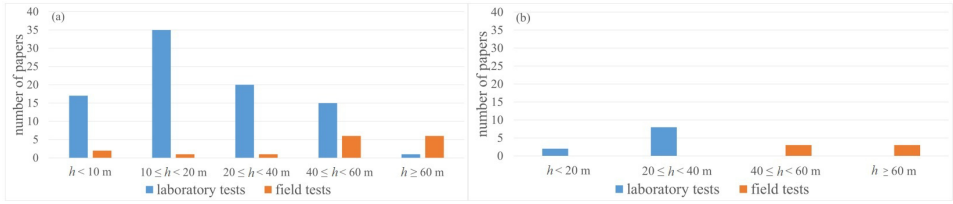


**Fig. 2.7:** Category #5: pre-transient pressure range,  $h$ . Number of the papers for: (a) single pipe and branched system, and (b) network.

### Category #6: inserted pressure wave

As mentioned, within TTBTs, the value of the inserted pressure wave,  $\Delta h$ , plays a very important role in leak detection. In fact, given all quantities, the larger  $\Delta h$ , the larger the pressure wave reflected by the leak. Accordingly, the larger  $\Delta h$  (e.g., in meters of water column), the more accurate the detection of a given leak.

For tests executed on a single pipe and branched system, the values of  $\Delta h$  have been bundled in five groups: i)  $\Delta h_1$ :  $\Delta h < 5$  m (n.15, i.e., about 19%); ii)  $\Delta h_2$ :  $5 \text{ m} \leq \Delta h < 10$  m (n.11, i.e., about 14%); iii)  $\Delta h_3$ :  $10 \text{ m} \leq \Delta h < 20$  m (n.25, i.e., about 32%); iv)  $\Delta h_4$ :  $20 \text{ m} \leq \Delta h < 30$  m (n.12, i.e., about 16%); and v)  $\Delta h_5$ :  $\Delta h \geq 30$  m (n.15, i.e., about 19%). The analysis (Fig. 2.8a) indicates that in most of the papers (i.e., about 32%), the inserted pressure wave ranges between 10 m and 20 m ( $\Delta h_3$ ).

For tests concerning networks, three ranges have been considered : i)  $\Delta h_6$ :  $\Delta h < 10$  m; ii)  $\Delta h_7$ :  $10 \text{ m} \leq \Delta h < 30$  m; and iii)  $\Delta h_8$ :  $\Delta h \geq 30$  m. In most of these tests (i.e. n.10, about 62% ),  $\Delta h$  ranges between 10 m and 30 m (Fig. 2.8b), whereas both the other two  $\Delta h$  ranges, have a percentage equal to 19%, with n. 3 tests.

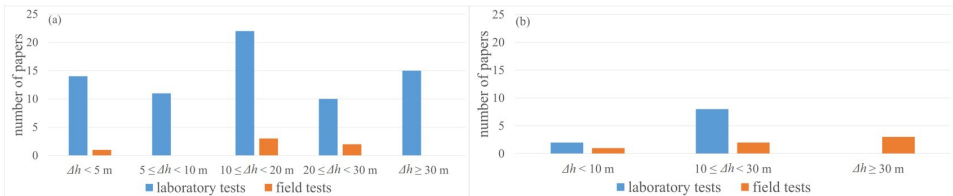


**Fig. 2.8:** Category #6: inserted pressure wave,  $\Delta h$ . Number of the papers for: (a) single pipe and branched system, and (b) network.

According to the available data, further tests should investigate the performance of transients giving rise to a very small pressure wave (i.e.,  $\Delta h$  of the order of

few meters) that are very attractive from the pipe system management point of view. In fact, they imply very safe test conditions for the investigated system and exclude the occurrence of pipe breaks. However, it is worth noting that the smaller  $\Delta h$  the higher the required quality of the measurement equipment.

### Category #7: pre-transient flow regime

The pre-transient flow regime has been characterized through the value of the Reynolds number,  $Re = \frac{VD}{\nu}$ , with  $V$  = pre-transient mean flow velocity, and  $\nu$  = kinematic viscosity. Irrespective from the system layout, tests have been divided in the following three groups: i)  $R_1$ :  $Re < 2000$  (n. 14, i.e., about 10 %); ii)  $R_2$ :  $2000 \leq Re < 8000$  (n. 13, i.e., about 9 %); and iii)  $R_3$ :  $Re \geq 8000$  (n. 113, i.e., about 81 %). The executed analysis (Fig. 2.9) indicates that most of the tests have been executed in a turbulent flow regime, whereas very few in laminar conditions. From such a result, it automatically descends that low Reynolds number pre-transient conditions should be explored more extensively. This would allow deepening the possible effects of the viscosity on the dynamics of the generated pressure waves in terms, as an example, of their damping while travelling along the test pipe (Martins et al., 2017; Martins et al., 2018). Moreover, since small values of the pre-transient  $Re$  usually imply small values of  $V$  and then of  $\Delta h$ , such a feature reconnects to the mentioned need of further tests with small values of the inserted pressure wave.

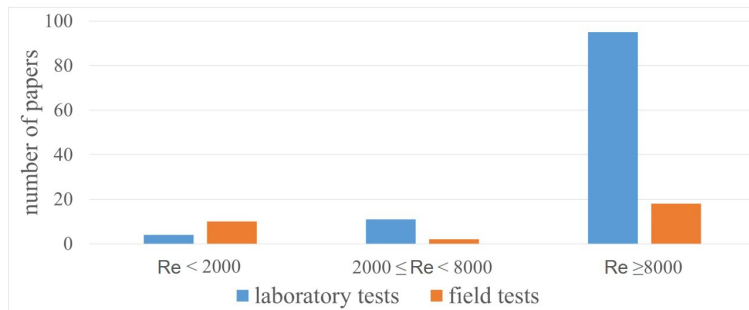


**Fig. 2.9:** Category #7: pre-transient flow regime. Number of the papers for the identified ranges of the Reynolds number,  $Re$ , for all the considered system layouts.

### Category #8: leak simulation

In this section, the expression *leak simulation* concerns both the characteristics of the device simulating the leak and its size.

The first result of the analysis indicates that the 95 % of the executed tests concerned a pipe with one leak, in seven cases there were two leaks whereas in

one case there were three leaks. Moreover, it is worth of noting that tests with multiple leaks have been executed only in labs.

In the 45 % of the tests, the leak has been simulated by means of a fixed orifice, in the 13 % and 35 % by means of a short pipe and a valve, respectively; only in the 7 % real leaks have been considered. With regard to the condition downstream of the leak, only in the 15 % of the tests, the leak is submerged.

With respect to the size, leaks are characterized on the basis of the value of the following quantities: i) leak effective area,  $C_{sv}A_L$ , ii) percentage of lost discharge,  $q/Q_{in}$ , and iii) leak percentage area,  $A_L/A$ ; with  $C_{sv}$  = leak coefficient of discharge,  $A_L$  = leak area,  $A$  = pipe cross-section area,  $q$  = discharge through the leak, and  $Q_{in}$  = discharge in the pipe upstream of the leak. In the below statistics, attention has been focused on tests executed on pipes with one leak; in case more than one quantity has been given to quantify leak size, the leak effective area has been chosen as a reference quantity.

With regard to the tests executed in the labs on a pipe with one leak, in terms of the leak effective area,  $C_{sv}A_L$ , papers have been grouped by considering the following four ranges: i)  $L_1$ :  $C_{sv}A_L < 5 \cdot 10^{-7} \text{ m}^2$ ; ii)  $L_2$ :  $5 \cdot 10^{-7} \text{ m}^2 \leq C_{sv}A_L < 5 \cdot 10^{-6} \text{ m}^2$ ; iii)  $L_3$ :  $5 \cdot 10^{-6} \text{ m}^2 \leq C_{sv}A_L < 5 \cdot 10^{-5} \text{ m}^2$ ; and iv)  $L_4$ :  $C_{sv}A_L \geq 5 \cdot 10^{-5} \text{ m}^2$  (Fig. 2.10 a).

For papers where leak size has been characterized by means of the percentage lost discharge,  $q/Q_{in}$ , the following five ranges have been considered: i)  $L_5$ :  $q/Q_{in} < 5 \%$ ; ii)  $L_6$ :  $5 \% \leq q/Q_{in} < 10 \%$ ; iii)  $L_7$ :  $10 \% \leq q/Q_{in} < 20 \%$ ; iv)  $L_8$ :  $20 \% \leq q/Q_{in} < 30 \%$ ; and v)  $L_9$ :  $q/Q_{in} \geq 30 \%$  (Fig. 2.10 b).

Finally, with regard to the leak percentage area,  $A_L/A$ , papers have been ascribed to the following three ranges: i)  $L_{10}$ :  $A_L/A < 5 \%$ ; ii)  $L_{11}$ :  $5 \% \leq A_L/A < 10 \%$ , and iii)  $L_{12}$ :  $A_L/A \geq 10 \%$  (Fig. 2.10 c).

According to the above graphs, it results that in most cases  $C_{sv}A_L$  is larger than  $5 \cdot 10^{-5} \text{ m}^2$ ,  $q/Q_{in}$  ranges between 10 % and 20 %, and  $A_L/A < 5 \%$ .

With regard to tests on a pipe with more than one leak,  $C_{sv}A_L$  ranged between  $5 \cdot 10^{-7} \text{ m}^2$  and  $5 \cdot 10^{-5} \text{ m}^2$ , whereas  $A_L/A$  was smaller than 5 %.

With regard to the field tests, less information are available. Precisely, nine tests concern a leaky pipe with  $C_{sv}A_L < 1 \cdot 10^{-4} \text{ m}^2$  ( $L_{13}$ ); in terms of  $q$ , in ten tests it was  $q < 0.50 \text{ L/s}$  ( $L_{14}$ ), whereas in two it was  $q \geq 0.50 \text{ L/s}$  ( $L_{15}$ ); finally, for one test a leak with  $A_L/A = 40 \%$  ( $L_{16}$ ) was considered.

In terms of leak simulation, future research could address the *extreme* value of the leak size, however it is characterised. In fact, very small leaks point out the accuracy of the method whereas very large leaks may change totally the transient response of the system with respect to the leak-free one. It is obvious that tests on pipes with multiple leaks would be very welcome.

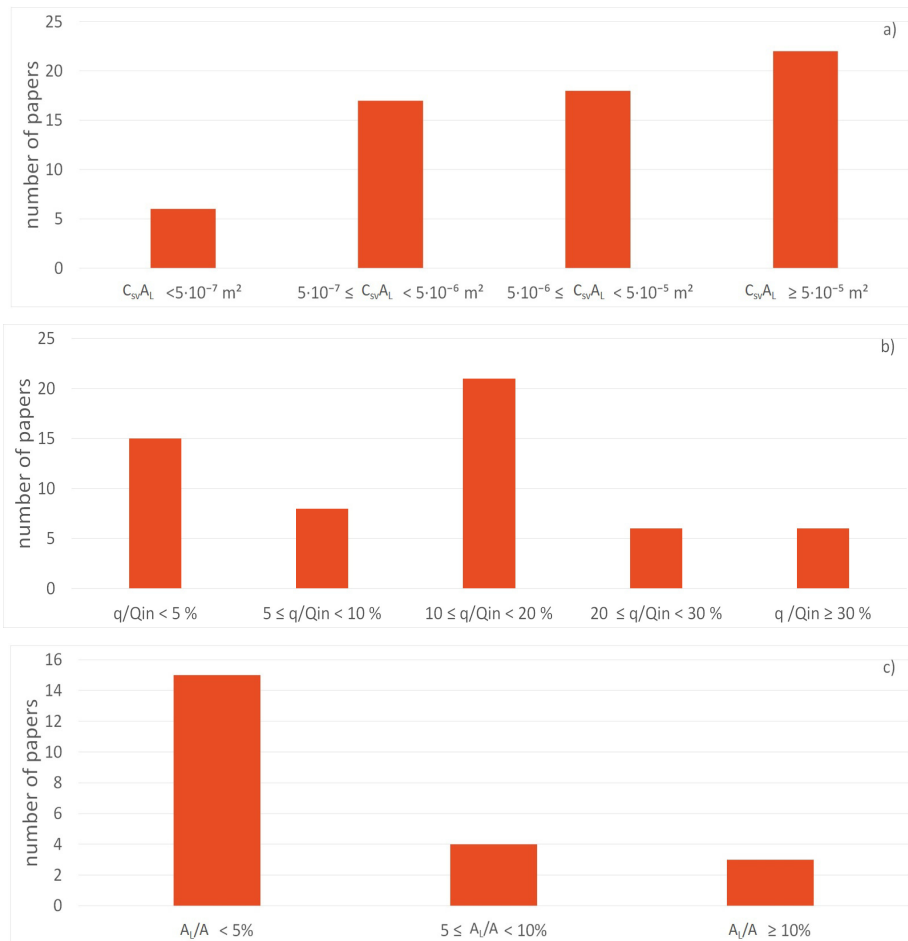


**Fig. 2.10:** Category #8: leak simulation. Number of the papers for laboratory systems with one leak for ranges of: leak effective area,  $C_{sv}A_L$ ; b) percentage lost discharge,  $q/Q_{in}$ ; and c) leak percentage area,  $A_L/A$ .

### 2.3.3. Conclusions

Since the 1990s, transients test-based techniques gained attention of technicians as a viable tool for fault (e.g., leak) detection in pressurised pipes. However, a systematic analysis of the results obtained both in laboratories and real systems has not been offered yet in literature. The intention of this work was to fill this gap in two ways: the first by presenting in an organic manner the experimental results from selected papers, the second by identifying desirable developments of future research.

With this aim, tests have been grouped by considering eight categories: complexity of the test system (layout), modality of transient generation, pipe material, pipe diameter, pre-transient pressure and flow condition, inserted pressure wave, and leak characteristics; moreover, each category has been divided in several sub-categories (Table 2.2). For each category, the main characteristics of the relevant tests have been discussed, as well as the possible specific issues to address for future research have been proposed. For the sake of clarity, such issues are synthesised in Table 2.4.

**Table 2.4:** Characteristics of future tests for each category to improve the knowledge about the transient response of leaky pipes.

Category (#)	Title	Future tests should concern
1	complexity of the test system	branched and looped systems, real systems
2	modality of transient generation	innovative devices for generating transients
3	pipe material	steel/iron/cast iron and PVC pipes
4	pipe diameter	large diameters ( $D > 500$ mm)
5	pre-transient pressure regime	small ( $h < 10$ m) and large ( $90$ m $\leq h < 100$ m) pressures
6	inserted pressure wave	$\Delta h$ of the order of few meters
7	pre-transient flow regime	laminar regime
8	leak simulation	<i>extreme</i> leak sizes; multiple leaks

To conclude, three general issues are worthy of the research community's attention.

The first issue concerns the great need of executing tests in real systems where the uncertainty about the boundary conditions plays a key role in the analysis of the results of the transient tests.

The second issue is about the need for a stable over time large experimental setup with large diameter and very long pipes where to test also hybrid systems

## Chapter 2. State of the art

(i.e., with different pipe materials) and looped systems. Something quite close to this idea has been active for some years at the Imperial College (Covas and Ramos, 2010), but with no loops.

The third issue concerns the creation of a global database as a repository of all the available experimental data. Such a project, that could be funded by water utilities, is fully in line with the new policy of almost all international Journals, requiring the availability of the used experimental data. Moreover, such an initiative would bridge the gap between the community of the researchers in the field of the pressurised pipe system management and the other research communities in terms of the methodologies for sharing the available experimental results (see, as an example, the Copernicus European Union's Earth observation programme).

### 2.4. Transient Test-Based Techniques for partial blockages detection

This section corresponds to the following research paper:

Brunone, B.; **Maietta F.**; Capponi, C.; Duan, H.-F.; Meniconi, S. Detection of Partial Blockages in Pressurized Pipes by Transient Tests: A Review of the Physical Experiments. *Fluids* 2023, 8, 19.

<https://doi.org/10.3390/fluids8010019>

#### 2.4.1. Introduction

Faults in pressurized pipe systems may affect several features, resulting in different consequences in terms of functioning conditions. Leaks, as an example, imply not only resource loss but also energy waste. The corrosion of the pipe's internal wall, as a second example, not only reduces the mechanical strength, but also facilitates biological processes at the wall that, for water pipes, may compromise potability. Moreover, over time, corrosion has external evidence, since it can lead to leakage. However, maybe the most insidious fault to detect and manage is the partial obstruction, the technical term for which is a "partial blockage"—hereafter referred to as a PB—which does not provide any external evidence. Indirect "symptoms" of a PB are a decrease in carrying capacity and pressure rise. However, such symptoms do not allow localizing nor viably characterizing PB by means of, as an example, steady-state measurements. In the case of water, PBs may result from the deposition of sand and excess calcium and hydrates, whereas in pipes carrying refined and crude oil, paraffins and asphaltene may obstruct the cross-section. Moreover, in the subsea pipelines, wax particles in the oil may crystallize and deposit on the inner surface because of the cold temperature (Alnaimat and Ziauddin, 2020). Plaques and clots behave as PBs in the venous and arterial systems. In all cases, "natural" PBs start from small growths in the roughness of inner pipe walls, and if not detected early, protrude transversely (in many cases, radially and then with a circumferential shape) and longitudinally, occluding progressively the internal pipe cross-sectional area (Duan et al., 2015). A PB can be also assimilated by an in-line valve negligently set as partially closed.

In liquid-filled pipelines, on which attention is focused in this chapter section, several methods have been proposed for detecting PBs (an early detection is the best action!): vibration analysis (Lile et al., 2012), pulse echo methodology (Duan et al., 2015), acoustic reflectometry (Papadopoulou et al., 2008), steady-state (Yang et al., 2019) and unsteady-state (Meniconi et al., 2011a; Duan et al., 2014; Louati et al., 2017) pressure measurements. An analysis of the characteristics of these methods, as previously explained, is beyond the scope of this work where attention is focused on the methods using unsteady-state pressure measurements – the so called transient test-based techniques

(TTBTs) – and, specifically, on the review of the available physical experimental data. The main reasons for such a choice is that the technicians responsible for large and long pipelines (i.e., those conveying water and oil) must be able to execute the diagnosis of the system whenever they need it to assure continuity and efficiency of service. Indeed, this is the case of TTBTs that are based on the clear properties of the pressure waves propagating in a pressurized pipe (see the next section) and do not need nor using an extremely sophisticated equipment nor the presence of external personnel.

As in Brunone et al. (2022), rational criteria for selecting the papers have been preliminary identified. Specifically, reasons for exclusion are:

- conference papers, research reports and PhD theses (in most cases, they include preliminary results with the complete series of data published in successive Journal papers);
- only experiments on “rigid” PBs are considered, with the consequent exclusion of tests where PB is due to an air pocket;
- papers where not complete information are provided about the experimental layout, modality of transient generation, and PB simulation.

With regard to such a last feature, an exception is made for the paper by Contractor (1965), a sort of milestone in the field, where regrettably very few information are given about the carried out experiments. As a result, 18 papers have been selected, published between 1965 and 2020.

The time-history of the published papers is reported in Fig. 2.11. Such a figure anticipates one of the results of this review: very few experimental papers deal with PB detection by means of transient tests with respect to those concerning leak detection (Brunone et al., 2022). In such a bleak scenario, the long gap between 1965 and 2005 (40 years!) with no contribution must be noticed as well as 2013 as a standing out year with four papers. For the sake of clearness and to make the paper easy to read, selected papers have been grouped into six categories, each of them labelled by a progressive number (Table 2.5). For some categories, sub-categories have been identified. For category “# 6 - PB simulation”, as an example, four subcategories have been considered: in-line valve, orifice, small bore pipe, and “other types”. Moreover, to make clear the classification criterion, it is worthy of pointing out that if, as an example, in a paper two different devices have been used for simulating a PB, such a paper is included in both the related two sub-categories. In Table 2.6, all the selected papers are listed with their main characteristics indicated according to the identified categories. Finally, in Table 2.7 the meaning of the abbreviations used in Table 2.6 is given.

According to the aims of this work, in section 2.4.2 the mechanisms of interaction between a pressure wave and a PB are synthesized. Each sub-section

## Chapter 2. State of the art

of section 2.4.3 concerns one of the above mentioned categories and includes a description of the main features, critical issues, and possible objectives for future research. In the Gaps of knowledge, some general comments on the literature review and hopes for the scientific community of the field are reported.

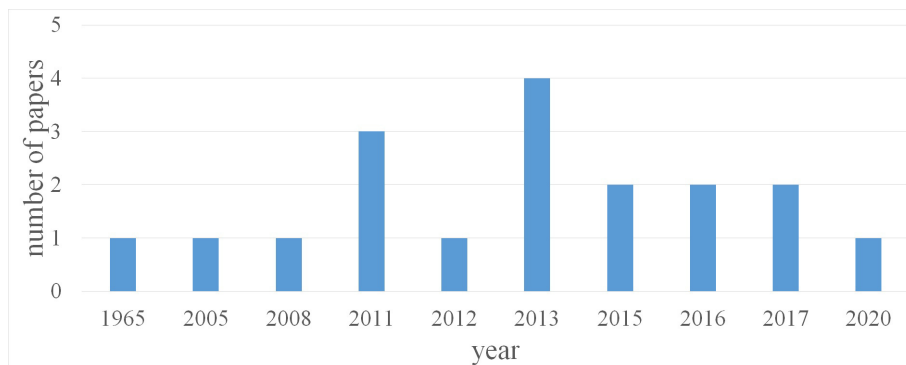


**Fig. 2.11:** Number of papers per year with physical experiments for partial blockage (PB) detection by transient tests.

**Table 2.5:** Categories identified for the analysis of the physical experimental tests.

Category (#)	Title
1	complexity of layout and modality of transient generation (CLM)
2	pipe material
3	pipe diameter
4	pre-transient pressure and flow regime
5	inserted pressure wave
6	partial blockage simulation

## Chapter 2. State of the art

**Table 2.6:** Selected papers with the main characteristics of the executed physical experimental tests.

Paper number	CLM	Mat.	$D$	$h$	$Re$	$\Delta h$	Type	Size	$L_b$	$\Delta t_b$
Contractor (1965)	L, SP, VC	-	-	$h_1,$ $h_3$	$Re_1,$ $Re_3$	$\Delta h_3,$ $\Delta h_4$	O	-	-	-
Duan et al. (2013)	L, SP, VC	Fe	$D_2$	-	$Re_1,$ $Re_3$	-	SBP	$B_1$	from 6.06 to 12.07	-
Duan et al. (2017)	L, SP, VC	Fe	$D_2$	-	$Re_2,$ $Re_3$	-	SBP	$B_1$	5.59	0.0085
	L, SP, VC	Fe	$D_2$	-	$Re_2,$ $Re_3$	-	OT	$B_3$	5.54, 5.59	0.0106, 0.0110
Lee et al. (2015)	L, SP, VC	Fe	$D_2$	-	$Re_2$	-	SBP	$B_1$	12.2480	0.0181
Louati et al. (2017)	L, SP, PPWM	PE	$D_2$	$h_2$	$Re_0$	$\Delta h_1$	SBP	$B_1$	3.6, 24	0.0185, 0.1234
Massari et al. (2015)	L, SP, VC	PE	$D_2$	$h_2$	$Re_3$	$\Delta h_3$	SBP	$B_1$	3.56	0.0180
Meniconi et al. (2011a)	L, SP, VC	PE	$D_2$	$h_2$	$Re_3$	$\Delta h_3,$ $\Delta h_4$	IV	$B_1$	-	-
	L, SP, VC	PE	$D_2$	$h_2$	$Re_3$	$\Delta h_4$	O	$B_1$	-	-
Meniconi et al. (2011b)	F, BS, VC	Fe	$D_3$	$h_2$	$Re_3$	$\Delta h_5$	IV	-	-	-
Meniconi et al. (2011c)	L, SP, PPWM	PE	$D_2$	$h_2$	$Re_0$	$\Delta h_1$	SBP	$B_1$	7.06	0.036
	L, SP, PPWM	PE	$D_2$	$h_2$	$Re_0$	$\Delta h_1$	IV	-	-	-
Meniconi et al. (2012a)	L, SP, VC	PE	$D_2$	$h_2$	$Re_3$	$\Delta h_3$	SBP	$B_1$	from 0.06 to 100	from 0.0003 to 0.5141

## Chapter 2. State of the art

Meniconi et al. (2013b)	L, SP, VC	Fe	$D_2$	-	$Re_1$	$\Delta h_1$	SBP	$B_1$	from 6.06 to 12.07	from 0.088 to 0.0176
Meniconi et al. (2016)	L, SP, VC	PE	$D_2$	$h_2$	$Re_3$	$\Delta h_3,$ $\Delta h_5$	IV	$B_2$	-	-
	L, SP, VC	PE	$D_2$	$h_2$	$Re_3$	$\Delta h_3,$ $\Delta h_5$	SBP	$B_1$	0.48	0.0025
	L, SP, VC	PE	$D_2$	$h_2$	$Re_3$	$\Delta h_3,$ $\Delta h_5$	OT	$B_1$	0.12, 0.48	0.0006, 0.0025
Sattar et al. (2008)	L, SP, OM	Cu	$D_1$	-	$Re_3$	-	-	$B_4$	-	-
Sun et al. (2016)	L, SP, VC	Fe	$D_1$	$h_1$	$Re_2,$ $Re_3$	$\Delta h_5$	SBP	$B_2$	5	-
Tuck and Lee (2013)	L, SP, VC	Fe	$D_2$	$h_2$	$Re_2$	$\Delta h_2$	SBP	$B_4$	10.4070	0.0158
Tuck et al. (2013)	L, SP, VC	Fe	$D_2$	-	$Re_2,$ $Re_3$	-	SBP	$B_1,$ $B_2$	from 2.866 to 12.0680	from 0.0045 to 0.0176
Wang et al. (2005)	L, SP, VC	-	$D_1$	-	$Re_2$	-	IV	-	-	-
Zouari et al. (2020)	L, SP, PPWM	PE	$D_2$	$h_2$	$Re_0$	$\Delta h_3,$ $\Delta h_4$	SBP	$B_1,$ $B_3$	24	0.1206, 0.1234
	L, SP, VC	PE	$D_2$	$h_2$	$Re_3$	$\Delta h_3$	SBP	$B_1,$ $B_3$	24	0.1206, 0.1234

**Table 2.7:** Meaning of the abbreviations used in Table 2.6.

Category #1: CLM	
Complexity of the functioning conditions	Symbol
Laboratory tests	$L$
Field tests	$F$
Complexity of the test system	Symbol
Single pipes	$SP$

## Chapter 2. State of the art

Branched systems	<i>BS</i>
<b>Modality of transient generation</b>	<b>Symbol</b>
Valve closure	<i>VC</i>
Portable Pressure Wave Maker or Other Maneuver	<i>PPWM/OM</i>
<b>Category #2: material (Mat.)</b>	
<b>Type</b>	<b>Symbol</b>
Steel - Cast iron	<i>Fe</i>
Copper	<i>Cu</i>
Polyethylene	<i>PE</i>
<b>Category #3: pipe diameter (<i>D</i>)</b>	
<b>Symbol</b>	<b>Range [mm]</b>
<i>D</i> <sub>1</sub>	$20 \leq D < 50$
<i>D</i> <sub>2</sub>	$50 \leq D < 100$
<i>D</i> <sub>3</sub>	$D \geq 100$
<b>Category #4: pre-transient pressure (<i>h</i>) and flow regime (<i>Re</i> number)</b>	
<b>Symbol</b>	<b>Range [m]</b>
<i>h</i> <sub>1</sub>	$h < 20$
<i>h</i> <sub>2</sub>	$20 \leq h < 50$
<i>h</i> <sub>3</sub>	$h \geq 50$
<b>Symbol</b>	<b>Range [-]</b>
<i>Re</i> <sub>0</sub>	$Re = 0$
<i>Re</i> <sub>1</sub>	$Re < 2000$
<i>Re</i> <sub>2</sub>	$2000 \leq Re < 8000$
<i>Re</i> <sub>3</sub>	$Re \geq 8000$
<b>Category #5: inserted pressure wave (<math>\Delta h</math>)</b>	
<b>Symbol</b>	<b>Range [m]</b>
$\Delta h$ <sub>1</sub>	$\Delta h < 5$
$\Delta h$ <sub>2</sub>	$5 \leq \Delta h < 10$
$\Delta h$ <sub>3</sub>	$10 \leq \Delta h < 20$
$\Delta h$ <sub>4</sub>	$20 \leq \Delta h < 50$
$\Delta h$ <sub>5</sub>	$\Delta h \geq 50$
<b>Category #6: partial blockage simulation</b>	
<b>Partial blockage type</b>	
<b>Type</b>	<b>Symbol</b>
In-line Valve	<i>IV</i>
Orifice	<i>O</i>
Other type	<i>OT</i>
Small Bore Pipe	<i>SBP</i>
<b>Partial blockage size</b>	
<b>Symbol</b>	<b>Range [%]</b>
<i>B</i> <sub>1</sub>	$B < 25$
<i>B</i> <sub>2</sub>	$25 \leq B < 50$
<i>B</i> <sub>3</sub>	$50 \leq B < 75$
<i>B</i> <sub>4</sub>	$B \geq 75$

**Partial blockage extension (only for SBP and OT)**

**Length,  $L_b$  [m]**

**Characteristic time,  $\Delta t_b = 2L_b/a_b$  [s]**

### 2.4.2. Interaction between pressure waves and partial blockage

In one-dimensional flow in pressurized pipes – with the conduit wall and the fluid being linearly elastic – for the case of slightly compressible fluids and low velocities, the continuity equation can be written as

$$\frac{\partial h}{\partial s} + \frac{1}{g} \frac{\partial V}{\partial t} = 0 \quad (2.1)$$

and, if the friction term is neglected, the equation of motion is:

$$\frac{g}{a^2} \frac{\partial h}{\partial t} + \frac{\partial V}{\partial s} = 0 \quad (2.2)$$

where  $h$  = piezometric head,  $g$  = gravity acceleration,  $V$  = mean flow velocity,  $a$  = pressure wave speed,  $t$  = time, and  $s$  = spatial co-ordinate (Wylie and Streeter, 1993; Swaffield and Boldy, 1993).

The D'Alembert general solution of Eqs. (2.1) and (2.2) is given by:

$$h - h_0 = F\left(t + \frac{s}{a}\right) + f\left(t - \frac{s}{a}\right) \quad (2.3)$$

$$V - V_0 = -\frac{g}{a} \left[ F\left(t + \frac{s}{a}\right) - f\left(t - \frac{s}{a}\right) \right] \quad (2.4)$$

where the arbitrary functions  $F\left(t + \frac{s}{a}\right)$  and  $f\left(t - \frac{s}{a}\right)$  may be interpreted as a pressure wave (in meters of fluid column) propagating in the  $-s$  and  $+s$  direction, respectively. In Eqs. (2.3) and (2.4), the subscript 0 and  $+s$  indicate the pre-transient values and flow direction, respectively. These equations describe the transient where  $F\left(t + \frac{s}{a}\right)$  is the generated pressure wave, whereas  $f\left(t - \frac{s}{a}\right)$  is the reflected one due to a change in the boundary condition, as illustrated later in this section. For the sake of simplicity, hereafter  $F\left(t + \frac{s}{a}\right)$  and  $f\left(t - \frac{s}{a}\right)$  are indicated as  $F_i$  and  $f_i$ , respectively, with the subscript referring to the part of the pipe where these pressure waves happen. It is worth noting that the frictionless hypothesis implies that the solution given by Eqs. (2.3) and (2.4) provides reliable results only in the first phases of the transients (e.g., Pezzinga et al., 2014), precisely those considered in this paper.

With the aim of highlighting clearly the basic principles of TTBTs, below the “genesis” of the reflected pressure wave,  $f_i$ , is discussed for the specific case of PBs. Precisely, it is discussed the interaction of the incoming pressure wave,  $F_i$ , with boundaries, i.e. with “something” different in terms of geometry or flow condition with respect to the pipe with uniform characteristics in which

$F_i$  is propagating. In such a context, notwithstanding the considered analytical approach can be found in several textbooks and papers (e.g., Wylie and Streeter, 1993; Swaffield and Boldy, 1993; Contractor, 1965) it is presented here in a unitary form. As a confirmation of the obtained relationships providing  $f_i$ , a comparison with physical experimental results is offered. This also allows pointing out the difference between “discrete” and “extended” PBs. Such a distinction can be based on their transient response. If a single reflected pressure wave characterizes the pressure time history at the measurement section – or, if the maneuver is not instantaneous, a single train of reflected pressure waves – this is the case of “discrete” PBs. On the contrary, if several reflected pressure waves – or several trains of pressure waves – are identified, this is the case of “extended” PBs. It is worth noting that in capturing the pressure waves generated by the PB, for given pipe characteristics, the value of the sampling frequency at the measurement section plays a crucial role. Accordingly, two cases are examined below: the in-line orifice (Figs. 2.12) and small bore pipe (SBP) (Fig. 2.13), as examples of “discrete” and “extended” PBs, respectively (the subscript  $b$  refers quantities to the PB).

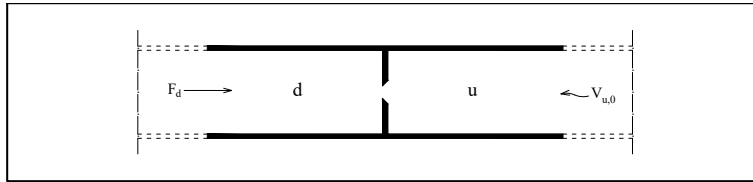


Fig. 2.12: Sketch of discrete partial blockage: in-line orifice.

For an in-line orifice (Fig. 2.12), diameter reduction (Fig. 2.13b), and expansion (Fig. 2.13c), it can be written:

$$h_{d,t} - h_{d,0} = F_d + f_d$$

$$h_{u,t} - h_{u,0} = F_u$$

since no reflected wave  $f_u$  is generated yet (the subscripts  $u$  and  $d$  indicate the upstream and downstream branch, respectively), and

$$V_{d,t} - V_{d,0} = -\frac{g}{a} (F_d - f_d)$$

$$V_{u,t} - V_{u,0} = -\frac{g}{a} F_u$$

For the in-line orifice, which behaves as a partially closed in-line valve for a given opening degree, a minor loss occurs Contractor (1965):

$$h_{u,0} - h_{d,0} = \zeta_0$$

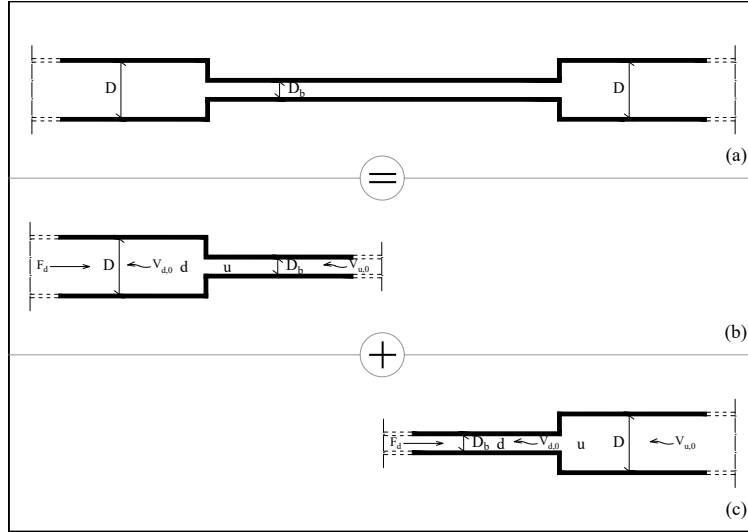


**Fig. 2.13:** Sketch of extended partial blockage: a) small bore pipe (SBP), as an ideal sum of b) diameter reduction (shrinkage), and c) diameter increase (expansion).

and

$$h_{u,t} - h_{d,t} = \zeta_t$$

Moreover, as it is  $A_d = A_u$ , and there is no storage in the orifice, it is  $V_{d,0} = V_{u,0}$  and  $V_{d,t} = V_{u,t}$ . Assuming that the velocity behind  $F_d$  is zero or very nearly zero ( $\zeta_t = 0$ ), as in the case when the incoming  $F_d$  is generated by a complete closure, the pressure wave reflected by the orifice is given by

$$f_d = \frac{1}{2} \zeta_0 \quad (2.5)$$

According to Eq.(2.5), an in-line orifice, and then a partially closed in-line valve, generates a positive reflected pressure wave. Such a feature is confirmed by the pressure signal reported in Fig. 2.14b where  $y_{PB}$  characterizes the transient response of the PB at the measurement section M. The shape of the pressure rise due to the arrival of the reflected pressure wave is linked to one of the maneuver generating the incoming pressure wave. Precisely, an instantaneous (or nearly instantaneous) maneuver generates a single wave, whereas a maneuver with a given duration gives rise to a train of pressure waves.

A junction between two pipes (Ayed et al., 2023), where the diameter decreases ( $D_b \downarrow D$ ) in the direction of the  $F_d$  propagation (case of shrinkage - Fig. 2.13b), behaves as the downstream part of a small bore pipe simulating an extended PB. Assuming that the two pipes have the same Young's modulus and neglecting the effect on the pressure wave speed of the deposited material that reduces

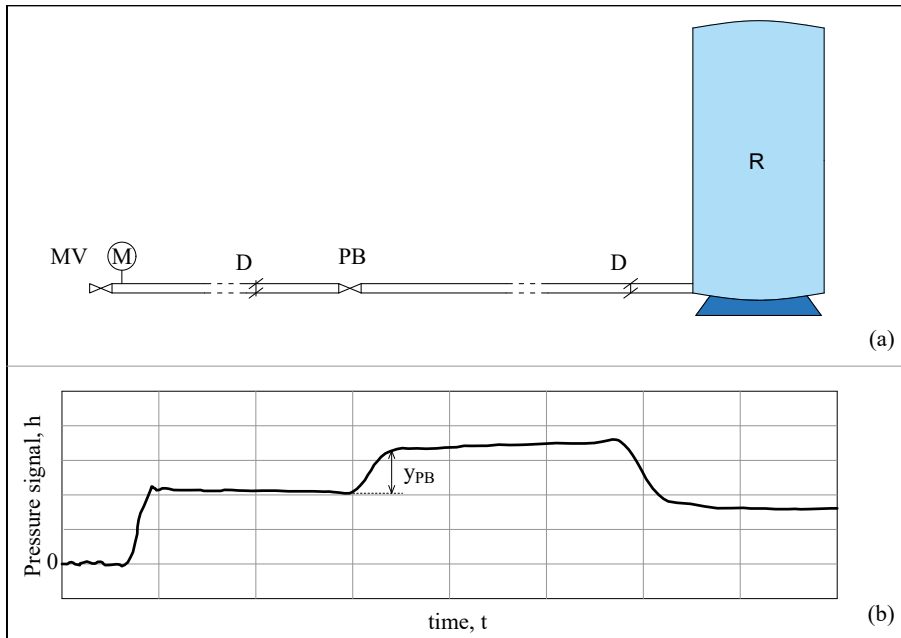


**Fig. 2.14:** Partially closed in-line valve simulating a discrete partial blockage: a) sketch of the experimental setup at the Water Engineering Laboratory (WEL) of the University of Perugia, Italy (MV = maneuver valve, M = measurement section, PB = (discrete) partial blockage, R = reservoir), and b) pressure signal during the transient generated by the complete closure of MV (modified from Meniconi et al. (2016)).]

## Chapter 2. State of the art

the diameter to  $D_b$ , it can be assumed  $a = a_b$ . At the junction, continuity of flow and commonality of the piezometric head (if the local loss is neglected) allow writing:

$$F_d + f_d = F_u$$

$$A(F_d - f_d) = A_b F_u$$

As a consequence, the reflection coefficient,  $C'_{R_J}$ , defined as the ratio between the reflected,  $f_d$ , and incoming,  $F_d$ , pressure wave, is given by the following relationship:

$$C'_{R_J} = \frac{f_d}{F_d} = \frac{A - A_b}{A + A_b} \quad (2.6)$$

According to Eq. (2.6), a junction with a diameter decreasing in the direction of the generated pressure wave is characterized by a positive reflection coefficient. On the contrary, for the case of a junction with the diameter increasing in the direction of the  $F_d$  propagation (case of expansion - Fig. 2.13c), following a procedure similar to that for Eq. (2.6), the following expression is obtained for the reflection coefficient:

$$C''_{R_J} = \frac{A_b - A}{A + A_b} \quad (2.7)$$

Then, a junction with a diameter increasing in the direction of the generated pressure wave is characterized by a negative reflection coefficient.

As a consequence, in a small bore pipe, the mechanisms of interaction synthesized by Eqs. (2.6) and (2.7) give rise to a bell-shaped feature, linked to  $L_b$ , in the pressure signal. Precisely, firstly a pressure rise happens due to shrinkage, and then the expansion gives rise to a pressure decrease. Such a feature is confirmed by the experimental pressure signal reported in Fig. 2.15b where  $y_{PB}$  is the maximum value in the pressure signal due to the PB at the measurement section M.

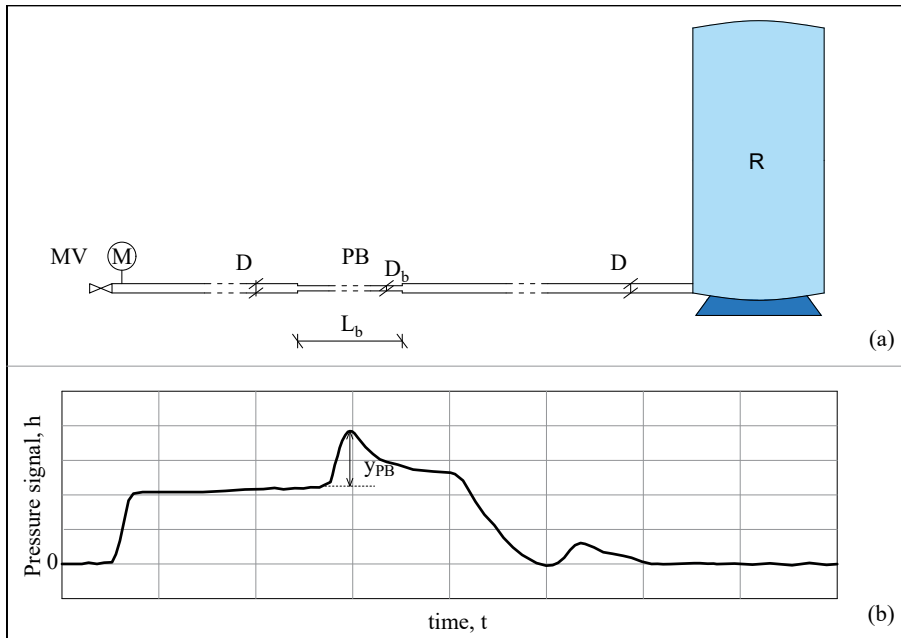


**Fig. 2.15:** Small bore pipe simulating an extended partial blockage: a) sketch of the experimental setup at the Water Engineering Laboratory (WEL) of the University of Perugia, Italy (MV = maneuver valve, M = measurement section, PB = (extended) partial blockage, R = reservoir), b) pressure signal during the transient generated by the complete closure of MV (modified from Meniconi et al. (2012a)).

### 2.4.3. Laboratory and field tests

As anticipated, in this section the available physical experiments are analysed referring to the categories reported in Table 2.5.

#### Category #1: complexity of layout and modality of transient generation (CLM)

The relevance of such aspects merits a specific section even if a very narrow range of types of experimental setups has been explored. In fact, 94 % of the tests has been executed in a laboratory (L) and on a single pipe (SP). One paper (Meniconi et al., 2011b) concerns field (F) tests carried out in a branched system (BS). In most papers (n.14, equal to 78%) the valve closure (VC) has been considered, whereas in one paper (Sattar et al., 2008) a sinusoidal oscillation has been used (OM - Other Maneuver). In two papers, the pressure waves have been inserted by means of the Portable Pressure Wave Maker (PPWM) device, refined at the Water Engineering Laboratory (WEL - <http://welabpg.com>) of the University of Perugia, Italy. In one paper, transients are generated by both valve closure and PPWM (Zouari et al., 2020).

#### Category #2: pipe material

Within TTBTs, the effect of the pipe material reflects mainly in the value of the pressure wave speed,  $a$ . Such a quantity influences the value of the inserted pressure wave,  $\Delta h$ , and requirements of the data acquisition system. Precisely, the larger  $a$  (e.g., as in metallic and concrete pipes), the larger  $\Delta h$  (for a given velocity change), the larger the sampling frequency needed to capture the behavior of the traveling pressure waves. As shown in Fig. 2.16, the available experiments share almost equally between metallic (with very few tests in copper pipes) and polyethylene pipes, whereas no tests have been executed in PVC and concrete pipes. The lack of experiments with PVC pipes can be assigned to the fact that they are usually assimilated to the polyethylene ones. The lack of experiments with concrete pipes is due to the fact that almost all available tests have been executed in laboratories where concrete pipes cannot be used because their diameter is usually quite large.

#### Category #3: pipe diameter

The diameters used in laboratory and field tests have been divided in the following three ranges (Table 2.7): i)  $D_1$ :  $20 \text{ mm} \leq D < 50 \text{ mm}$ ; ii)  $D_2$ :  $50 \text{ mm} \leq D < 100 \text{ mm}$ ; and iii)  $D_3$ :  $D \geq 100 \text{ mm}$  (note that in some cases the value of the internal diameter is given whereas in some others the nominal diameter

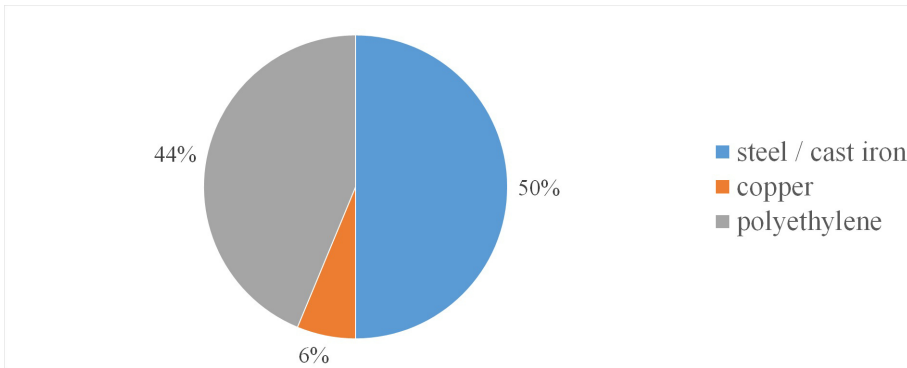


**Fig. 2.16:** Category #2: pipe material. Percentage of the papers in terms of pipe material: steel/cast iron (Fe), polyethylene (PE), and copper (Cu).

is provided). Fig. 2.17, where the percentage of such ranges are reported, indicates that most tests (76 %) have concerned the  $D_2$  range. As for the pipe material, the lack of tests in large diameter pipes is due to the fact that very few tests have been executed in real systems. Moreover, the use of large diameter pipes implies large values of the discharge, a feature quite difficult to achieve in the laboratories.

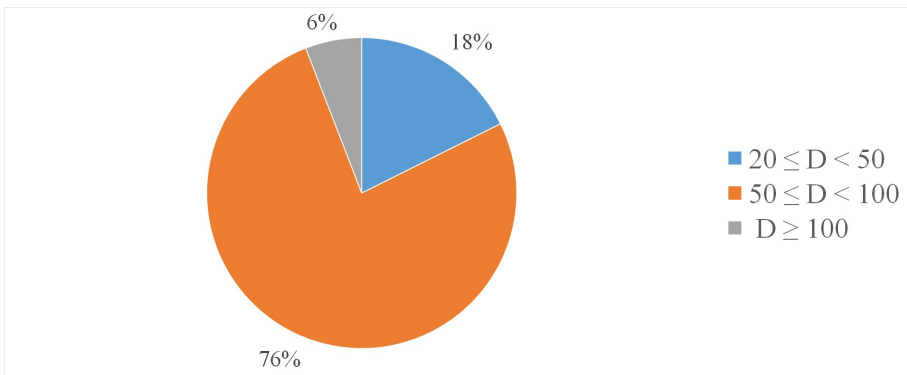


**Fig. 2.17:** Category #3: pipe diameter. Percentage of the papers for the three diameter ranges.

#### Category #4: pre-transient pressure and flow regime

According to the executed tests, four pressure ranges have been considered (Table 2.7). Most of tests (82 %) have been carried out in the range  $h_2$  ( $20 \text{ m} \leq h < 50 \text{ m}$ ); much less (12 %) in the range  $h_1$  ( $h < 20 \text{ m}$ ) and very few (6 %) in the  $h_3$  ( $h \geq 50 \text{ m}$ ) one. For eight tests, the pre-transient pressure is not

reported (the main reason is that only dimensionless plots are included).

The value of the Reynolds number,  $Re = \frac{V_0 D}{\nu}$ , with  $\nu =$  kinematic viscosity, characterizes the pre-transient flow conditions. The available tests have been divided in the following four groups: i)  $Re_0$ :  $Re = 0$ ; ii)  $Re_1$ :  $0 < Re < 2000$ ; iii)  $Re_2$ :  $2000 \leq Re < 8000$ ; and iv)  $Re_3$ :  $Re \geq 8000$ . The related percentages, reported in Fig. 2.18, indicate that most tests (50 %) have been carried out in turbulent conditions; in tests with  $Re = 0$  the PPWM has been used. According to Brunone et al. (2021), where it is shown that the smaller  $Re$  the more stable the pressure signal and then the easier the detection of the pressure waves reflected by any fault, it is of interest to execute further tests in laminar conditions. Moreover, to identify the possible mechanisms of interaction with the pressure waves, the characteristics in such conditions of the flow field around a PB – particularly downstream of it – must be investigated by means of appropriate tools (e.g., three-dimensional Computational Fluid Dynamics (CFD) models (Yang et al., 2019; Martins et al., 2021)).

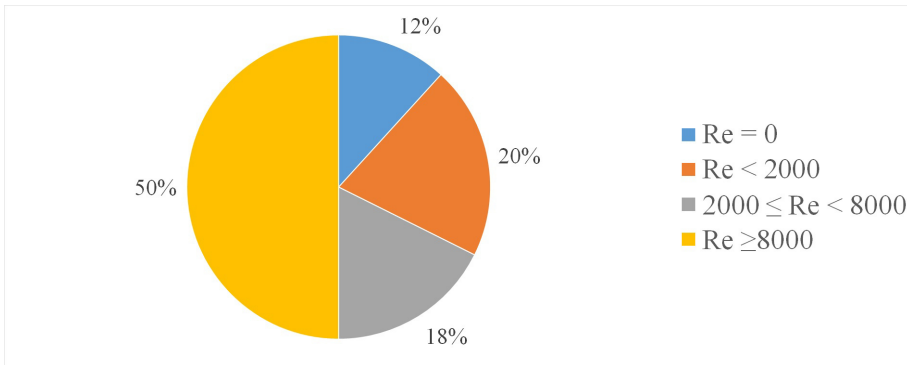


**Fig. 2.18:** Category #4: pre-transient Reynolds number,  $Re$ . Percentage of the papers for the four ranges.

### Category #5: inserted pressure wave

Within TTBTs it is quite evident that the larger the inserted pressure wave,  $\Delta h$ , the more effective the fault detection. In other words, the larger  $\Delta h$ , the smaller the minimum detectable fault and/or the larger the number of detectable faults for given pipe system characteristics and measurement section. However, since TTBTs stand for being an “on demand” procedure (i.e., whenever a fault is suspected, transient tests are executed), small  $\Delta h$  should be inserted to avoid fatigue phenomena. As a consequence, the value of  $\Delta h$  is the result of a series of compromises. In line with this consideration (Fig. 2.19), for most the available tests it is  $\Delta h < 20$  m.

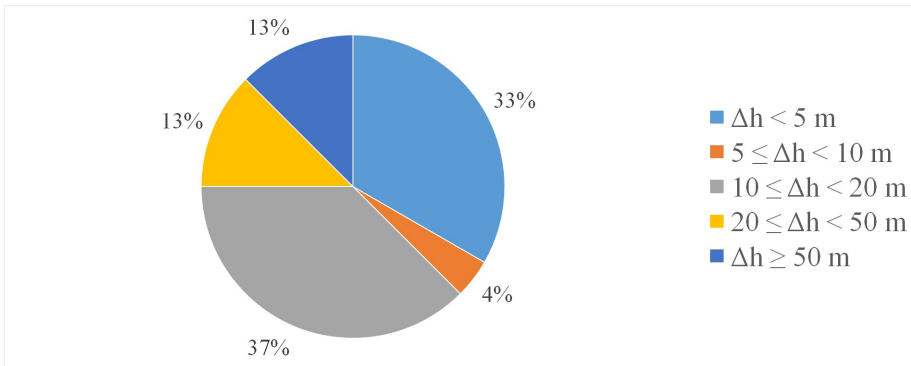


**Fig. 2.19:** Category #5: inserted pressure wave,  $\Delta h$ . Percentage of the papers for the five ranges.

### Category #6: Blockage simulation

In this section, the characteristics of the devices used in the experiments to simulate PBs are described. In the available experiments (Table 2.6), four types of devices have been identified (Fig. 2.20): i) in-line valve, ii) orifice, iii) small bore pipe, and iv) “other” (i.e., irregular rock aggregate or rough coconut coir (Duan et al., 2017), very short PB and longitudinal body PB (Figs. 3 and 4 in Meniconi et al. (2016), respectively)). As shown in Fig. 2.20, the most used device is the small bore pipe that captures indeed the characteristics of the real “extended” PBs (Brunone et al., 2008a). Fig. 2.21 shows that most tests have been executed in polyethylene pipes with the PB simulated by a small bore pipe.

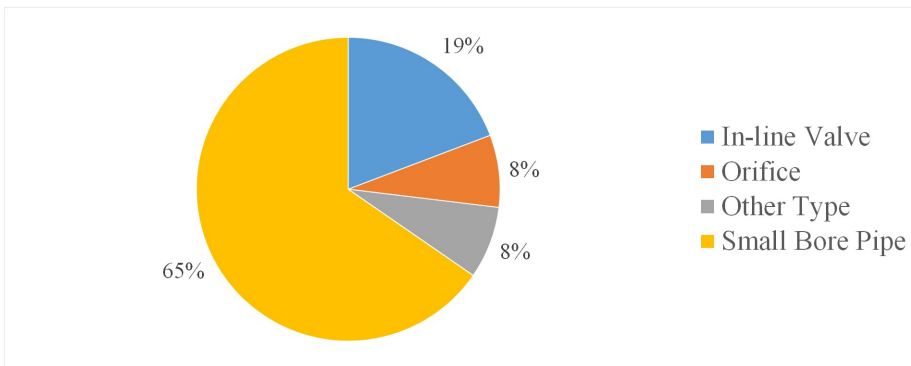


**Fig. 2.20:** Category #6: types of the devices used for simulating PBs.

In terms of the PB severity, three parameters have been considered. The first one,  $B$ , is given by the ratio between the cross-sectional area of the PB,  $A_b$ ,

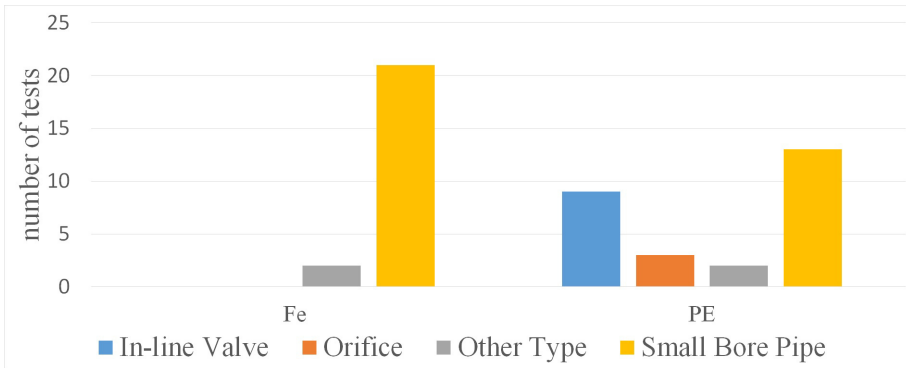


Fig. 2.21: Pipe material and PB type.

and the pipe,  $A$  ( $B = A_b/A$ ). For each setup with a small bore pipe or an orifice,  $A_b$  is a constant value whereas when the PB is simulated by means of an in-line valve, different values of  $A_b$  have been considered for a given valve. The analysis of the executed tests indicates that most of them ( $= 65\%$ ) has been executed for  $B = B_1 (< 25\%)$ , i.e., for the most favourable conditions from the experimental point of view (the smaller  $A_b$  the easier the PB detection). This implies that experiments concerned mainly PBs at a late stage (i.e.,  $A_b \ll A$ ). As a consequence, future experiments should be carried out in pipe systems with a larger value of  $B$ , i.e. with PBs at an early stage. The second and third parameters – appropriate only for “extended” PBs – are defined in terms of the length,  $L_b$ , and time interval,  $\Delta t_b$ ; the latter is a sort of PB characteristic time ( $\Delta t_b = 2L_b/a_b$ ). In other words,  $\Delta t_b$  is the time interval that the pressure wave takes to travel along the PB and be reflected back. It gives an idea of the frequency of acquisition needed to capture the length,  $L_b$ , of the PB. In terms of  $L_b$ , most experiments concerned quite “short” PBs (i.e., with  $L_b$  of the order of few meters); in terms of  $\Delta t_b$ , it is  $\Delta t_{b,min} = 0.0003$  s and  $\Delta t_{b,max} = 0.5141$  s; such values can guide future research.

#### 2.4.4. Conclusions

In the last decades, transients test-based techniques (TTBTs) established as a viable tool for fault detection, particularly in the poorly inaccessible pressurized transmission mains (e.g., Meniconi et al., 2022). Although TTBTs are based on the well known properties of the pressure waves generated during transients, to be considered as a practicable procedure, it has been necessary that many experiments validated them. Accordingly, papers reviewing and analysing the available experimental results may help reassuring pipe system managers about the performance of the TTBTs. This is hopefully the case, for the leaks, of

Brunone et al. (2022) and this paper for partial blockages (PBs).

The first outcome of the review of the available physical experiments presented in this paper is the quite small number of papers focused on the use of the pressure waves for detecting PBs with respect to those concerning leak detection (18 vs 49). A possible reason is the underestimation of the problem represented by PBs that have no external evidence and make their effect felt in the long run and, more importantly, through indirect manifestations. Precisely, the increase of the energy consumption and decrease of the carrying capacity in the rising mains and gravity systems, respectively, are the result of the progressively growth of PBs. In most cases, when such indirect effects are evident, the PB size and length can be very severe and, maybe, difficult to counter with simple actions. In other words, it is too late and the pipe branch in question must be replaced.

The second outcome of this review is the extremely small number of tests executed in real systems. Such a feature causes the fact that no experiments have been carried out in large diameter pipes. As a further consequence, no experiments have been carried out in concrete pipes.

The third outcome concerns the lack of experiments in pipe networks both in the laboratories and, as mentioned above, real systems. This is a serious shortcoming since the multiple reflections of the pressure waves and their overlapping in complex pipe systems could highlight possible weak points of the TTBTs.

The fourth outcome is that there is no test executed in systems with “multiple” faults – e.g., a combination of several PBs and/or leaks – which is very frequent in real systems (the three orifices in series considered in Contractor (1965) were so close that they behaved as a unique PB).

To conclude this chapter section could encourage researchers to devote themselves to physical experimentation as a necessary action in parallel with the development of numerical methods for PB detection. In addition to the recommendation to present the results in dimensional quantities and with an accurate description of the experimental setup, two issues must be pointed out. The first one is that there is a need to refine reliable devices for generating fast transients that give rise to sharp pressure waves (easier to analyse). The second issue is that the time is ripe to fine-tune guidelines for carrying out transient tests in an optimal way within TTBTs.

## 3. Transients modelling

### 3.1. Introduction

Unsteady flows in pressure conduits are usually generated by sudden changes in flow rate, due to the operation of a regulating device that is placed in a generic flow section.

The change in flow rate propagates across the flow as a wave, which causes changes in the pressure, speed, and flow rate, in space and time. Such disturbance (hydraulic transient) moves from one section to another of the flow with a speed – called pressure wave speed – which is a function of the characteristics of the fluid and the pipeline.

Moreover, the hydraulic transient propagating along the flow is modified and reflected in correspondence with each variation of the boundary conditions: changes in pipe diameter, pipe-wall thickness, pipe-wall material, leak water, partial blockage, and also devices.

In this chapter, the one-dimensional differential equations of continuity and motion of the fluid are presented, as well as the assumptions necessary for the water hammer analysis, which takes into account the unsteady friction losses, and also the linear-viscoelastic behaviour of the pipe-wall. Such a feature is of considerable importance in plastic pipes.

### 3.2. Classic waterhammer problem

Classic waterhammer analysis is normally used in the design of water pipeline systems since describes adequately pressure fluctuations.

The hypotheses at the basis of the problem are (Covas, 2003):

- (i) Mono-phase, homogenous and compressible fluid. During transient events, density and temperature changes are neglected with respect to pressure and flow rate changes.
- (ii) The flow is one-dimensional with a velocity profile uniform in each cross-

### Chapter 3. Transients modelling

section of the pipe, whereas the head losses are calculated by common friction formulae of the steady-state.

- (iii) The pipe material is linear elastic. The dynamic fluid-pipeline interaction is neglected, and the pipe is straight and uniform with a constant cross-section, without flow variation.

The equations that describe unsteady-state flow in pressurized pipes (Wylie and Streeter, 1993) are the continuity equation:

$$\frac{dH}{dt} + \frac{a_0^2}{gA} \frac{\partial Q}{\partial s} = 0 \quad (3.1)$$

and the momentum equation:

$$\frac{\partial H}{\partial s} + \frac{1}{gA} \frac{dQ}{dt} + h_f = 0 \quad (3.2)$$

where:

$Q$  = flow rate;  $H$  = piezometric head;  $a_0$  = elastic wave speed, which depends on the fluid compressibility and physical properties of the pipe;  $g$  = gravity acceleration;  $A$  = pipe cross-sectional area;  $s$  = axial coordinate;  $t$  = time;  $h_f$  = the friction term.

By the Euleian rule of derivation, the total derivative of a generic quantity  $G$  is written as:

$$\frac{dG}{dt} = \frac{\partial G}{\partial t} + \frac{\partial G}{\partial s} \frac{ds}{dt}$$

Therefore, in most engineering applications, neglecting the convective term, the continuity equation, and the momentum equation can be simplified:

$$\frac{\partial H}{\partial t} + \frac{a_0^2}{gA} \frac{\partial Q}{\partial s} = 0 \quad (3.3)$$

$$\frac{\partial H}{\partial s} + \frac{1}{gA} \frac{\partial Q}{\partial t} + h_f = 0 \quad (3.4)$$

Integrating numerically<sup>1</sup> the Basic Equations 3.3 and 3.4, with appropriate boundary conditions, the unsteady-state flow in pressurized pipes is modelled.

For linear-elastic pipes the elastic wave speed,  $a_0$ , can be described by the following formula (Meniconi et al., 2012b; Covas, 2003):

$$a_0 = \sqrt{\frac{\frac{K}{\rho}}{1 + \frac{\alpha D}{e} \frac{K}{E_0}}} \quad (3.5)$$

<sup>1</sup>The partial differential equations are usually solved with the Method of Characteristics, Finite-difference method, and Finite-element method. The Method of Characteristics (MOC) is extensively used for the solution of 1-D hydraulic transients, and a section (3.4) will be dedicated to it in this chapter.

## Chapter 3. Transients modelling

in which  $E_0$  = Young's modulus of elasticity of pipe walls;  $K$  = bulk modulus of elasticity of fluid;  $\rho$  = fluid density;  $D$  = pipe internal diameter;  $e$  = pipe-wall thickness;  $\alpha$  = dimensionless parameter that depends on the pipe axial constraints. There are several formulae to estimate  $\alpha$  parameters for various pipeline conditions (Wylie and Streeter, 1993).

The formula 3.5, due to the uncertainty associated with the pipe's characteristics, only provides an estimate of the wave speed.

### 3.3. Unconventional waterhammer problems

The classical analysis of waterhammer doesn't take into account the following problems:

- unsteady friction;
- non-linear elastic behaviour of the pipe;
- transient cavitation and water column separation;
- fluid-structure interaction;
- distributed lateral flow

which can occur in particular situations and change the transient response of a pipe system (Covas, 2003).

In this section, we will only discuss the unsteady friction losses and non-elastic and viscoelastic behaviour of the pipe material.

#### 3.3.1. Unsteady friction losses

In presence of slow transients, frictional losses are commonly calculated by steady-state formulae. During rapid transient events the instantaneous velocity profile changes rapidly with significant increase of the level of turbulence in the flow. Therefore, to account for effects of the non-uniform velocity profile and unsteady friction losses in 1-D transient flow, in the momentum equation (Eq. 3.4) the slope of the energy line  $h_f$  is decomposed into two terms:

$$h_f = h_{fs} + h_{fu} \quad (3.6)$$

where  $h_{fs}$  and  $h_{fu}$  are the steady-state and the unsteady-state friction components, respectively.

The steady-state friction component, is calculated for turbulent flows by:

$$h_{fs} = \lambda \frac{Q |Q|}{2gDA^2} \quad (3.7)$$

### Chapter 3. Transients modelling

or may be calculated by common steady-state formulae. Whereas, for laminar flows is calculated by:

$$h_{fs} = \frac{32\nu' Q}{gD^2 A} \quad (3.8)$$

where  $\lambda$  = Darcy-Weisbach friction factor;  $D$  = pipe inner diameter;  $\nu'$  = kinematic fluid viscosity.

The unsteady-state friction component, can be calculated by different formulations present in literature. In this thesis work,  $h_{fu}$  is evaluated within an instantaneous acceleration-based model by means of the following relationship (Brunone et al., 1995; Pezzinga, 2000; Bergant et al., 2001; Meniconi et al., 2012b):

$$h_{fu} = \frac{k_d}{2gA} \left( \frac{\partial Q}{\partial t} + a_0 \text{sign}(Q) \left| \frac{\partial Q}{\partial s} \right| \right) \quad (3.9)$$

in which  $\text{sign}(Q) = +1$  for  $Q \geq 0$  or  $= -1$  for  $Q < 0$ .

#### 3.3.2. Non-elastic and viscoelastic behaviour of the pipe material

Viscoelastic materials, in contrary to elastic materials that strain instantaneously by applying a stress and return to their original state once it is removed, present a different rheological behaviour. Their response to the application of instantaneous circumferential stress does not follow Hooke's law, and the total strain is divided into two components: the instantaneous ( $\varepsilon_i$ ) and retarded strain ( $\varepsilon_r$ ):

$$\varepsilon = \varepsilon_i + \varepsilon_r \quad (3.10)$$

In viscoelastic materials when the stress is held constant the deformation increases or decreases over time, and occurs viscoelastic creep or viscoelastic relaxation respectively. Moreover, the rate of application of the load affects the effective stiffness. Instead, a cyclic load leads to a phase lag (hysteresis) followed by a reduction of mechanical energy. At last, in the viscoelastic pipe, the pressure or acoustic waves experience a fast attenuation (Meniconi et al., 2012b).

The total strain generated by a continuous application of a stress,  $\sigma(t)$ , is:

$$\varepsilon(t) = J_0\sigma(t) + \int_0^t \sigma(t-t') \frac{\partial J(t')}{\partial t'} dt' \quad (3.11)$$

in which  $J_0$  = instantaneous creep-compliance and  $J(t')$  = creep function at time  $t'$ .

For linear-elastic materials, the creep compliance  $J_0$  is equal to the inverse modulus of elasticity,  $J_0 = 1/E_0$ .

Assuming that the pipe material (i) is homogeneous and isotropic, (ii) has linear viscoelastic behaviour for small strains, and (iii) has a constant Poisson's ratio

### Chapter 3. Transients modelling

$\nu$  so that the mechanical behaviour is only dependent on creep compliance, the circumferential strain is:

$$\begin{aligned} \varepsilon(t) = & \frac{\alpha_0 \rho g D_0}{2e_0} [H(t) - H_0] J_0 + \\ & + \frac{\alpha(t - t') \rho g D(t - t')}{2e(t - t')} \int_0^t [H(t - t') - H_0] \frac{\partial J(t')}{\partial t'} dt' \end{aligned} \quad (3.12)$$

where  $H(t)$  = piezometric head at time  $t$ ;  $H_0$  = initial steady-state piezometric head;  $J_0$  = instantaneous creep compliance;  $J(t)$  = creep compliance function (obtained experimentally) defined by  $J(t) = \varepsilon(t)/\sigma$  for a constant circumferential stress  $\sigma$ ,  $\sigma = \alpha \frac{\rho g H D}{2e}$ ;  $D(t)$  and  $D_0$  = inner diameter at time  $t$  and  $t=0$ , respectively;  $e(t)$  and  $e_0$  = wall thickness at time  $t$  and  $t=0$ , respectively;  $\alpha(t)$  and  $\alpha_0$  = pipe wall constraints coefficient at time  $t$  and  $t = 0$ , respectively. The first term of this equation corresponds to the elastic strain  $\varepsilon_i$  and the integral part to the retarded strain  $\varepsilon_r$  (Covas et al., 2004c)

One of the physical model to simulate the viscoelastic behavior is the Kelvin-Voigt model, where an elastic spring and viscous damper are placed in parallel. This element is jointed to a simple elastic spring in series (with instantaneous Young's modulus of elasticity  $E_0$ ), (Meniconi et al., 2012b). The spring describes the elastic-instantaneous response of the material.

The creep compliance function can be expressed by the following expression:

$$J(t) = J_0 + \sum_{k=1}^N J_k \left(1 - e^{-\frac{t}{\tau_k}}\right) \quad (3.13)$$

where:  $J_0$  = creep-compliance of the first spring defined as  $J_0 = 1/E_0$ ,  $J_k$  = creep compliance of the spring of the Kelvin-Voigt element  $k$  ( $J_k = 1/E_k$ , where  $E_k$  = modulus of elasticity of the spring of  $k$ -element),  $\tau_k$  = retardation time of the dashpot of  $k$ -element ( $\tau_k = \mu_k/E_k$ , where  $\mu_k$  = the viscosity of the dashpot of  $k$ -element).

A viscoelastic solid, as a polyethylene pipe, can be described by an infinite number of elements (Fig. 3.1).

The number and type of elements used improves the accuracy of the solution and the computational effort (Covas et al., 2004c).

If a single Kelvin-Voigt element is combined jointed to a simple elastic spring in series, the instantaneous circumferential stress can also be written as:

$$\sigma = E_r \varepsilon_r + \mu_r \frac{d\varepsilon_r}{dt} \quad (3.14)$$

and the variation in time of  $\varepsilon_r$  is given by:

$$\frac{d\varepsilon_r}{dt} = \frac{1}{\tau_r} \left( \alpha \frac{\rho g H D}{2e E_r} - \varepsilon_r \right) \quad (3.15)$$

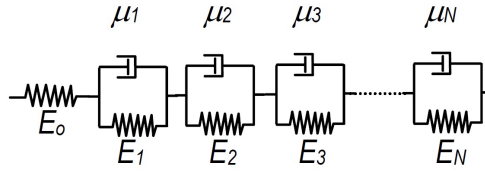


**Fig. 3.1:** Generalised Kelvin-Voigt Model (Source figure: Covas, 2003).

Taking into account the relationship between cross-section area,  $A$ , and total hoop strain,  $\varepsilon$ :

$$\frac{dA}{dt} = 2A \frac{d\varepsilon}{dt}$$

and the components of strain (Eq. 3.10), the continuity equation (Eq. 3.3) for viscoelastic pipes becomes:

$$\frac{\partial H}{\partial t} + \frac{a_0^2}{gA} \frac{\partial Q}{\partial s} + \frac{2a_0^2}{g} \frac{d\varepsilon_r}{dt} = 0 \quad (3.16)$$

where the term  $\frac{d\varepsilon_r}{dt}$  is the rate of change in time of the retarded strain,  $\varepsilon_r$ , and it takes into account the different behavior of plastic pipes with respect to metal and concrete ones (Meniconi et al., 2012b).

The Eq. 3.16 solved with Eq. 3.4 describes the pressure-flow changes and circumferential strain along a pressurised linear viscoelastic pipe.

### 3.4. Method of Characteristics

Method of Characteristics (MOC) has the attractive feature of allowing the transformation of the set of equations (Eqs. 3.16 and 3.4) into a system of ordinary differential equations. Once the initial and boundary conditions have been defined, it is possible to directly integrate the system. The simplicity of programming and efficiency of computations made it very popular (Covas et al., 2004c).

Therefore, combining linearly the Eqs. 3.16 and 3.4, using an unknown multiplier ( $\pm \frac{g}{a}$ ), we obtain the two total differential equations valid along the characteristic lines  $ds/dt = V \pm a_0$  (Wylie and Streeter, 1993; Covas, 2003):

$$C^+ : \begin{cases} \frac{dH}{dt} + \frac{a_0}{gA} \frac{dQ}{dt} + \frac{2a_0^2}{g(V+a_0)} \left( V \frac{d\varepsilon_r}{dt} + a_0 \frac{\partial \varepsilon_r}{\partial t} \right) + a_0 h_f = 0 \\ \frac{ds}{dt} = V + a_0 \end{cases} \quad (3.17)$$

$$C^- : \begin{cases} \frac{dH}{dt} - \frac{a_0}{gA} \frac{dQ}{dt} + \frac{2a_0^2}{g(V-a_0)} \left( V \frac{d\varepsilon_r}{dt} - a_0 \frac{\partial \varepsilon_r}{\partial t} \right) - a_0 h_f = 0 \\ \frac{ds}{dt} = V - a_0 \end{cases} \quad (3.18)$$

Generally, fluid velocity is negligible compared to the wave speed propagation  $V \ll a_0$ , leading to approximate straight characteristic lines, i.e.  $ds/dt = \pm a_0$ , and characteristic equations  $C^+$  and  $C^-$  can be further simplified to:

$$C^+ : \begin{cases} \frac{dH}{dt} + \frac{a_0}{gA} \frac{dQ}{dt} + \frac{2a_0^2}{g} \left( \frac{\partial \varepsilon_r}{\partial t} \right) + a_0 h_f = 0 \\ \frac{ds}{dt} = +a_0 \end{cases} \quad (3.19)$$

$$C^- : \begin{cases} \frac{dH}{dt} - \frac{a_0}{gA} \frac{dQ}{dt} + \frac{2a_0^2}{g} \left( \frac{\partial \varepsilon_r}{\partial t} \right) - a_0 h_f = 0 \\ \frac{ds}{dt} = -a_0 \end{cases} \quad (3.20)$$

Using a rectangular computational grid (Figure 3.2), in which the pipe is divided in sections of length  $\Delta s$ , the following finite difference scheme is used valid along  $\frac{\Delta s}{\Delta t} = \pm a_0$  (Covas, 2003; Covas et al., 2004c):

$$C^+ : \begin{cases} (H_{i,j} - H_{i-1,j-1}) + \frac{a_0}{gA} (Q_{i,j} - Q_{i-1,j-1}) + \frac{2a_0^2(\Delta t)}{g} \left( \frac{\partial \varepsilon_r}{\partial t} \right)_{i,i-1} + a_0(\Delta t)h_f = 0 \\ \frac{\Delta s}{\Delta t} = +a_0 \end{cases} \quad (3.21)$$

$$C^- : \begin{cases} (H_{i,j} - H_{i+1,j-1}) - \frac{a_0}{gA} (Q_{i,j} - Q_{i+1,j-1}) + \frac{2a_0^2(\Delta t)}{g} \left( \frac{\partial \varepsilon_r}{\partial t} \right)_{i,i+1} - a_0(\Delta t)h_f = 0 \\ \frac{\Delta s}{\Delta t} = -a_0 \end{cases} \quad (3.22)$$

In the Eqs. 3.21 and 3.22 the term  $h_f$  is calculated as described in Subsection 3.3.1, whereas the total retarded strain  $\varepsilon_r$  and the retarded strain time-derivative  $\frac{\partial \varepsilon_r}{\partial t}$  are calculated as the sum of these partial terms for each Kelvin-Voigt element  $k$  (Covas, 2003):

$$\varepsilon_r(i,j) = \sum_{k=1 \dots N} \varepsilon_{rk}(i,j) \quad (3.23)$$

### Chapter 3. Transients modelling

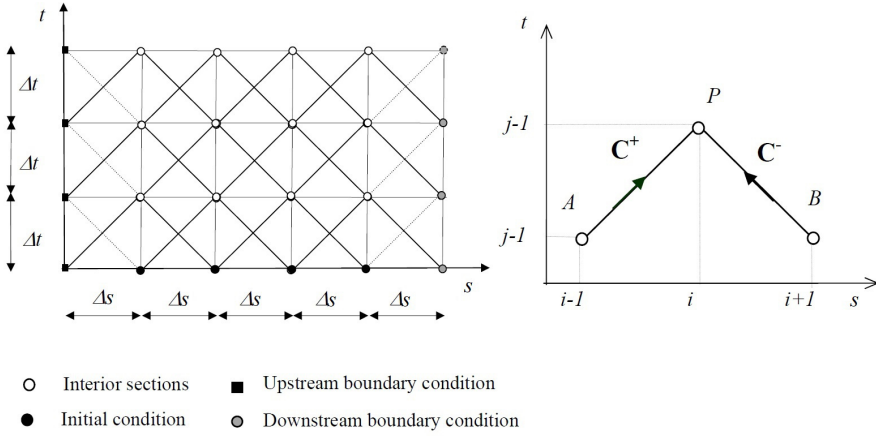


**Fig. 3.2:** Set of characteristic lines in time and space that constitutes a rectangular grid (Source figure: Covas, 2003.)

$$\left(\frac{\partial \varepsilon_r}{\partial t}\right)_{(i,j)} = \sum_{k=1 \dots N} \left(\frac{\partial \varepsilon_{rk}}{\partial t}\right)_{(i,j)} \quad (3.24)$$

The creep function (Eq. 3.13) can be directly differentiated in time:

$$\frac{\partial J(t)}{\partial t} = \frac{\partial}{\partial t} \left[ J_0 + \sum_{k=1}^N J_k \left(1 - e^{-\frac{t}{\tau_k}}\right) \right] = \sum_{k=1}^N \frac{J_k}{\tau_k} e^{-\frac{t}{\tau_k}} \quad (3.25)$$

Introducing this time-derivative in the retarded strain described by the second term of the Eq. 3.12, the total retarded strain is:

$$\varepsilon_{r(i,j)} = \sum_{k=1 \dots N} \left( \frac{\alpha \rho g D}{2e} \int_0^t [H(s, t - t') - H_0(s)] \frac{J_k}{\tau_k} e^{-\frac{t'}{\tau_k}} dt' \right) \quad (3.26)$$

and the retarded strain time-derivative is given by:

$$\left(\frac{\partial \varepsilon_r}{\partial t}\right)_{(i,j)} = \sum_{k=1 \dots N} \left( \frac{\alpha \rho g D J_k}{2e \tau_k} [H(s, t) - H_0(s)] - \frac{\varepsilon_{rk}(s, t)}{\tau_k} \right) \quad (3.27)$$

Then, the retarded strain for each Kelvin – Voigt element k is:

$$\varepsilon_{rk}(s, t) = \int_0^t F(s, t - t') \frac{J_k}{\tau_k} e^{-\frac{t'}{\tau_k}} dt' \quad (3.28)$$

with:

$$F(s, t) = \frac{\alpha \rho g D}{2e} [H(s, t) - H_0(s)]$$

### Chapter 3. Transients modelling

The strain time-derivative derivative is calculated by the analytical differentiation of equation Eq. 3.28. After mathematical manipulations, for each element  $k$ , we obtain (Covas, 2003; Covas et al., 2004c):

$$\frac{\partial \varepsilon_{rk}(s, t)}{\partial t} = \frac{J_k}{\tau_k} F(s, t) - \frac{\varepsilon_{rk}(s, t)}{\tau_k} \quad (3.29)$$

$$\varepsilon_{rk}(s, t) = J_k F(s, t) - J_k e^{-\frac{\Delta t}{\tau_k}} F(s, t - \Delta t) - J_k \tau_k (1 - e^{-\frac{\Delta t}{\tau_k}}) \frac{F(s, t) - F(s, t - \Delta t)}{\Delta t} + e^{-\frac{\Delta t}{\tau_k}} \varepsilon_{rk}(s, t - \Delta t) \quad (3.30)$$

#### 3.4.1. Compatibility equations

The two Eqs. 3.21 and 3.22, can be written in the following simplified linear form (Covas, 2003):

$$C^+ : Q_{i,j} = C_P - C_{a+} H_{i,j} \quad (3.31)$$

$$C^- : Q_{i,j} = C_N + C_{a-} H_{i,j} \quad (3.32)$$

where the coefficients  $C_N$ ,  $C_{a+}$ ,  $C_P$  and  $C_{a-}$  are known constants when the equations are applied at location  $i$  and time  $j$  (Covas, 2003).

The coefficients depend on the numerical model used to describe steady-state friction, unsteady friction and the rheological behaviour of the pipe. In a generic form, these coefficients are defined as follows (Covas, 2003):

$$C_P = \frac{Q_{i-1,j-1} + B H_{i-1,j-1} + C'_{P1} + C''_{P1} + C'''_{P1}}{1 + C'_{P2} + C''_{P2}} \quad (3.33)$$

$$C_N = \frac{Q_{i+1,j-1} + B H_{i+1,j-1} + C'_{N1} + C''_{N1} + C'''_{N1}}{1 + C'_{N2} + C''_{N2}} \quad (3.34)$$

$$C_{a+} = \frac{B + C'''_{P2}}{1 + C'_{P2} + C''_{P2}} \quad (3.35)$$

$$C_{a-} = \frac{B + C'''_{N2}}{1 + C'_{N2} + C''_{N2}} \quad (3.36)$$

The coefficients superscripts ', '' and ''' refer to the steady-state friction, the unsteady friction and the pipe mechanical behaviour component, respectively. The numerical description of each coefficient is presented in Table 3.1 (Covas, 2003).

**Table 3.1:** Coefficients  $C_{P1}$ ,  $C_{P2}$ ,  $C_{N1}$  and  $C_{N2}$  (Source: Covas, 2003)

Steady-state friction [']
Frictionless $C'_{P1} = C'_{P2} = 0$ $C'_{N1} = C'_{N2} = 0$
First-order accuracy $C'_{P1} = R\Delta t  Q_{i-1,j-1}  Q_{i-1,j-1}$ $C'_{N1} = R\Delta t  Q_{i+1,j-1}  Q_{i+1,j-1}$ $C'_{P2} = 0$ $C'_{N2} = 0$
Unsteady friction [']
No-unsteady friction $C''_{P1} = C''_{P2} = 0$ $C''_{N1} = C''_{N2} = 0$
Vitkovsky formulation $C''_{P1} = k'\theta Q_{i,j-1} - k'(1-\theta)(Q_{i-1,j-1} - Q_{i-1,j-2}) - k' \text{sign}(Q_{i-1,j-1})  Q_{i,j-1} - Q_{i-1,j-1} $ $C''_{N1} = k'\theta Q_{i,j-1} - k'(1-\theta)(Q_{i+1,j-1} - Q_{i+1,j-2}) - k' \text{sign}(Q_{i+1,j-1})  Q_{i,j-1} - Q_{i+1,j-1} $ $C''_{P2} = C''_{N2} = k'\theta$
Rheological behaviour of pipe-wall [''']
Linear-Viscoelastic $C'''_{P1} = -2a_0 A \Delta t C_0 \sum_{k=1 \dots N} \left\{ \frac{\tau_k}{\Delta t} \left( 1 - e^{-\Delta t / \tau_k} \right) \right\}$ $C'''_{N1} = -2a_0 A \Delta t \sum_{k=1 \dots N} \left\{ -C_0 \frac{J_k}{\tau_k} H_{t,0} + C_0 \frac{J_k}{\tau_k} \left[ 1 - (1 - e^{-\Delta t / \tau_k}) \frac{\tau_k}{\Delta t} \right] H_{i,0} + \right.$ $\left. - C_0 \frac{J_k}{\tau_k} \left[ (1 - e^{-\Delta t / \tau_k}) \frac{\tau_k}{\Delta t} - e^{-\Delta t / \tau_k} \right] (H_{i,j-1} - H_{t,0}) - \frac{e^{-\Delta t / \tau_k}}{\tau_k} \epsilon_{r(i,j-1)} \right\}$ $C'''_{P2} = -C'''_{P1}$ $C'''_{N2} = +C'''_{N1}$ $C_0 = \alpha_0 D_0 \rho g / (2e_0)$

Parameter  $B$  depends on the physical characteristics of the fluid and the pipe:

$$B = \frac{gA}{a_0} \quad (3.37)$$

whereas  $R$  is the pipe resistance coefficient, defined for turbulent flows by (Covas, 2003):

$$R = \frac{\lambda}{2gDA^2} \quad (3.38)$$

and for laminar flows by:

$$R = \frac{32\nu'}{gD^2A} \quad (3.39)$$

Flow parameters at section  $i$  and time  $j$ ,  $i_j$  and  $H_{i,j}$ , are calculated for all interior sections of the pipes as follows (Covas, 2003):

$$H_{i,j} = \frac{C_P - C_N}{C_{a+} + C_{a-}} \quad (3.40)$$

$$Q_{i,j} = C_N + C_{a+} H_{i,j} \tag{3.41}$$

At the ends of each pipe, auxiliary equations are needed to describe the boundary condition. Each boundary condition is solved independently of the other boundary conditions, and independently of the interior point calculations (Wylie and Streeter, 1993).

In this thesis work, only the boundary conditions used in the employed transient solver (chapter 7) are presented.

### 3.4.2. Boundary conditions

The piping systems are made up of different elements: the pipes (defined as Link-Elements) connected to each other by nodes, i.e. junctions, defined as Node-Elements. In complex systems can also be present different hydraulic devices, such as valves, reservoirs and pumps, defined as Non-Pipe Elements, which have a negligible length (Covas, 2003).

The Pipe Link-Element is composed of interior sections and two boundary sections at the extreme ends. Flow parameters  $Q$  and  $H$  are computed with the Eqs. 3.40 and 3.41 at the interior sections, whereas additional equations have to be specified at the extreme ends of each pipe (Covas et al., 2004c). The end condition are applied to adjacent pipes or other boundary elements. Also in this case each boundary condition is treated independently of the others.

A Node-Elements has  $N_C$  convergent pipes and  $N_D$  divergent pipes and only one Non-Pipe Element is linked to each node (Fig. 3.3).

The same piezometric head ( $H$ ) is assumed at the node at each instant of time:

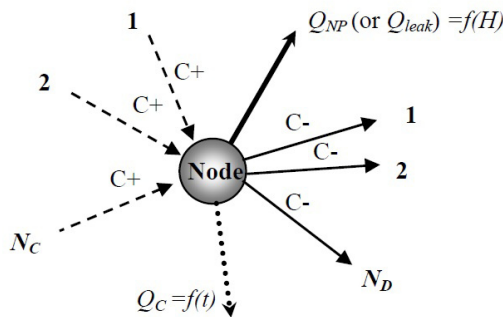


Fig. 3.3: Representation of a Node-Element (Source figure: Covas, 2003)

$$H_{p1} = H_{pN} \tag{3.42}$$

and the continuity equation must be satisfied at each instant of time:

$$\sum_{k=1\dots N}^{N_C} Q_{k,j} - \sum_{k=1\dots N}^{N_D} Q_{k,j} = Q_{NP} + Q_C \quad (3.43)$$

where  $Q_{k,j}$  is the flow from pipe  $k$  at time step  $j$ ,  $Q_{NP}$  is non-pipe element flow or leak,  $Q_C$  time-dependent demand (Covas, 2003).

Introducing the Eqs. 3.40 and 3.41 in the Eq. 3.43 for all pipe connected to node, the node equation is:

$$H_N = \frac{E_N - Q_{NP}}{B_N} \quad (3.44)$$

in which the the constants  $E_N$  and  $B_N$  are defined by:

$$E_N = \sum_{k=1}^{N_C} C_{P_k} - \sum_{k=1}^{N_D} C_{N_k} - Q_C \quad (3.45)$$

$$B_N = \sum_{k=1}^{N_C} C_{a+k} + \sum_{k=1}^{N_D} C_{a-k} \quad (3.46)$$

Node-Elements are computed after the calculation of interior sections of the pipes. These have two unknown parameters  $Q_{NP}$  and  $H_N$ , defined by Equation 3.44. If  $Q_{NP}=0$ :

$$H_N = \frac{E_N}{B_N} \quad (3.47)$$

else, an additional equation is required to solve these parameters, i.e. the Non-Pipe Element equation.

A Non-Pipe Element is any hydraulic device, such as a valve, pump, and reservoir (Covas, 2003). For these elements, negligible length, incompressible fluid, flow rate  $Q_P$  and piezometric heads  $H_u$  upstream and  $H_d$  downstream are assumed (Fig. 3.4).

The difference between piezometric heads at the upstream and the downstream ends (both defined by Eq. 3.44) is:

$$\Delta H_{NP} = H_u - H_d = E_E + B_E Q_{NP} \quad (3.48)$$

where parameters  $E_E$  and  $B_E$  are:

$$E_E = E_{Nd} - E_{Nu} \quad (3.49)$$

$$B_E = B_{Nu} + B_{Nd} \quad (3.50)$$

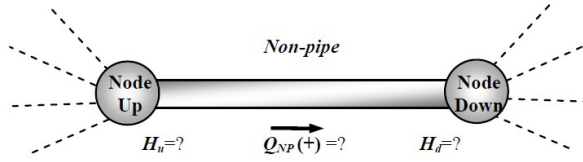


**Fig. 3.4:** Representation of a Non-Pipe Element (Source figure: Covas, 2003)

An additional equation is necessary to the system:

$$F(H_u, H_d, Q_{NP}) = 0 \quad (3.51)$$

or

$$H_u - H_d = f(Q_{NP}) \quad (3.52)$$

Introducing the Eq. 3.48 in Eq. 3.51 and 3.52 we obtain the characteristic equation of a Non-Pipe Element (Covas, 2003):

$$f(Q_{NP}) + B_E Q_{NP} + E_E = 0 \quad (3.53)$$

This equation can be (i) a linear algebraic equation (e.g. reservoir), (ii) a second-order algebraic equation (e.g. valve) or (iii) a non-linear ordinary equation that is solved by an iterative procedure (e.g. air vessel).

The reservoir is assumed to have an infinite volume. The piezometric head of this element is constant  $H_N = H_R$ , in which  $H_R$  is the reservoir level. If the reservoir level changes, this is defined from a sine function of an intermediate level. The flow-rate  $Q_{NP}$  is calculated with Eq. 3.36, from which (Covas, 2003):

$$Q_{NP} = E_N - B_N H_R \quad (3.54)$$

The valve at downstream end of pipe is a valve that discharges to the atmosphere. In this case, the flow energy is equal to node elevation plus kinetic energy, then the characteristic equation is (Covas, 2003):

$$\left( C(t) + \frac{1}{2gA_{sv}(t)^2} \right) |Q_{PE}| Q_{PE} + B_{Nu} Q_{PE} + (Z - E_{Nu}) = 0 \quad (3.55)$$

where  $A_{sv}(t)$  is the valve section at time  $t$ . The solution and the coefficients are (Covas, 2003):

$$C_E = C(t) + \frac{1}{2gA_{sv}(t)^2} \quad (3.56)$$

$$B_E = B_{Nu} \quad (3.57)$$

$$E_E = Z - E_{Nu} \quad (3.58)$$

The leak ( $Q_{leak}$ ) is solved as a Non-Pipe Element, analogous to an atmosphere-valve. The difference is that the local head losses at this element are not incorporated in  $C(t)$  but in leak effective area  $A_{Lef}$  (Covas, 2003):

$$\left( \frac{1}{2gA_{Lef}^2} \right) |Q_{PE}| Q_{PE} + B_{Nu} Q_{PE} + (Z - E_{Nu}) = 0 \quad (3.59)$$

where  $A_{Lef} = C_{sv} A_{sv}$ , and  $C_{sv}$  is the discharge coefficient, that depends on the shape of the orifice, the size and distance from the pipe's wall of the contracted section, and the local head losses. The solution and the coefficients are (Covas, 2003):

$$C_E = \frac{1}{2gA_{Lef}^2} \quad (3.60)$$

$$B_E = B_{Nu} \quad (3.61)$$

$$E_E = Z - E_{Nu} \quad (3.62)$$

If the pipeline contains a closed end we have a dead-end, where the flow  $Q_{NP} = 0$ . The piezometric head at this element is obtained directly from Eq.3.47, where the coefficients  $E_N$  and  $B_N$  are calculated for one pipe only (Covas, 2003).

### 3.5.The Lagrangian Model

To better understand the dynamic behavior of the network during the executed transient tests in the research project, a Lagrangian model (LM) simulating the pressure wave propagation is used in the chapter 6, (Keramat et al., 2019; Ferrante et al., 2009a). Such a model is based on the solution of the differential equations governing frictionless transients in pressurized elastic pipe systems (Swaffield and Boldy, 1993) and assumes an instantaneous maneuver. Specifically, the momentum (Eq.3.4) and continuity (Eq. 3.3) equations can be written:

$$\frac{\partial H}{\partial s} + \frac{1}{Ag} \frac{\partial Q}{\partial t} = 0 \quad (3.63)$$

$$\frac{\partial H}{\partial t} + \frac{a_0^2}{gA} \frac{\partial Q}{\partial s} = 0 \quad (3.64)$$

The omission of friction in Equation (3.63) is not limiting if, as in the chapter 6, only the first phase of the transient tests is considered. In fact, in such a period of time, the effect of both unsteady friction and for polymeric pipes, viscoelasticity, is quite negligible with respect to the evaluation of the extreme pressure values (Duan et al., 2010; Brunone et al., 2018). Moreover, the inclusion of the unsteady friction term in the momentum equation and the one simulating the change of the pipe cross-sectional area due to viscoelasticity in the continuity equation (Pezzinga et al., 2014) increases very significantly the complexity of the model from several points of view without a significant return in terms of performance. First of all, the computational burden increases significantly and may imply an unacceptable computational time because of the very large number of pipes of the WDNs. Secondly, to refine the model, a complicated preliminary calibration phase is needed for evaluating the unsteady friction and viscoelastic parameters. In particular, the dependence of the latter on the pipe material properties—often not known with sufficient accuracy—and geometrical characteristics increases significantly their number (Mitosek and Chorzelski, 2003; Pezzinga et al., 2016). On the contrary, as discussed below, the use of the LM implies evaluating only the pressure wave speed and geometric parameters of the singularities.

The LM allows following the propagation of the pressure waves generated by the maneuver and their interaction with the successive singularities (i.e., junctions, leaks, partially closed in-line valves, etc.). Accordingly, the paths of the reflected and transmitted pressure waves and their arrival times at any node can be evaluated. In other words, the LM identifies which pressure waves pass the measurement sections and provides the instants of passage. Specifically, the arrival of an incident pressure wave,  $F_j$ , travelling along a given pipe, say pipe  $j$ , to a singularity generates a reflected pressure wave,  $F_{R,j}$ ,—propagating backward—and a transmitted pressure wave,  $F_{T,i}$ , in each of the pipes connected downstream (with  $i \neq j$ ). The coefficients of reflection,  $C_R$ , and transmission,  $C_T$ , are defined as:

$$C_R = \frac{F_{R,j}}{F_j} \quad (3.65)$$

and

$$C_T = \frac{F_{T,i}}{F_j}, i \neq j \quad (3.66)$$

respectively, with  $i$  indicating the generic pipe connected to the singularity, except pipe  $j$ . Table 3.2 summarizes the values of such coefficients for all the singularities of the laboratory network, i.e., a constant head reservoir, a dead end, and a generic junction connecting  $n$  pipes, each with its pressure wave speed,  $a$ , and cross-sectional area,  $A$ .

**Table 3.2:** The reflection and transmission coefficients given by the Lagrangian model (LM) for the singularities of the network.

Singularity	Reflection Coefficient, $C_R$	Transmission Coefficient, $C_T$
constant head reservoir	-1	0
closed valve/dead end	1	0
junction	$\frac{A_j/a_j - (\sum_{i=1, i \neq j}^n A_i/a_i)}{\sum_{i=1}^n A_i/a_i}$	$\frac{2A_j/a_j}{\sum_{i=1}^n A_i/a_i}$

### 3.6. Conclusions

Hydraulic transients have been widely described by classic waterhammer theory based on the assumptions of linear elastic behaviour of pipe-walls and quasi-steady state friction-losses. However, when the hydraulic transients are generated by rapid changes in flow conditions, the hypotheses at the basis of the theory are not sufficient to describe the phenomenon. Therefore it is necessary to implement the unstable friction and the rheological behavior of the pipe wall, not negligible in plastic pipes (e.g. PE) and important for the accurate description of transient events.

Typically the water hammer equations are solved using the Method of characteristics, in which several boundary and internal conditions are imposed. This method, as well as unsteady friction and linear viscoelastic behaviour of the pipe-wall, have been implemented in the solver (Hydraulic Transient Solver), used during the research project.

Finally, to better understand the dynamic behavior of the transients in the first phase it is possible to use the Lagrangian model.

## 4. Experimental data collection programme

### 4.1. Introduction

From the literature review (Chapter 2) it emerges that in the few papers based on physical experiments, transients are generated by maneuvers in the supply lines (e.g., pump trip) and their effects are analyzed in the main pipes; whereas the role of the location of the transient source and the effects of the transients generated within the network (i.e., in the service lines) due to water consumption variations aren't analyzed.

To fill this gap, this thesis work focuses on the experimental analysis of the effects of transients due to changes in the users' water consumption, which are surely the most frequent source of pressure variations in a WDN. The motivation is that, for the intrinsic characteristics of WDNs, only laboratory tests allow isolating and understanding the nature of the transients. In fact, in real systems, since boundary conditions change in an uncontrolled way, repeatability of tests is a very hard task to achieve and then it is quite arduous to examine in detail the effect of each cause of transients.

The analysis is carried out considering transients due to both deterministic and stochastic consumption variations. In the deterministic consumption variation, just one consumption variation is imposed. This will allow distinguishing each single pressure wave arriving from each singularity of the system. Consequently, the response of the complex topological network could be interpreted without any doubts. On the contrary, the stochastic consumption variation is generated by randomly opening and closing three downstream end valves by following a real pattern of consumption (Marsili et al., 2022). This will allow reproducing the real dynamic behavior of a WDN and, consequently, providing useful information for detecting the most vulnerable parts of the network and their management.

The transient behavior of a looped WDN (two 100x100 m square loops) – with one or more active service lines in different locations – is analyzed via experiments conducted in the Water Engineering Laboratory (WEL) at the University of Perugia, Italy. During tests, pressure signals are acquired both in the main pipes and service line, where the downstream end valve simulates an end-user located downstream of the water meter. Transients are generated by the fast and total closure of such a valve simulating the effect of rapid maneuvers of an end-user. In the following, the experimental set-up, and the preliminary tests for characterizing the end-user and the service line will be described. Moreover, a brief description of the laboratory transient tests and the key quantities that will be used for the experimental test interpretation will be done.

### 4.2. The experimental set-up

The experimental set-up at the Water Engineering Laboratory (WEL) of the University of Perugia, Italy (Fig. 4.1) is a pipe network with two loops — indicated as I and II— simulating a DMA (Fig. 4.2). All the pipes are high-density polyethylene (HDPE) pipes and are supplied by a pressurized tank (Fig. 4.3a) in which the head is assured by a pump (Fig. 4.3b). The two loops of the DMA are supplied by a 42.3 m long pipe with an internal diameter,  $D$ , equal to 93.3 mm, nominal diameter DN110, and wall thickness  $e = 8.1$  mm. Loop I has four 100 m long pipes with  $D = 63.8$  mm, DN75, and  $e = 5.6$  mm, whereas loop II has four pipes one in common with the first loop and the other three ones with  $D = 42.6$  mm, DN50,  $e = 3.7$  mm, and a length of 100 m (Fig. 4.2b). In order to simulate a service line, a DN25 branch ( $D = 20$  mm, and  $e = 3$  mm) with a length of 23.6 m has been alternatively or simultaneously installed at sections 5, 6, and 7 (Table 4.1).

To simulate the end-user, at the downstream end of the service line (i.e., at nodes 5u, 6u, and 7u – Table 4.1) a solenoid valve in series with a ball valve is installed (Fig. 4.4). The ball valve – equipped with a protractor to check the actual opening degree – allows simulating different water consumption, whereas the solenoid valve generates controlled, repeatable, and fast transients. It is worthy of noting that fast transients imply sharp pressure waves. Such a requirement for pressure waves is of great importance not only when they are used for fault detection Brunone et al. (2021) but also for understanding the mechanisms of interaction with the system component as in this thesis work.

In all the considered layouts of the system, the supplied steady-state discharge is measured at section 2, located at a distance of 22.2 m from the tank, by means of an electromagnetic flow meter (Fig. 4.2b). Pressure is monitored at nodes 1, 4, 5, 6, 7, and 8, as well as at the measurement sections denoted with two numbers indicating the closest and the farthest junction, respectively (Fig. 4.2b). As an example, the measurement section 32 is located at a distance



**Fig. 4.1:** View of the Water Engineering Laboratory (WEL) of the University of Perugia, Italy.

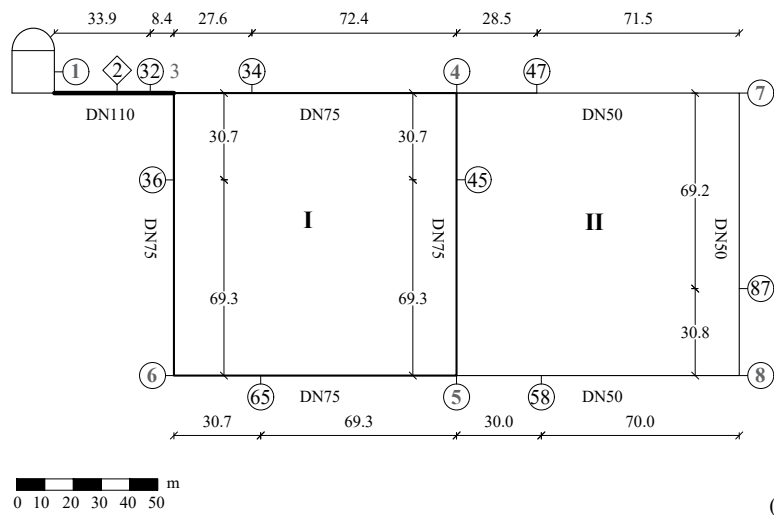


**Fig. 4.2:** The two-loop network at the Water Engineering Laboratory (WEL) of the University of Perugia, Italy: (a) picture, and (b) layout with the pipe length and location of the measurement sections indicated.



Fig. 4.3: At WEL: (a) pressurized tank, (b) pump.



**Fig. 4.4:** end-user (i.e. nodes 5u, 6u, and 7u).

of 8.4 m from node 3, whereas it is farther (= 11.7 m) from node 2. Finally, each junction connected to the service line has been fully monitored by adding a measurement section at a distance of 1 m in each main pipe connected to it. As an example, for the node 5, very close to the junction pressure signals are also acquired at nodes 5<sub>8</sub>, 5<sub>4</sub>, and 5<sub>6</sub> located 1 m from junction 5 along the three main pipes connected to it (with the subscript indicating the closest node); Figure 4.5a indicates the location of the measurement sections around junction 5 (shown in Figure 4.5b).

To capture properly the features of the system transient response, during tests, pressure is sampled at a frequency of 2048 Hz by a National Instrument cDAQ-9188 data acquisition system with a maximum analog input single-channel sampling rate of 51.2 kilosamples per second. Relative (G) piezoresistive pressure transducers have been installed with a full scale ( $f_s$ ) variable from 6 bar G to 10 bar G in the network. To capture eventual relative negative pressure in the service line, absolute (A) piezoresistive transducers are used from 15 bar A to 16 bar A. All these transducers have an accuracy of 0.25%  $f_s$ . For all tests, the water temperature is quite constant and equal to about 18 °C.

It is worth noting that the experimental set-up has been designed in order to be representative of real WDNs, on the one side, and allow an effective analysis and comprehension of the phenomena, on the other side. Indeed, it has to be pointed out that: (i) the loops of the experimental set-up consist of pipes of different diameters, thus allowing a proper analysis of the effects of the pipe size on the system response to the user water consumption change, (ii) the water consumption change can be physically modelled in parts of the system with different characteristics such as at connection of three pipes of different diameters, large and small diameters (see node 5) or at the connection of a couple of pipes with the same diameter (both large or small, such as node 6 and 7, respectively), and (iii) given its topological structure, the system allows taking into account transmission and reflection of the pressure waves at nodes

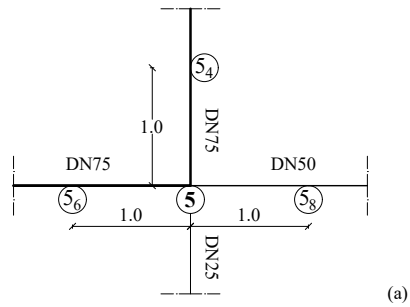


**Fig. 4.5:** (a) Location of the measurement sections around junction 5; and (b) junction 5 (as an example of the service line connection to the WDN).

featuring different geometrical characteristics (number of the connected pipes, ratio of the diameters of the pipes), as in real systems. Furthermore, pipe lengths and diameters, as well as the types of connection considered in this system, are quite common. Indeed, the system is conceived taking a cue from a part of the real WDN considered in the field analysis by (Marsili et al., 2020).

### 4.3. Preliminary tests for the end-user and service line characterization

In order to characterize the end-user and service line, some preliminary tests have been executed. Firstly, the ball valve at the end-user has been geometrically characterized. Precisely, the relationship between the valve relative opening  $\phi$  ( $\phi = 0$  for fully closed valve and  $\phi = 1$  for fully open valve) and dimensionless cross-sectional area  $A_v/A$ —with  $A_v$  = ball valve cross-sectional area, and  $A$  = pipe area—has been obtained by means of a 3D AutoCAD model and checked by a photographic analysis. Figure 4.6a shows the good agreement between such a geometric relationship and the results by Idel'cik (1986).

Secondly, steady-state tests have been carried out for evaluating the end-user hydraulic characteristics. Precisely, the local head loss,  $\zeta$ , across the two installed in series valves has been measured for different values of  $\phi$  and discharge,  $Q$ .

According to the usual flow conditions in real pipe systems, experiments concerned turbulent flow with values of the Reynolds number that ranges from 6,700 to 183,000. Accordingly, for any given relative opening,  $\phi$ , the constant value of the in series valve effective area ( $C_{sv}A_{sv}$ ) has been determined by means of the following equation:

$$Q = C_{sv}A_{sv}\sqrt{2g\zeta} \quad (4.1)$$

with  $A_{sv}$  ( $C_{sv}$ ) = in series valve area (discharge coefficient), and  $g$  = gravity acceleration ( $= 9.806 \text{ m/s}^2$ ). Figure 4.6b shows the experimental hydraulic characteristics of the end-user—i.e., the relationship between  $\phi$  and  $C_{sv}A_{sv}/A$ —and the corresponding fitting function ( $C_{sv}A_{sv}/A = 0.802\phi^2 - 0.035\phi$ ).

Further preliminary experiments allowed evaluating the pressure wave speed,  $a$ , of both the network pipes and service line by measuring the pressure wave travel time. As a result, the following values have been obtained:  $a_{DN25} = 455.91 \text{ m/s}$ ,  $a_{DN50} = 379.81 \text{ m/s}$ ,  $a_{DN75} = 387.89 \text{ m/s}$ , and  $a_{DN110} = 398.82 \text{ m/s}$ , with the subscripts indicating the corresponding pipe nominal diameters. Such values are compatible with the geometrical and mechanical characteristics of the pipes.

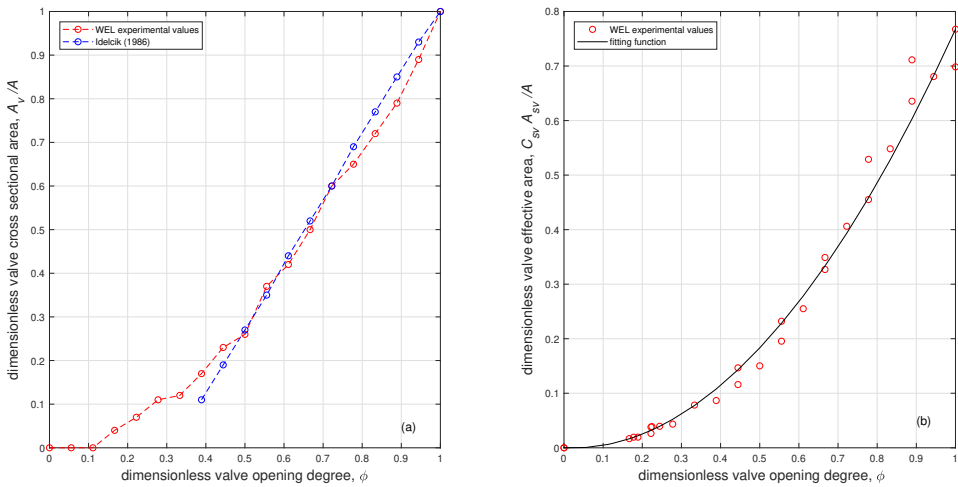


**Fig. 4.6:** (a) Comparison of the geometric characteristics of the ball valve obtained at WEL and by Idel'c'ik (1986); (b) hydraulic characteristics of the end-user.

#### 4.4. Laboratory transient tests

Table 4.1 shows the main characteristics of some of the tests carried out at WEL. Such tests differ for the layout, boundary conditions, and initial discharge of the end-user,  $Q_{0,yu}$ , with subscripts 0 and  $yu$  indicating the steady-state conditions and the end-user (with  $y = 5, 6, \text{ and } 7$ , alternately), respectively. For a given relative opening of the end-user,  $\phi$ , the discharge  $Q_{0,yu}$  has been obtained by Eq. (4.1). To simulate actions initiated in the plumbing system – i.e., the shutting off the valve, shower heads or the automatic off of the solenoid valve on the washing machine – transients are generated by the complete closure of the end valve. Such a maneuver emphasizes the dynamic response of the system, and the variation of the discharge,  $\Delta Q_{yu}$ , generating the overpressure  $\Delta_{yu}$ , coincides to  $Q_{0,yu}$ .

In particular, tests with  $Q_{0,yu}$  smaller than about  $0.4 \times 10^{-3} \text{ m}^3/\text{s}$  are consistent with the typical consumption of sanitary appliances Blokker et al. (2010). On the contrary, tests with larger values of  $Q_{0,yu}$  refer to more important users (e.g., of industrial or commercial type).

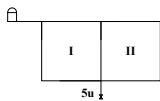
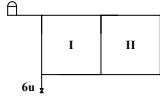
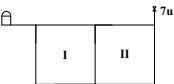
During test series #1, #2, and #3, only one end-user is active (precisely: node 5u, 6u, and 7u, respectively). The aim of these tests is to analyze the effect of the discharge variation, when the generated pressure waves propagate in a completely closed network. Moreover, with such tests we want to analyze the effect of the topology and location of the pressure waves generation point on the network transient response. Accordingly, the executed tests differ for the network layout, boundary conditions, and water consumption at the end-user,  $Q_{0,yu}$ , with the subscripts 0 and  $yu$  indicating the steady-state conditions and the end-user (with  $y = 5, 6, \text{ and } 7$ , alternately), respectively. On the contrary,

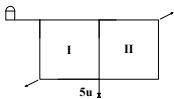
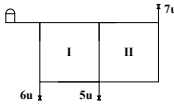
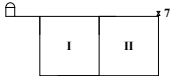
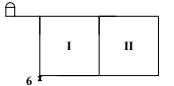
during test series #4, several users are still active (precisely: nodes 6 or/and 7), after the completion of the maneuver at the end-user 5u. This series allows examining the effect of the WDN functioning conditions (i.e., the pressure regime and the values of the discharge in the pipes).

In addition, in order to consider realistic and randomly varying water consumption patterns at different nodes of the system, a test featuring one hour of random water consumption variations in all the three end-users (i.e., nodes 5u, 6u and 7u), for more than one hundred and fifty opening and closing maneuvers, is performed (test series #5). The water consumption pattern simulated in each node is definitively representative of the operations of users in pipe networks since it has been obtained by field monitoring of real users (Marsili et al., 2020, Marsili et al., 2022).

Finally, other series of tests were carried out for numerical simulation of the network in unsteady state conditions. In these tests, transients are generated directly on the network. Specifically, they are due to the complete and fast closure of a valve located at node 7 for test series #6 and #8, and at node 6 for test series #7. Moreover, the network is damaged during test series #7 with a leak at node 47. Test series #6 is used to calibrate the flow rate curve of the valve during the maneuver and the creep function parameters, whereas test series #7 is used to validate the performed calibration. Furthermore, test series #8 is used to validate the model also in the leak case. Steady-state tests were executed for evaluating the effective area of the leak at node 47 ( $C_{sv}A_{sv}=1.7E-05$ ) by means of Eq. 4.1.

**Table 4.1:** Main characteristics of some of the tests carried out at WEL.

Test series (#)	Layout	Other open sections	Discharge [ $10^{-3} \text{ m}^3/\text{s}$ ]
1 (closure at 5u)		-	$Q_{0,5u} = 0.04$ $Q_{0,5u} = 0.1$ $Q_{0,5u} = 0.2$ $Q_{0,5u} = 0.4$ $Q_{0,5u} = 0.7$ $Q_{0,5u} = 0.9$
2 (closure at 6u)		-	$Q_{0,6u} = 0.04$ $Q_{0,6u} = 0.1$ $Q_{0,6u} = 0.2$ $Q_{0,6u} = 0.4$ $Q_{0,5u} = 0.7$ $Q_{0,5u} = 0.9$
3 (closure at 7u)		-	$Q_{0,7u} = 0.04$ $Q_{0,7u} = 0.1$ $Q_{0,7u} = 0.2$ $Q_{0,7u} = 0.4$

			$Q_{0,7u} = 0.6$
			$Q_{0,7u} = 0.9$
			$Q_{0,7u} = 1.1$
4 (closure at 5u)		6	$Q_{0,5u} = 0.4$ $Q_{0,6} = 0.3$
		7	$Q_{0,5u} = 0.4$ $Q_{0,7} = 0.3$
		6, 7	$Q_{0,5u} = 0.4$ $Q_{0,6} = 0.3$ $Q_{0,7} = 0.3$
5 (random opening and closure at 5u, 6u, and 7u)		variable	variable
6 (closure at 7)		-	$Q_{0,7} = 0.3$
7 (closure at 6)		-	$Q_{0,6} = 0.1$
8 (closure at 7)		47	$Q_{0,7} = 0.3$

#### 4.5. Key quantities characterizing the network transient response

To compare different transient tests, the dimensionless pressure signal is considered:

$$h = \frac{H - H_e}{\Delta_u} \quad (4.2)$$

where  $H$  (m) is the pressure head, the subscript  $e$  indicates the end conditions achieved when the effect of the maneuver fully vanishes, and  $\Delta_u$  (m) denotes the pressure head variation generated by the maneuver at a given end-user. In Eq. 4.2, pressure head is referred to  $H_e$  since this value is more representative of the dynamics of the transient event. In fact, after the completion of the

## Chapter 4. Experimental data collection programme

maneuver, pressure oscillates around  $H_e$  which represents the end state, or the new steady-state, of the system, that can be also very far from the pre-transient conditions. Moreover, in order to capture the propagation of  $\Delta_u$  in the network, the dimensionless first pressure variation,  $\delta$ , is evaluated as:

$$\delta = \frac{\Delta}{\Delta_u} \quad (4.3)$$

with  $\Delta$  = first pressure variation at a given measurement section. Finally, to point out the most stressed part of the network, not only during the first characteristics time but along time, the instantaneous hoop stress, given by the classical Mariotte formula ( $= \frac{HD\gamma}{2e}$ ) is considered, with  $\gamma$  = liquid specific weight. More precisely, to take into account the whole time-history of the pressure variations,  $|H - H_e|$ , to which is subjected each measurement section, the cumulative value of the hoop stress,  $\sigma$ , is calculated as:

$$\sigma = \sum_t \frac{|H - H_e| D\gamma}{2e} \quad (4.4)$$

with  $t$  = time elapsed since the beginning of the manoeuvre.

## 5. Consumption change-induced transients in a water distribution network

This chapter corresponds to the research paper:

Meniconi, S., **Maietta F.**, Alvisi, S., Capponi, C., Marsili, V., Franchini, M., Brunone, B. (2022). Consumption change-induced transients in a water distribution network: Laboratory tests in a looped system. *Water Resources Research*, 58, e2021WR031343. DOI: 10.1029/2021WR031343.

### 5.1. Introduction

The wide experimental program, already described in chapter 4 is analyzed to understand the dynamic response of the system to transients caused by a change in water consumption. As mentioned, to emphasize such a response, transients are generated by the complete and fast closure of an end-user, located at the downstream end of a service line. In this concern, the entity of these variations and their frequency of occurrence are analyzed from two different points of view: on the water utility and user side Loganathan and Lee (2005).

During tests, the combined effect of simultaneous consumers, whose consumption is varied both deterministically and stochastically, has been analyzed. The tests allow examining the propagation of the generated pressure waves within the network for different water consumption variations, and end-user locations. The lessons learnt from the experimental results may help the water utility managers to identify the reasons for the higher frequency of occurrence and severity of faults in some specific portions of water distribution networks apparently “similar” to others where damages are less frequent and severe.

This chapter is organized as follows: the possible occurrence of cavitation in the service line and the acquired pressure signals for no-cavitating flows are

shown in Sections 5.2, and 5.3, respectively. Section 5.4 focuses on the effect of the end-user discharge variations during the first phases of the transients and along time. The combined effect of simultaneous consumers – with consumption varied both deterministically and stochastically – is highlighted in Section 5.5. Finally, conclusions are drawn in Section 5.6.

### 5.2. Occurrence of cavitation in the service line

As an example of the generated transients, Fig. 5.1 shows the pressure signals (i.e., the time-history of the pressure head),  $H$ , acquired during test series #1, with  $Q_{0,5u} = 0.1$ , and  $0.7 \times 10^{-3} \text{ m}^3/\text{s}$  at four sections, considered as exemplary: the downstream end section of the service line (Fig. 5.1a), junction 5 (Fig. 5.1b), the connections in series 6 and 7, in the first (Fig. 5.1c) and second loop (Fig. 5.1d), respectively. It is worthy pointing out that in all figures of Sections 5.2 and 5.3, each line refers to a different flow-rate at the end-user. As highlighted in Fig. 5.1a, for both the discharges most of the incident pressure wave is reflected back by junction 5 with a negative sign. Then it doubles at the now closed user, whereas very small amplitude wave propagate into the network (Figs. 5.1b, 5.1c, and 5.1d). Specifically, for the largest value of the discharge, the pressure ranges between  $-10.33 \text{ m}$  and  $118 \text{ m}$  in the service line, and between  $15 \text{ m}$  and  $30 \text{ m}$  in the network. In other words, according to Lee et al. (2012), Fig. 5.1a confirms the risk of the occurrence of the water column separation in the service line, but not in the main pipes. This implies that for  $Q_{0,5u} = 0.7 \times 10^{-3} \text{ m}^3/\text{s}$  (with cavitation), the pressure signal at the measurement section 5u exhibits a quite different dynamics (Cannizzaro and Pezzinga, 2005) with respect to the test for  $Q_{0,5u} = 0.1 \times 10^{-3} \text{ m}^3/\text{s}$  (without cavitation). The depressurization generated by large users can pose severe problems in the service line: not only the generation of vapor bubbles or water column separation, as for  $Q_{0,5u} = 0.7 \times 10^{-3} \text{ m}^3/\text{s}$ , but also the possible intrusion of contaminants – e.g., Collins et al. (2012).

### 5.3. Pressure signals for no-cavitating flows

To analyze a larger range of no-cavitating flows, the pressure signals acquired during test series #3 are taken into account (Fig. 5.2). Specifically, Fig. 5.2a confirms that, also at the end-user 7u, the pressure variation generated by the maneuver gets trapped into the service line. In fact, this branch is overexcited since most of the pressure wave incident at junction 7 is reflected back. However, it does not achieve cavitating conditions, even for higher consumption variations, as it happens for test series #1. This difference is mainly due to the fact that node 7 is a multiway junction connecting three pipes instead of four, as for junction 5. Consequently, the transmitted waves towards the network

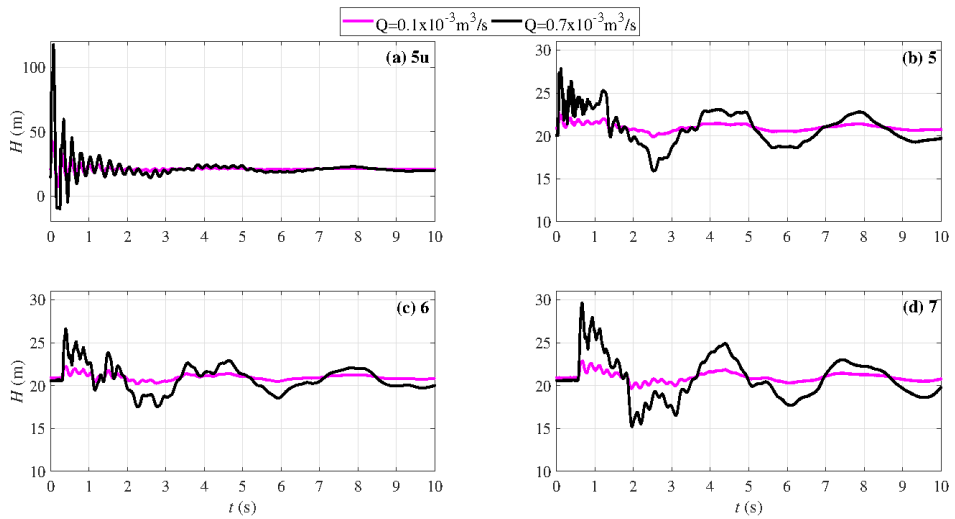


**Fig. 5.1:** Test series #1 – pressure signals for  $Q_{0,5u} = 0.1$  and  $0.7 \times 10^{-3} \text{ m}^3/\text{s}$  acquired at nodes: (a) 5u, (b) 5, (c) 6, and (d) 7.

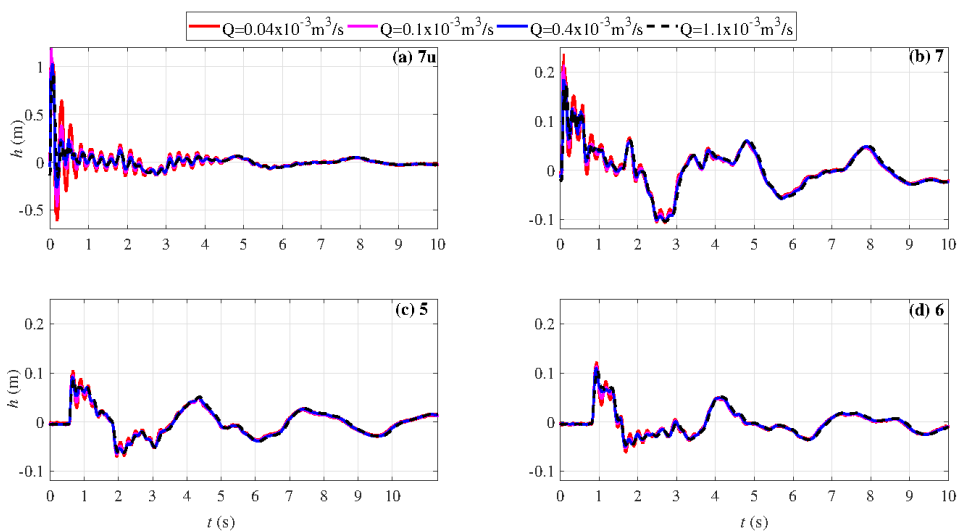


**Fig. 5.2:** Test series #3 – dimensionless pressure signals for  $Q_{0,7u} = 0.04, 0.1, 0.4, 1.1 \times 10^{-3} \text{ m}^3/\text{s}$  acquired at nodes: (a) 7u, (b) 7, (c) 5, and (d) 6.

are larger – since the energy is diverted into less paths – and the reflected one towards the service line is smaller. Indeed, the transmitted pressure waves are about 23% and 10% of the incident pressure wave for test series #3 and #1, respectively, whereas the reflected one is 77% and 90%. However, as it will be discussed below, for both the layouts, the most stressed part of the network is the one at nodes 7 (reported in Fig. 5.2b) and 8 (not shown for the sake of shortness). Such a result is corroborated by an in depth analysis carried out both in the short and long terms with regard to the dimensionless first pressure variation,  $\delta$  and the cumulative hoop stress,  $\sigma$ , respectively, that will be discussed in the next sections.

In addition, it has been numerically verified (on the basis of the numerical model explained in Chapter 7 and not shown for the sake of brevity) that this result is also valid for slower maneuvers of the order of a fraction of a second (Marsili et al., 2022).

### 5.4. Effect of the end-user discharge change

#### 5.4.1. Transient response of the network during the first phases

In order to explain more clearly the mechanism of propagation inside the network of the pressure wave generated by maneuvers at the end-user, in Fig. 6.1, the behavior of  $\delta$  at most of the measurement sections in the network is shown. First, for a given measurement section, a clear dependence of  $\delta$  on the consumption has not been observed. This confirms the fact that during the first phase of the transients the topology of the network prevails on the system hydrodynamics. Second, for a given test series, the most excited section is node 7. This result does not surprise for test series #3 where the maneuver is carried out at 7u: node 7 is the first node reached by  $\Delta_u$  (Fig. 6.1f). For test series #1, and #2, such a feature can be ascribed to the particular topology of the system (uniform material and length of the loop pipes). As highlighted in Figs. 6.1d and 6.1e, this is due to the almost simultaneous arrival of different pressure waves at node 7. Third, a global analysis of the three test series in the short term suggests that the most excited scenario is the one where the maneuver is carried out at node 7u. On the one hand, comparing series #1 and #3, this is due to the already mentioned simpler shape of junction 7 with respect to junction 5: a larger amplitude pressure wave does enter into the network. On the other hand, this remark cannot explain the different behavior of test series #2 and #3, since junctions 6 and 7 have the same shape. However, it is worthy pointing out the crucial role of the ratio between the main pipe cross sectional areas connected to the service line, and the service line itself, for a given pipe material: the smaller this ratio – i.e., the higher the pipe impedance ratio =  $a/(gA)$ , with  $A$  = pipe area – the larger the transmitted pressure wave

(Swaffield and Boldy, 1993, Bohorquez et al., 2020b). This is the reason why series #3 experiences the largest range of the no-cavitating flow in the service line.

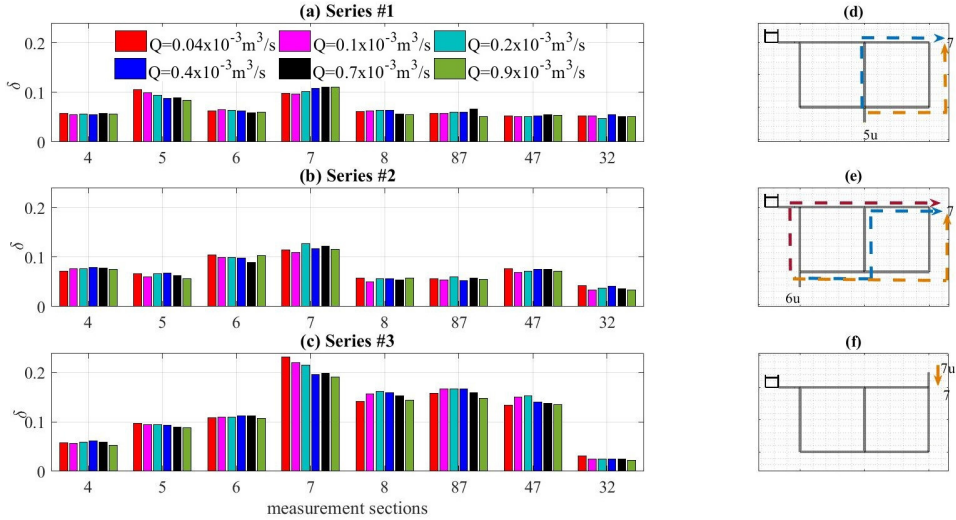


**Fig. 5.3:** The dimensionless first pressure variation at the measurement sections,  $\delta$ , for different  $Q_{0,yu}$  and the propagation of the pressure wave generated by the maneuver towards node 7 for: (a) and (d) test series #1, (b) and (e) test series #2, and (c) and (f) test series #3.

### 5.4.2. Transient response along time

To better emphasize the effect of the discharge along time, the cumulative hoop stress given by Eq. (4.4) is evaluated for pressure signals of Figs. 5.2 and reported in Figs. 5.4. As expected, the larger  $Q_{0,7u}$ , the larger the stress. It is worth pointing out that nodes 5 (Fig. 5.4c) and 4 (not shown for the sake of shortness) are quite similar in terms of stress. However, the closer the node to the tank, the smaller the stress (see, for example, node 6 in Fig. 5.4d) with node 32 (not shown) the least excited because of the damping effect due to the tank. Finally, for a given discharge, it should be noted that the most stressed part of the system is the one with the smallest pipe diameters (i.e., nodes 7 – shown in Fig. 5.4b and 8 – not shown), and not the one in the close proximity of the end-user  $7u$  (and then the service line). The reason of this important result will be explained in the following. In order to pinpoint the most excited part of the network in the successive phases of the transients, in Fig. 5.5 the values of the hoop stress achieved at the end of the transient,  $\sigma_e$ , are evaluated for all the series. The analysis of this figure offers two comments, in line with

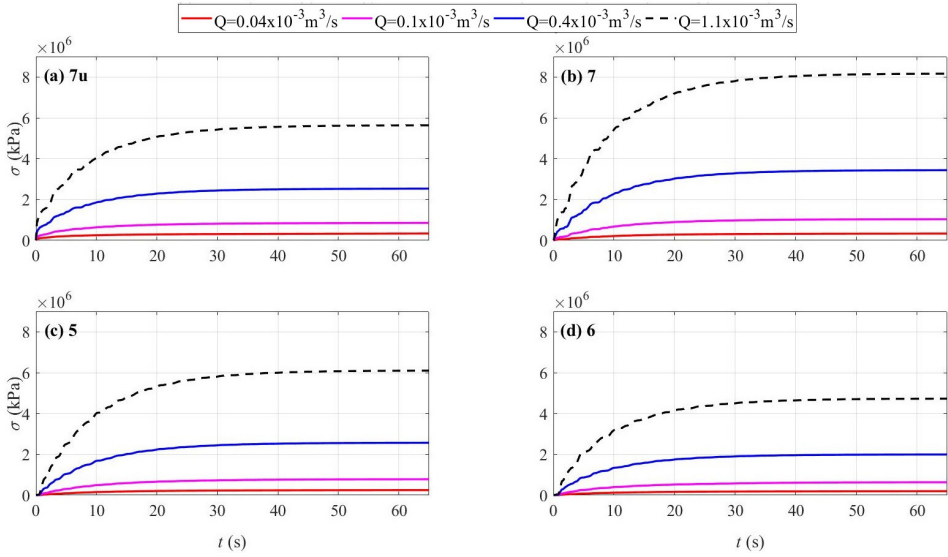


**Fig. 5.4:** Test series #3 – time-history of the cumulative hoop stress,  $\sigma$ , for  $Q_{0,7u} = 0.04, 0.1, 0.4, 1.1 \times 10^{-3} \text{ m}^3/\text{s}$  acquired at nodes: (a) 7u, (b) 7, (c) 5, and (d) 6.

the results already mentioned. Firstly, in all the measurement sections, the extreme values of  $\sigma_e$  are achieved in series #2, and #3. Precisely, the smallest values are attained in series #2 (Fig. 5.5b) because of the proximity of the transient generation point to the tank that damps the pressure waves. On the contrary, the largest values occur in series #3 (Fig. 5.5c), since the generation point is located not only far away from the tank, but also in the portion of the network with the smaller diameter pipes. Secondly, in line with this remark, for all the test series, the most excited portion of the main network is the one with smaller diameter pipes (i.e., nodes 7 and 8), regardless of where the transient is generated. This can be explained by the fact that larger amplitude pressure waves enter in such pipes but smaller amplitude ones exit. In other words, in a contraction, the transmitted wave is larger than the reflected one and the vice-versa happens in an enlargement. The so called “head accumulation” – already tested in Bohorquez et al. (2020b) but in a single pipe (with a connection in series) for transients generated in the larger diameter pipe (low impedance) – happens also in a WDN for transients generated in the downstream end section of a service line.

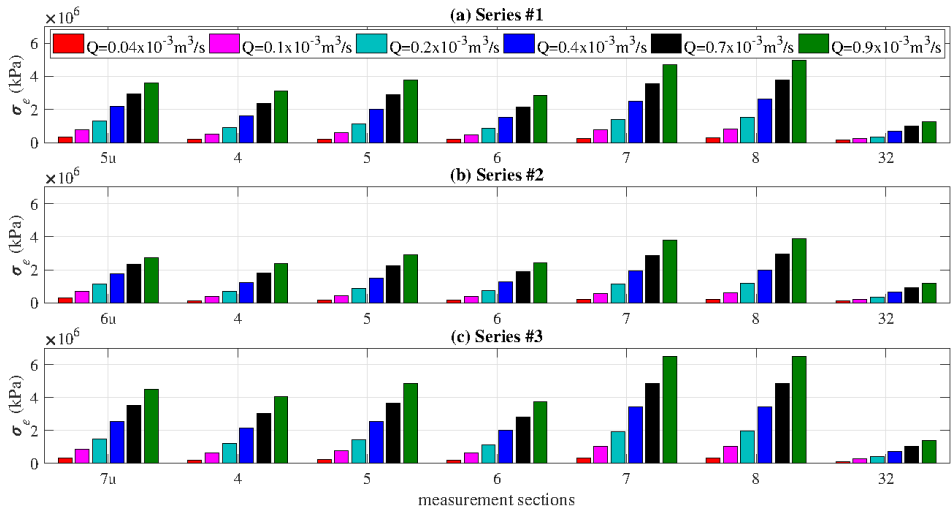


**Fig. 5.5:** (a) Test series #1, (b) test series #2, and (c) test series #3 – the end value of the cumulative hoop stress,  $\sigma_e$ , at the measurement sections for different discharge variations.

## 5.5. Combined effect of simultaneous consumers

### 5.5.1. Effect of deterministic water consumption variations

In order to better understand the combined effect of further consumers, test series #4 of Table 4.1 has been carried out and compared with those of test series #1. In series #4, transients are generated by the fast and total closure of the end-user 5u, as for series #1, but with users still active at connections 6 or/and 7 (hereafter, referred to as users 6 or/and 7, for the sake of brevity). The dimensionless pressure signals are reported in Fig. 5.6, for a given consumption variation,  $Q_{0,5u} (= 0.4 \times 10^{-3} \text{ m}^3/\text{s})$ . The larger the consumption at the users 6 or/and 7, the smaller the pressure variations in all the measurement sections. In fact, total reflection does not occur at the active users that do not behave as a dead end, where pressure variations double. Moreover, for a given discharge,  $Q_{0,6} = Q_{0,7} (= 0.3 \times 10^{-3} \text{ m}^3/\text{s})$ , the damping of the pressure waves is larger when the user 7 is active with respect to the case of the active user 6. This feature is justified by the already mentioned key role of the portion of the network with smaller diameter pipes, that amplifies the reflection of the pressure waves. Such a behavior is confirmed by the time-history of the hoop stress of tests of Fig. 5.6, shown in Fig. 5.7: the larger the total consumption through the users 6 or/and 7, the less stressed the network, as well as the service line. Moreover, it is clear that, for a given consumption, the location of the active user is crucial. In fact, the stress in the whole network is smaller when user 7

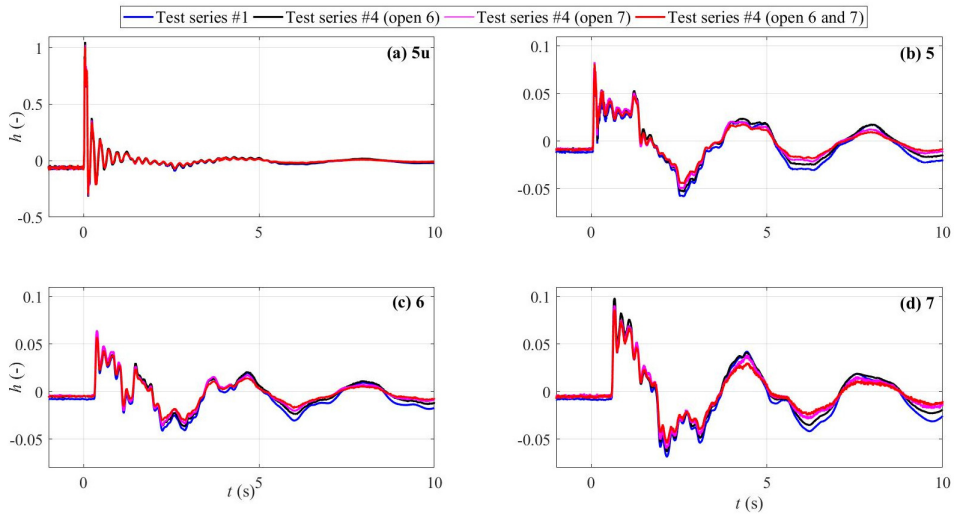


**Fig. 5.6:** Test series #1 (with  $Q_{0,5u} = 0.4 \times 10^{-3} \text{ m}^3/\text{s}$ ) vs. test series #4 – dimensionless pressure signal,  $h$ , at nodes: (a) 5u, (b) 5, (c) 6, and (d) 7.

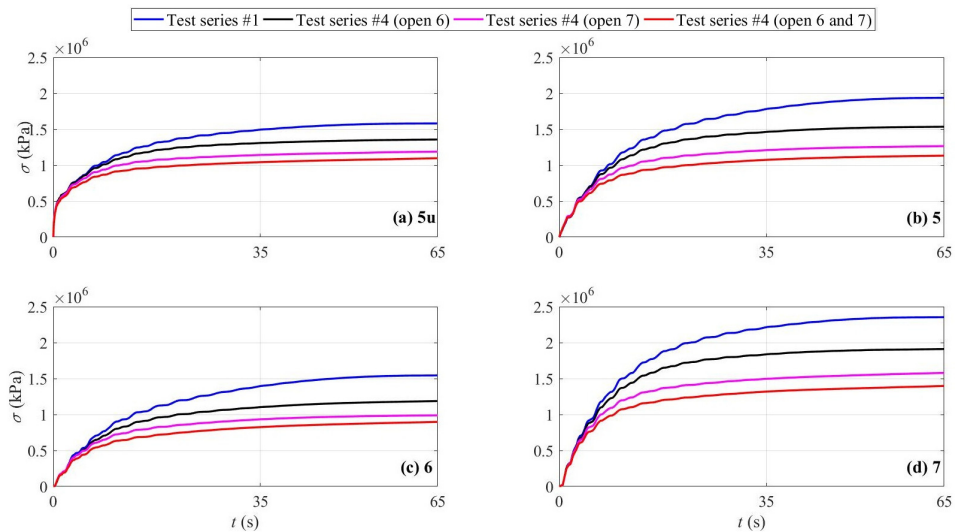


**Fig. 5.7:** Time-history of the cumulative hoop stress,  $\sigma$ , at sections: (a) 5u, (b) 5, (c) 6, and (d) 7 for test series #1 (with  $Q_{0,5u} = 0.4 \times 10^{-3} \text{ m}^3/\text{s}$ ) vs. test series #4.

is active. Finally, even if the network is open, in any case the most excited part of the network still remains the one with the smaller diameters (as an example, node 7 in Fig. 5.7d).

### 5.5.2. Effect of random water consumption variations

In test series #5, the transient behavior of the laboratory DMA is checked considering one hour of random water consumption variations in all the three end-users (i.e., nodes 5u, 6u and 7u), for a total of more than one hundred and fifty opening and closing maneuvers, according to the field monitoring of real users (Marsili et al., 2020, Marsili et al., 2022). More specifically, the water consumption variations, imposed at the three end-users, are equivalent: each end-valve is set to generate a water consumption variation of  $0.2 \times 10^{-3} \text{ m}^3/\text{s}$ , when all the other end-users are closed. Furthermore, the same pattern, but opportunely offset, is imposed at each end-user. The resulting cumulative hoop stress in all measurement sections is reported in Fig. 5.8. Such a plot confirms that the most stressed part of the network is the one with the smallest diameter pipes (nodes 7 and 8): along time, such a part becomes more stressed than the service lines themselves (nodes 5u, 6u, and 7u).

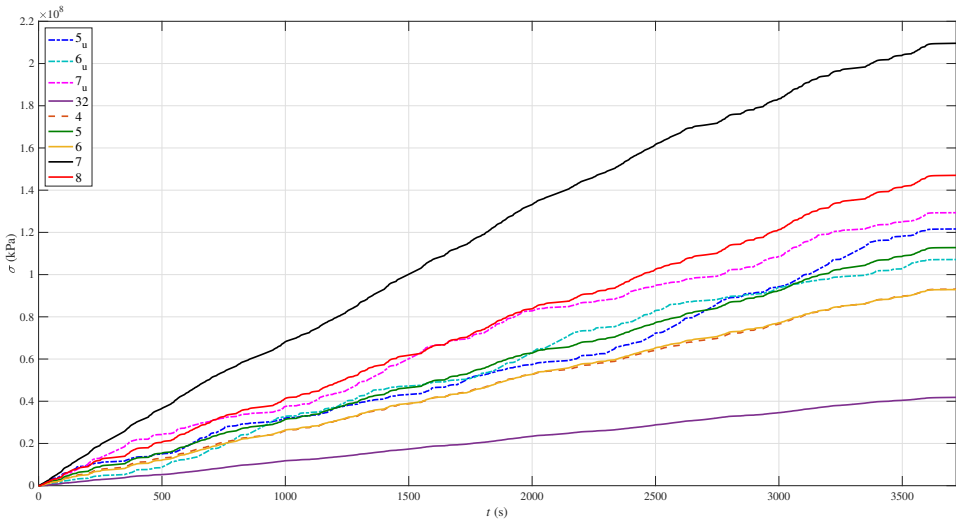


**Fig. 5.8:** Series #5: time-history of the cumulative hoop stress,  $\sigma$ , at all measurement sections.

## 5.6. Conclusions

The carried-out tests emphasize the dynamic response of the system and enable highlighting the mechanism of interaction of pressure waves with the network components.

Transients differ in the entity of the water consumption variation, location and number of the active end-users.

The major findings of this study are as follows:

- the tests show that the service lines are overexcited and cavitation can occur particularly when the discharge in the service line is large (Fig. 5.1);
- cavitation does not occur when the service connection differs less in diameter from the nearby pipes, as for junction 7 (Fig. 5.2);
- the larger the water consumption at the end-users is, the larger the pressure variations (Fig. 5.1), and the more stressed both the service line and the main pipes are (Fig. 5.4);
- the most stressed part of the WDN is the one with the smaller diameters regardless of where the transient is generated when the water consumption varies both deterministically (Fig. 5.5) and stochastically (Fig. 5.8);
- the active end-users behave like pressure relief valves that dampen the transient events (Fig. 5.6);
- for a given consumption, the largest transient pressure damping occurs when consumers are located in the part of the network with the smallest diameter pipes (Fig. 5.6);
- the most severe transients occur when there are no further end-users consuming water beyond the one where the maneuver is carried out (Fig. 5.7).

The lessons learnt from such findings may help the water utility managers to identify the possible reasons of the higher frequency of occurrence and severity of faults in some specific parts of WDNs apparently “similar” to other parts where damages are less frequent and severe. The first reason could be the occurrence of severe consumption change due to the activity of important users during the night when large parts of the network are almost inactive. The second reason could be the repetitive and fast maneuvers (not necessarily severe) especially when they are carried out in the night (see above). The third reason could be the percentage of small diameter pipes. Moreover, the higher the diameter gradient, with respect to the nearby pipe diameters, the larger the head accumulation (i.e., the progressive exaltation of the pressure waves). Such findings can help the water utility managers to better understand the WDN behavior in the view of its transient response: a larger number of leaks/faults is

expected in areas with large consumers in the night or in the network with regular fast maneuvers carried out in the night, in areas with the smallest diameters and a higher diameter gradient with respect to the nearby pipe diameters.

## 6. The most vulnerable areas of a water distribution network due to transients generated in a service line

This chapter corresponds to the research paper:

Meniconi, S.; **Maietta F.**; Alvisi, S.; Capponi, C.; Marsili, V.; Franchini, M.; Brunone, B. (2022). A Quick Survey of the Most Vulnerable Areas of a Water Distribution Network Due to Transients Generated in a Service Line: A Lagrangian Model Based on Laboratory Tests. *Water* 2022, 14, 2741. DOI: 10.3390/w14172741.

### 6.1. Introduction

This chapter analyses the propagation and mechanisms of interaction of a pressure wave in a looped water distribution network by means of laboratory and numerical tests. Specifically, the analysis executed by means of a Lagrangian model (LM) highlights the effect of the network topology and the location of the transient generation point but in a more expeditious way with respect to the use of a complete transient model. By means of the refined LM – which is able to capture the pressure extreme values occurring in the first phases of the transient – the most excited part of the network will be localized and explained, and the vulnerability maps of the network are provided. Such maps identify the nodes subjected to the most severe pressure waves in terms of both frequency and amplitude. The exposure level to transients of each node is synthesized by the value of the vulnerability index proposed.

A description of the experimental setup and the preliminary tests executed to characterize the end-user and service line are described in chapter 4. For the

## Chapter 6. The most vulnerable areas of a water distribution network due to transients generated in a service line

sake of clarity, Table 6.1 lists the tests of Table 4.1 considered in this chapter.

**Table 6.1:** Main characteristics of the executed laboratory tests.

Test No. (#)	Layout	Maneuver Type	Discharge [ $10^{-3}$ m <sup>3</sup> /s]
1	service line at node 5	Total closure of 5u	$Q_{0,5u} = 0.1$
2	service line at node 6	Total closure of 6u	$Q_{0,6u} = 0.1$
3	service line at node 7	Total closure of 7u	$Q_{0,7u} = 0.1$

The organization of this chapter is as follows. The effect of the network topology and the transient generation point is highlighted and discussed in Sections 6.2 and 6.3, respectively. Successively, a procedure for implementing the map of vulnerability that points out the parts of the network more exposed to transient effects, is described. Finally, conclusions are drawn in Section 6.5.

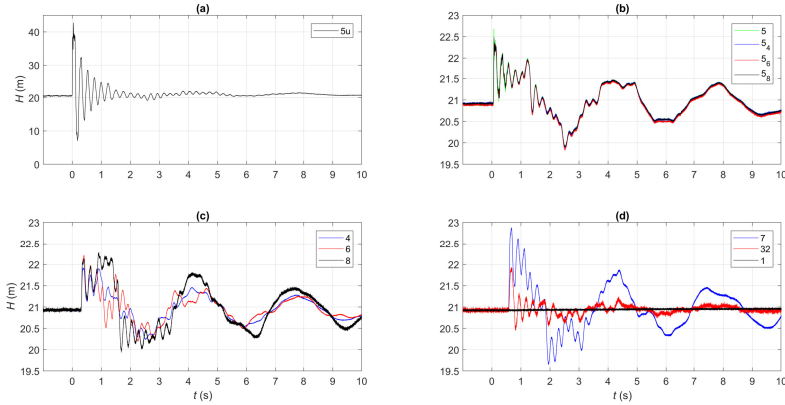
### 6.2. The Effect of the Network Topology

Figure 6.1 shows the pressure signals,  $H$ , acquired during test #1; in this figure,  $t = 0$  indicates the manoeuvre starting time. Figure 6.1a highlights that at 5u the pressure variation due to the manoeuvre becomes trapped into the branch. Thus, the service line is overexcited since most of the incident pressure wave is reflected back by junction 5, whereas very small pressure waves propagate into the network.

Figure 6.1b reports the pressure signals acquired at the measurement sections in the proximity of junction 5: nodes 5, 5<sub>4</sub>, 5<sub>6</sub>, and 5<sub>8</sub> of Figure 4.4. According to Lee (2015), because of the overlapping of the incident and reflected pressure waves, these signals are almost indistinguishable; their extreme values are smaller than the ones measured at the end-user 5u (Figure 6.1a). Such a feature reflects the fact that node 5, located at the upstream-end of the service line, experiences the same pressure variations occurring at 5u only for an extremely short time interval – and, then, not acquirable – because of the proximity of the junction.

Successively, the transmitted pressure waves arrive at the closest nodes 4, 6, and 8. The pressure signals of Figure 6.1c point out that the pressure variation at node 4 is slightly smaller than the ones at nodes 6 and 8, whereas the damping of the pressure peaks is quite similar at nodes 4 and 6, but smaller at node 8. The pressure signals at the measurement sections 7 and 32 and at the upstream tank (node 1) are reported in Figure 6.1d. The first pressure wave arriving at node 7 is significantly larger than all the other ones, whereas node 32 is the least stressed one because of its proximity to the tank.

**Chapter 6. The most vulnerable areas of a water distribution network due to transients generated in a service line**



**Fig. 6.1:** Test #1—pressure signals acquired at measurement sections: (a) 5u; (b) 5, 5<sub>4</sub>, 5<sub>6</sub>, and 5<sub>8</sub>; (c) 4, 6, and 8; (d) 7, 32, and 1. Note that to highlight the pressure variations into the network, the y-axis of (b–d) is significantly reduced with respect to the one at 5u (a).

Figure 6.2 shows one of the paths travelled by the pressure wave generated at end-user 5u: at 5u (Figure 6.2a); at junction 5, connecting the service line to the network (Figure 6.2b); at the two measurement sections along the pipe connecting this junction to node 4: 5<sub>4</sub> (Figure 6.2c) — 1 m from junction 5 — and 45 (Figure 6.2d) — 69.3 m from junction 5; at junction 4 (Figure 6.2e); at the measurement section 47 — 28.5 m from junction 4 (Figure 6.2f); and finally at connection 7 (Figure 6.2g).

In this figure, the pressure variations due to the maneuver,  $\Delta_m$ , are also highlighted, with the subscript  $m$  indicating the measurement section. In Figure 6.2a,  $\Delta_{5u}$  ( $=18.01$  m) occurs at  $t = t_{5u} = 0$ . At junction 5,  $\Delta_{5u}$  is reduced by about 90 % because of the already mentioned interaction at this junction, resulting in quite a small pressure variation at  $t_5 = 0.05$  s ( $\Delta_5 = 1.78$  m in Figure 6.2b) and  $t_{5_4} = 0.053$  s ( $\Delta_{5_4} = 1.42$  m in Figure 6.2c). Successively, this pressure wave arrives at node 45 at  $t_{45} = 0.219$  s, with  $\Delta_{45} = 1.28$  m (Figure 6.2d). Then, at  $t_4 = 0.307$  s,  $\Delta_{45}$  interacts with junction 4, causing a smaller pressure variation ( $\Delta_4 = 0.99$  m in Figure 6.2e). In fact, part of the pressure wave is reflected back toward junction 5, and part is transmitted toward nodes 7 and 3. The transmitted pressure wave arrives at nodes 47 and 7 at  $t_{47} = 0.384$  s (Figure 6.2f), and  $t_7 = 0.577$  s (Figure 6.2g), respectively. Moreover, the amplitude of the transmitted pressure wave  $\Delta_{47}$  ( $=0.92$  m) is unexpectedly amplified at node 7 ( $\Delta_7 = 1.75$  m). Such a rise cannot be ascribed to the geometrical and mechanical characteristics of node 7 that is a connection in series between two DN50 equivalent pipes. On the contrary, it can be associated to the almost simultaneous arrival of different pressure waves, as it will be clarified below. To better explain such a behavior, the LM is used. In Figure 6.3,

**Chapter 6. The most vulnerable areas of a water distribution network due to transients generated in a service line**

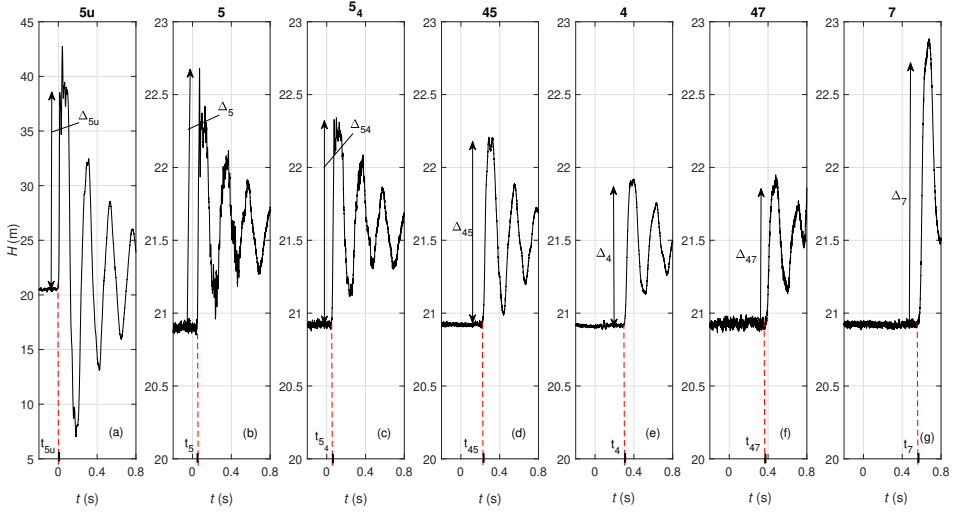


**Fig. 6.2:** Test #1—one of the paths of the generated pressure wave of Figure 6.1 in the network—pressure signals at measurement sections: (a) 5u; (b) 5; (c) 5<sub>4</sub>; (d) 45; (e) 4; (f) 47; and (g) 7.

the results of the LM are compared to the experimental pressure disturbances,  $H - H_0$ , at some of the measurement sections (black lines). The blue stems represent the pressure waves given by the LM (i.e., the impulse response function),  $\Delta H_n$ , whereas the red lines depict the LM simulation,  $H_n - H_{n,0}$ . Figure 6.3b shows that the excitation at junction 5 is almost twice as the one at the end-user 5u (Figure 6.3a). In fact, the reflection coefficient at junction 5,  $C_{R,5}$ , is equal to  $-0.93$ , for a pressure wave arriving from 5u. In other words, the incident pressure wave is always followed by a reflected one with approximately the same amplitude but opposite sign. The transmitted pressure wave at junction 5 reaches the closest sections (junction 4 and connections 6 and 8). However, while these pressure waves cross undisturbed connections 6 (Figure 6.3d) and 8 (Figure 6.3e), with  $\Delta H_{n,8} = \Delta H_{n,6} = 1.19$  m, junction 4 (Figure 6.3c) causes a reflection and a smaller resulting pressure variation ( $H_{n,4} - H_{n,4,0} = 0.97$  m). In addition, the first experimental pressure variation at node 8,  $\Delta_8 (=1.13$  m), is smaller than the one at node 6,  $\Delta_6 (=1.17$  m), because of the larger friction losses along a DN50 pipe with respect to a DN75 one. Moreover, at connection 7 the close arrival of the two pressure waves transmitted at junction 4 and 8 causes the mentioned large pressure variation (Fig. 6.3f). Finally, because of the interaction with junction 3, the simultaneous arrival of the pressure waves from connection 6 and junction 4 at the measurement section 32 (Figure 6.3g) causes a smaller global pressure variation ( $H_{n,32} - H_{n,32,0} = 1.06$  m).

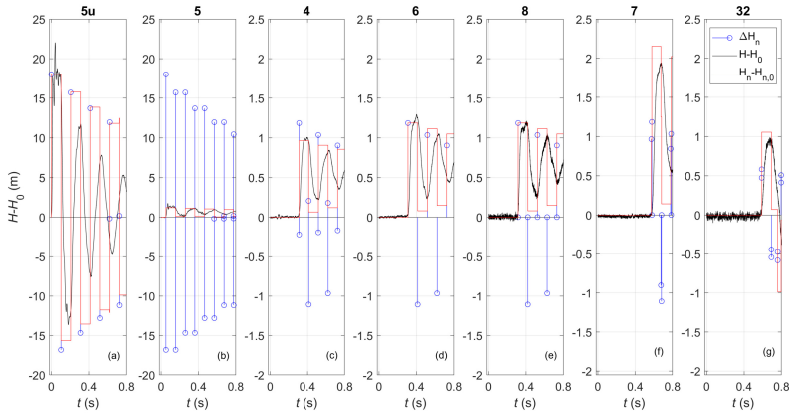


**Fig. 6.3:** Test #1—experimental pressure disturbances,  $H - H_0$ , vs. the impulse response function,  $\Delta H_n$  (blue stems), and numerical reconstruction,  $H_n - H_{n,0}$  (red line), carried out by the Lagrangian model (LM) at measurement sections: (a) 5u; (b) 5; (c) 4; (d) 6; (e) 8; (f) 7; and (g) 32.

### 6.3. The Effect of the Transient Generation Point

In order to point out the effect of the transient generation point on the dynamic behavior of the network, transients generated by the closure of the end-users at 6u (test #2) and 7u (test #3) are compared with test #1. In particular, Figure 6.4 compares the pressure signals acquired at the main nodes among those of Figure 6.1 with the ones of tests #2 and #3 for a given steady-state discharge ( $Q_{0,5u} = Q_{0,6u} = Q_{0,7u} = 0.12$  L/s). Specifically, Figure 6.4a highlights that, even if the maneuver is the same, during the first phases of the transient, the service line is more excited when the maneuver is executed at the end-user 5u. In fact, as confirmed by the LM results (Figures 6.3 and 6.5),  $C_R$  at the junction that connects the service line to the network is larger in absolute terms in the case of a cross junction (as node 5 with  $C_{R,5} = -0.93$ ) than a Y junction (as node 6, with  $C_{R,6} = -0.92$  and node 7, with  $C_{R,7} = -0.83$ ). The value of  $C_{R,7}$  is smaller than the one of  $C_{R,6}$ , because of the smaller diameters of the pipes connected to the junction. Thus, this means that for test #3, larger pressure waves are transmitted from node 7 towards the network (Figure 6.4f vs. Figure 6.4d,e). Moreover, the LM confirms that in the first phases of all the considered tests the most stressed part of the network is that with the smallest diameter pipes: nodes 7 and 8 (Figure 6.4f,g).

### 6.4. Maps of Vulnerability by the Lagrangian Model (LM)

The extreme values of the pressure variations are reached in the first phases of the transients. As shown, in such a period, the LM can be considered a good compromise between the computational efforts (quite limited) and its reliability.

## Chapter 6. The most vulnerable areas of a water distribution network due to transients generated in a service line

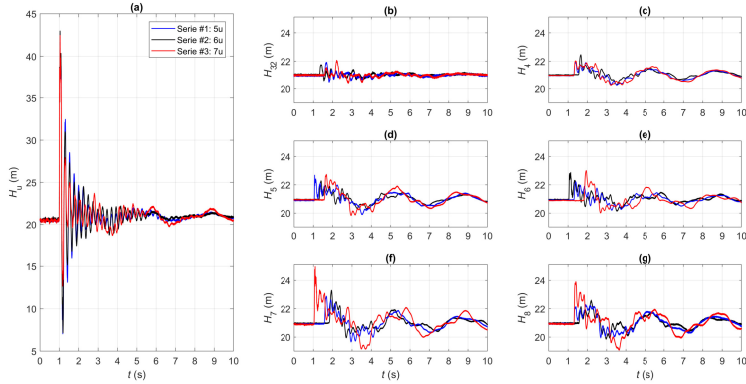


**Fig. 6.4:** Pressure signals acquired during tests #1 (blue lines), #2 (black lines), and #3 (red lines) with  $Q_{0,5u} = Q_{0,6u} = Q_{0,7u} = 0.12$  L/s at measurement sections: (a) end-user (5u/6u/7u); (b) 32; (c) 4; (d) 5; (e) 6; (f) 7; and (g) 8.

Accordingly, it allows pinpointing the most excited part of the network in the first period. The substantial limitation of the LM—i.e., the fact that it does not simulate the damping of the pressure waves—does not appear decisive. In fact, with respect to transmission mains in a WDN, it makes less sense to assume that the boundary conditions and related flow condition last for a long period of time. In fact, as demonstrated in Marsili et al. (2022), because of the users' behavior, flow conditions change so frequently that a stochastic approach is needed. In this context, the frequency distribution,  $f$ , of the numerical relative amplitude of the pressure waves,  $\delta$ , defined as:

$$\delta = \frac{|\Delta H_{n,m}|}{\Delta H_{AJ}} \quad (6.1)$$

has been evaluated for all measurement sections  $m$ , by considering pressure variations  $\delta$ , larger than a given value,  $\delta^*$ ; in Equation (6.1)  $\Delta H_{AJ}$  is the Allievi–Joukowski overpressure. Figure 6.6—where it has been assumed, as an example,  $\delta^* = 4\%$ —shows the frequency distribution, with a uniform width of 4 %, of the histogram bins. In particular, the largest values of  $\delta$  occur for the service line: the start node (5) and end node (5u) behave equivalently, with  $\delta$  being 10 times larger than all the other sections in the network. This confirms the results of the laboratory tests. However, the frequency of these large pressure variations is quite limited, with  $f = 2$  for  $\delta \geq 50\%$ . To emphasize the behavior of the network nodes, a magnified vision of the frequency distribution for  $4\% \leq \delta \leq 8\%$  is reported in Figure 6.6b–f. As already pointed out, the network is less excited than the service line. Moreover, the smaller the diameter, the larger the frequency: the maximum value of  $f$  ( $=15$ ) is achieved at nodes 7 and 8, whereas it is  $f = 0$  at node 32. This frequency distribution is used to synthesize the transient response of the system: both the frequency of

Chapter 6. The most vulnerable areas of a water distribution network due to transients generated in a service line

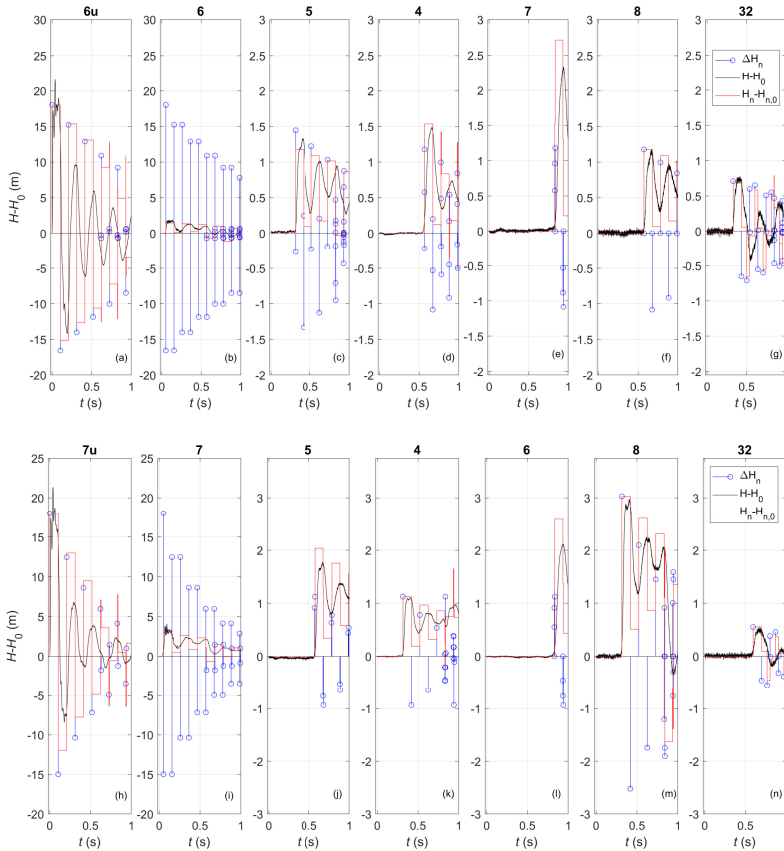


**Fig. 6.5:** Tests #2, and #3—experimental pressure disturbances,  $H - H_0$ , vs. the impulse response function,  $\Delta H_n$ , (blue stems) and numerical reconstruction,  $H_n - H_{n,0}$ , (red line) carried out by the Lagrangian model (LM) at measurement sections: (a) 6u; (b) 6; (c) 5; (d) 4; (e) 7; (f) 8; and (g) 32, for test #2, and (h) 7u; (i) 7; (j) 5; (k) 4; (l) 6; (m) 8; and (n) 32, for test #3.

## Chapter 6. The most vulnerable areas of a water distribution network due to transients generated in a service line

occurrence of a specific  $\delta$ , and the amplitude of  $\delta$  are taken into account in the vulnerability index,  $\nu$ , defined as:

$$\nu = \sum_i f_i \delta_i \quad (6.2)$$

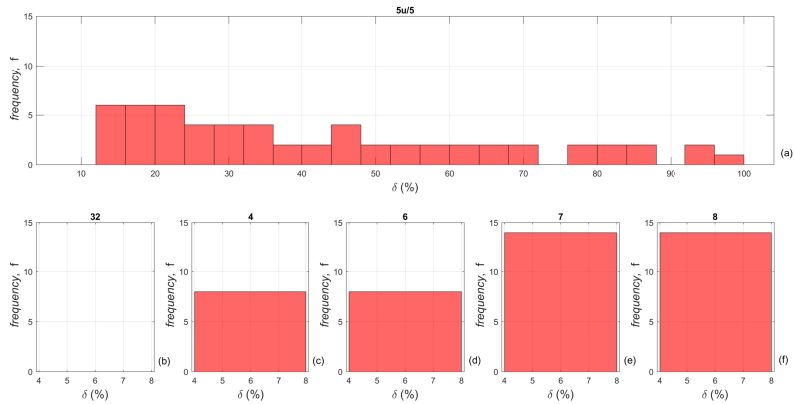


**Fig. 6.6:** Frequency distribution of the relative amplitude of the pressure waves given by the LM for test #1 at measurement sections: (a) 5u and 5; (b) 32; (c) 4; (d) 6; (e) 7; (f) 8.

For all nodes of the network, the map of vulnerability is provided for the configurations of tests # 1, 2, and 3 (Figure 6.7), based on the values of  $\nu$ . The aim of these maps is to quickly identify the areas where the impact of transients is expected to be the largest and that may therefore require particular attention, in terms, as an example, of high-frequency pressure monitoring. As expected, according to the experiments, in all configurations the most stressed area is the service line. Moreover, the more complex the junction and the larger the diameter of pipes connected to the junction, the larger  $\nu$ . Finally, for all the tests, the most excited portion of the main network is the one with smaller diameter pipes (i.e., nodes 7 and 8), regardless of where the transient is generated.

### 6.5. Conclusions

In recent years, the idea that the effect of transients in water distribution networks is not negligible is gaining ground in the management of such systems. This is due to two main reasons. The first one is the more and more frequent occurrence of not negligible transients, due to the unavoidable users' consumption variations and daily pump or automatic valve operation for system management. All these events, difficult to suppress or prevent by the water utilities, can lead to the deterioration of the system safety and long-term life

Chapter 6. The most vulnerable areas of a water distribution network due to transients generated in a service line

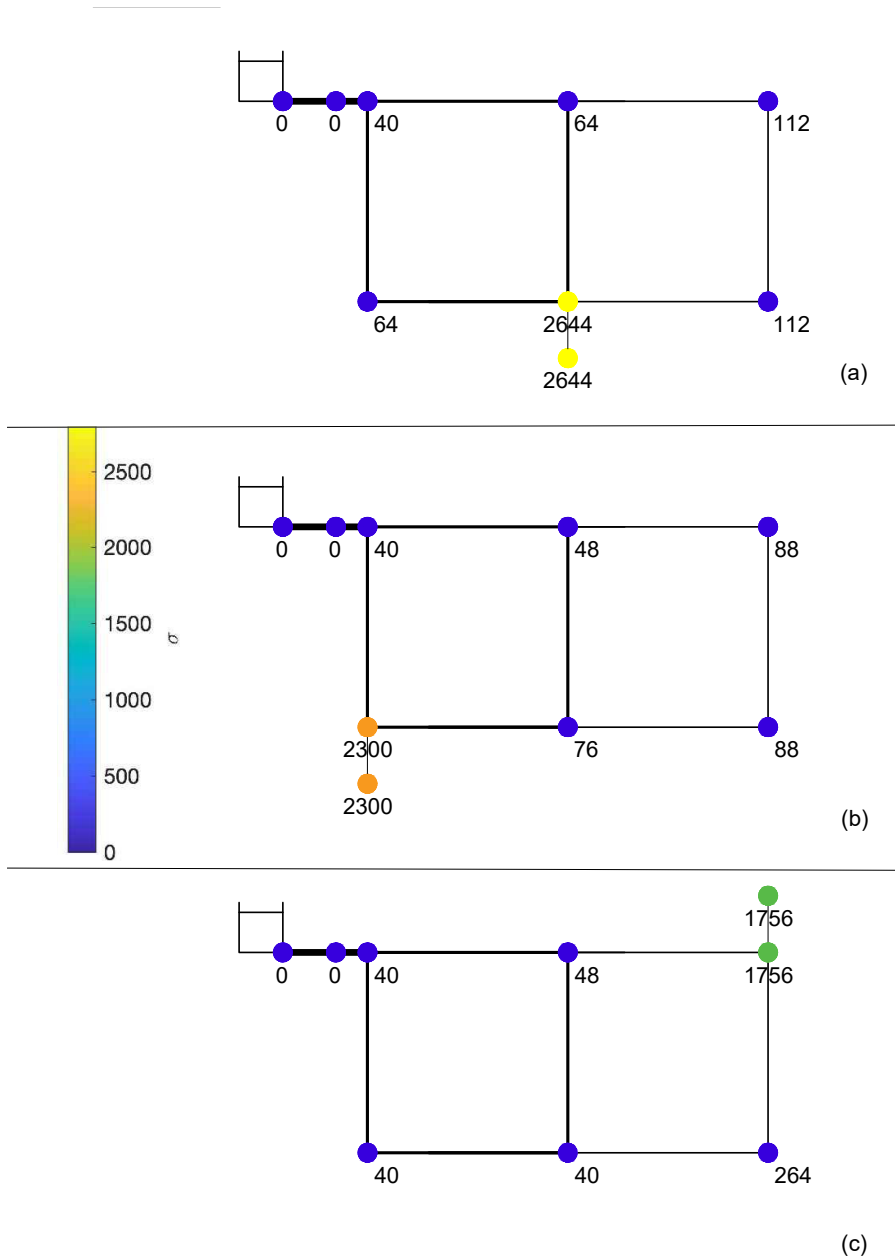


**Fig. 6.7:** Map of vulnerability evaluated by the LM for tests: (a) #1; (b) #2; and (c) #3; respectively (numbers at nodes indicate the value of the index of vulnerability,  $V$ ).

## Chapter 6. The most vulnerable areas of a water distribution network due to transients generated in a service line

cycles. In fact, the conventional surge protection devices (e.g., air vessel) are usually installed in the main pipes. The second reason is the fact that the steady-state modelling and low-frequency monitoring (i.e., of the order of  $10^{-3}$  Hz) do not allow identifying the causes of leakage and faults occurring in only some parts of the network substantially equal to other ones in terms of pipe material, maintenance, and pressure regime. A possible explanation of such a feature could derive from an inappropriate identification of the nature of the actually dangerous transients and the different exposure to pressure waves of the different parts of the considered network.

This work experimentally analyses the effects of a transient simulating an end-user closure in a looped water distribution network. The the end-user located at the downstream end section of a quite long service line allows capturing each single pressure wave inserted into the network. The experimental tests and the successive analysis by means of a Lagrangian model highlights the effect of the network topology and the location of the transient generation point, but in a more expeditious way with respect to the use of a complete transient model. The assumption of the Lagrangian model of neglecting the friction terms and maneuver duration does not limit its use for interpreting the dynamic response of the system in the first phases of the transients.

In particular, the tests point out that the most excited part of the system is the one in close proximity of the end-user and then the corresponding service line. In fact, the generated pressure wave becomes trapped in the service line because of the severe reflection from the junction that connects the service line to the network.

In addition, when different pipe materials are considered, the general results could be considered analogous (not shown for the sake of brevity). In fact, even if the metallic pipes have a stronger compressive capacity than the plastic ones, a pressure variation in a metallic pipe generated by a given water consumption change is much larger (about double) than the one generated in a plastic pipe with the same diameter.

Furthermore, notwithstanding the transient generation point, the pressure waves entering into the network are 80–90% smaller than the generated one and accumulate in the parts of the network with the smallest diameter pipes. To demonstrate that the obtained results are not dependent on the chosen layout, the distribution of DN50 and DN75 pipes has been changed and revised, and the indexes of vulnerability have been evaluated. As an example, Figure 6.8 shows the map of vulnerability, when the maneuver has been executed at node 5u. The results confirm that the service line is overexcited, and the smaller the diameter, the larger the pipe vulnerability, with the larger values of  $\nu$  occurring at nodes 3, 4, and 6 that are in this case the junctions connecting the smallest diameter pipes.

It is worth pointing out that not the entity but the frequency of such waves could be potentially risky for infrastructure safety through fatigue loading. In

## Chapter 6. The most vulnerable areas of a water distribution network due to transients generated in a service line

other words, the regular occurrence of pressure transients (even if small) could contribute to the degradation of pipe materials, pipeline accessories, pipe support, and instrument failures (e.g., Starczewska et al., 2015b).

In conclusion, by means of the Lagrangian model, which has been verified to be able to capture the pressure extreme values occurring in the first phases of the transient, the vulnerability maps of network are provided. These maps identify the nodes subjected to the most severe pressure waves in terms of both frequency and amplitude. The level of exposure to transients of each node is synthesized by the value of the vulnerability index proposed in this work. Such an outcome could be of paramount importance for system maintenance and management and to address appropriate guidelines for fault prevention.

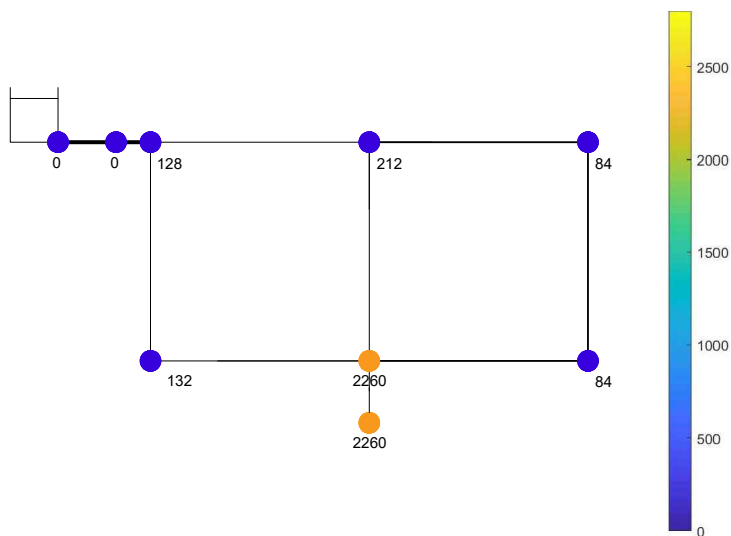


**Fig. 6.8:** Map of vulnerability evaluated by the LM for a numerical test equivalent to test #1, but with a diameter distribution reversed with respect to the laboratory layout (numbers at nodes indicate the value of the index of vulnerability,  $V$ ).

## 7. Hydraulic transient solver calibration in a water distribution network

The current chapter is based on the following scientific publication:

Covas D.I., **Maietta F.**, Cabral M., Meniconi S., Capponi C., Brunone B. (2022) Hydraulic Transient Solver Calibration in a Viscoelastic Pipe Network: Lessons Learnt. Proceedings of the 39th IAHR World Congress. Granada (Spain), doi:10.3850/IAHR-39WC2521711920221665 (ISBN: 978-90-832612-1-8).

### 7.1. Introduction

A transient solver for pressurized water pipe is important to better understand the dynamic behaviour of a system, both under normal conditions (e.g., manoeuvres in valves, start-up or shut-down of pumps and turbines) and under occasional emergency situations caused by failure of the electrical power grid (pump or turbine stoppage) or by sudden pipe bursts (Koelle and Almeida, 1991; Chaudhry, 2014; Wylie and Streeter, 1993). The transient pressure waves, generated by different operational conditions, are reflected in singularities of the system (e.g., valves, tee junctions, leaks) and transport information on their location and size. This information can be very useful for a better understanding of the current condition of valves (e.g., Meniconi et al., 2011a), the presence of blockages (Che et al., 2019; Duan et al., 2017; Jing et al., 2018; Louati et al., 2018; Meniconi et al., 2013b; Meniconi et al., 2016; Zouari et al., 2020), the existence and location of leaks and bursts (Brunone et al., 2021; Meniconi et al., 2021a; Pan et al., 2022), the presence of entrapped air pockets (Alexander et al., 2020; Eldayih et al., 2020; Ferreira et al., 2021) and also the existence of pipe connections (Meniconi et al., 2011d; Meniconi et al., 2018; Pan et al., 2022).

Several techniques can be used for the detection and location of those features that can be based on time analysis (Brunone, 1999), wavelet analysis (Beck et al., 2006; Ferrante et al., 2007; Srirangarajan et al., 2013), artificial neural networks (Ayati et al., 2022; Bohorquez et al., 2020a; Capelo et al., 2021; Guo et al., 2021; Hu et al., 2021; Wang et al., 2021) and inverse engineering (Blocher et al., 2020; Choura et al., 2021; Covas and Ramos, 2010; Soares et al., 2011).

Inverse transient techniques require the use of reliable and calibrated transient solvers as well as of an optimization algorithm (Covas, 2003; Covas and Ramos, 2010; Pudar and Liggett, 1992). The calibration process involves the estimation of values of a set of non-measurable parameters, such as manoeuvres of valves (opening-time), friction (pipe roughness), elastic wave speed, leak sizes and the creep behaviour of plastic pipes. The inverse approach can also be used for calibration as long as the optimization algorithm includes those parameters to be determined. Many authors have used inverse engineering for leak detection and viscoelastic effect calibration in single pipes, but there are very few studies regarding its application in pipe networks with several loops using real data (e.g. Fathi-Moghadam and Kiani, 2020).

The current chapter aims at the calibration of main parameters in hydraulic transient solvers in a multi-pipe system with viscoelastic pipes using inverse analysis and at the discussion of the main uncertainties associated with the calibration.

In the detail, a transient solver developed for pressurized water pipe networks incorporating unsteady friction and pipe wall viscoelasticity is used. The most relevant parameters are calibrated: the valve initial opening and time-manoeuve, the elastic wave speed, the unsteady friction and the Kelvin-Voigt (K-V) parameters associated with the pipe wall viscoelastic behaviour function. The calibration of the Kelvin-Voigt parameters is carried out using an inverse transient solver incorporating the Levenberg-Marquardt optimization technique. Additionally, pressure signals are collected in an experimental high-density polyethylene pipe network assembled at the Water Engineering Laboratory of the University of Perugia, Italy.

A description of the experimental setup, simulating a District Metered Area (DMA), and the preliminary tests carried out to characterize the end-user, the service line and the leaks are described in Chapter 4. Table 7.1 presents the set of tests depicted in Table 4.1 that are analysed in this chapter, in which the location of the valve and the initial steady-state discharge are indicated.

**Table 7.1:** Main characteristics of the laboratory tests.

Test series (#)	Layout	Maneuver Type	Leak	Discharge [ $10^{-3} \text{ m}^3/\text{s}$ ]
1	service line at 5u	closure of 5u	-	$Q_{0,7u} = 0.1$
6	no service line	closure of 7	-	$Q_{0,5u} = 0.3$
7	no service line	closure of 6	-	$Q_{0,6u} = 0.1$
8	no service line	closure of 7	47	$Q_{0,7u} = 0.3$

The organization of this chapter is as follows. A brief description of the Inverse Transient Solver is presented in Section 7.2. The hydraulic model construction and calibration are described in Section 7.3. Hydraulic model calibration and validation for the no leak case and hydraulic model validation for the one leak case (in different locations) are discussed in Sections 7.4 and 7.5, respectively. Subsequently, the procedure is carried out for a new network layout in no leak case (Section 7.6). Finally, conclusions are highlighted in Section 7.7.

## 7.2. Forward and inverse solvers

A hydraulic transient solver developed for multipipe systems is used for the simulation of transients (hereafter, referred to as Forward Transient Solver, FTS). This solver is based on the continuity and the momentum equations that describe one-dimensional transient flow in pressurised pipes (Eqs. 3.16 and 3.4) and integrates additional terms to describe unsteady friction and pipe wall viscoelasticity (Covas, 2003; Covas et al., 2004b, Covas et al., 2004c, Covas et al., 2005). The steady-state component of friction losses is calculated by Eqs. 3.7 or 3.8 for turbulent and laminar flow, respectively. The viscoelastic behavior of the pipe is described by the Kelvin-Voigt mechanical model (Covas, 2003). The retarded strain time-derivative  $\frac{\partial \varepsilon_r}{\partial t}$ , is calculated by the sum of the strain time-derivative of each Kelvin-Voigt element  $k$ ,  $\frac{\partial \varepsilon_{rk}}{\partial t}$  by Eq. 3.29. This equation depends on the strain of each Kelvin-Voigt element  $k$ ,  $\varepsilon_{rk}$ , that is described by Eq. 3.30.

An Inverse Transient Solver (ITS) has been implemented and used for the calibration of several parameters using collected transient pressure data. Parameter identification is an optimization problem in which the system's behavior is simulated by the FTS and the difference between observed and calculated variables is minimized by means of an optimization model integrated in the ITS (Covas and Ramos, 2010).

The ITS includes an optimization algorithm that searches for the best-fitted solution by minimizing the average least-square errors (LSEs) between observed

and calculated variables:

$$MinOF(p) = \frac{1}{M} [q^* - q(p)]^T [q^* - q(p)] = \frac{\sum_{i=1}^M [q_i^* - q_i(p)]^2}{M} \quad (7.1)$$

in which  $OF(p)$  = objective function;  $p$  = parameter-vector with  $N$  variables;  $q(p)$  = predicted system response vector (with  $M$  elements) for a given parameter vector  $p$ ;  $q^*$  = the observation-vector (with  $M$  elements), whose elements are measured heads;  $M$  = number of measurements. Observed data are pressure measurements.

Different optimisation techniques can be used to search for the best-fitted solution in the ITS. Two optimisation algorithms were implemented in the ITS: Genetic Algorithms and Levenberg-Maquardt.

The genetic algorithms (GA) are global search methods that seek the solution in the variable space: however, these methods can not be carried out for a local search due to limitations in the operators used (e.g. mutation). The advantages of GA over traditional search methods are: (i) conservation of a population of well-adapted sample points and then increasing the chance of reaching the global optimum, (ii) probability rules for the transition from one set of trial solutions to the next, and (iii) flexibility, since these methods admit many types of objective functions without requiring the continuity and existence of their derivatives (Soares et al., 2011).

The Levenberg–Maquardt (LM) algorithm is an iterative technique that locates a local minimum of a function that is expressed as the sum of squares of several nonlinear real-valued functions. It has been widely used for dealing with data-fitting applications, such as nonlinear Least Square Error (LSE) problems. When the current solution is close to a local minimum, LM algorithm shows fast convergence, once the initial values are accurate enough. However, it works with only function evaluations and gradient information (Jacobian matrix) and it estimates the Hessian matrix using the sum of the outer products of the gradients. The main disadvantages of the LM method are the need for the calculation of gradients and matrix inversion as part of the update process and, also, depending on the nature of the optimization problem to be solved, can be stuck in a local minimum solution (Soares et al., 2011).

### 7.3. Hydraulic model construction and calibration

#### 7.3.1. Main steps

The hydraulic model of the system describes the transient pressure variations in a pressurized pipe given a set of initial and boundary conditions. The construction and calibration of the model is a procedure characterized by several steps and requires the estimation of several parameters, as described and discussed

in Carriço et al. (2016). The most relevant parameters of the transient solver are the valve initial opening and the time-manoeuvre, the elastic wave speed, unsteady friction (very important in elastic pipes) and the Kelvin-Voigt parameters associated with the pipe wall viscoelastic behaviour function (in plastic pipes).

The main steps are:

- i) definition of the pipe-system layout;
- ii) calibration of the valve manoeuvre;
- iii) calculation of the elastic wave speed;
- iv) definition of the unsteady friction model and calibration of model parameters, in the case of elastic pipes;
- v) definition of the unsteady friction model and of the values of the respective parameters (if these exist) and calibration of the K-V parameters in the case of viscoelastic pipes.

These steps are presented and illustrated in the following sections.

### 7.3.2. Definition of the pipe-system layout

The definition of the pipe-system layout (step i) consists of the clear establishment of all relevant link-elements (e.g., reservoirs, tanks, pumps, valves, pipes) defined between two extreme nodes connecting. Also, additional pipes and nodes can be added to create intermediate nodes associated with potential locations of leaks or transducers. Each link-element and node should be characterized by a different identifier (e.g., pipe 1, pipe 2, . . . , node 1, node 2, . . . ). In the cases considered, the system layout is composed of one tank, one valve (representing the two inline valves), 17 pipes and 17 nodes in Test series #6, #7 and #8; whereas in Test series #1, the system layout has 18 pipes and 18 nodes. Initially, Test series #6 is used for calibration purposes with the transient generated by the closure of valve 7-9 (Figure 7.1).

### 7.3.3. Calibration of the valve initial opening and the valve manoeuvre

The first step in the FTS calibration is the adjustment of valve manoeuvre (step ii). This calibration corresponds to the calculation of the initial percentage of opening,  $\tau$ , for a given valve diameter, or alternatively, the adjustment of the diameter of a fully open valve in order to deliver the measured flow rate. In the present study, the last procedure is used: the real valve diameter is 4 mm, whereas the calibrated diameter is 4.25 mm for a ball valve fully open that discharges 0.27 L/s. The flow in the pipes is considered laminar for pipes with

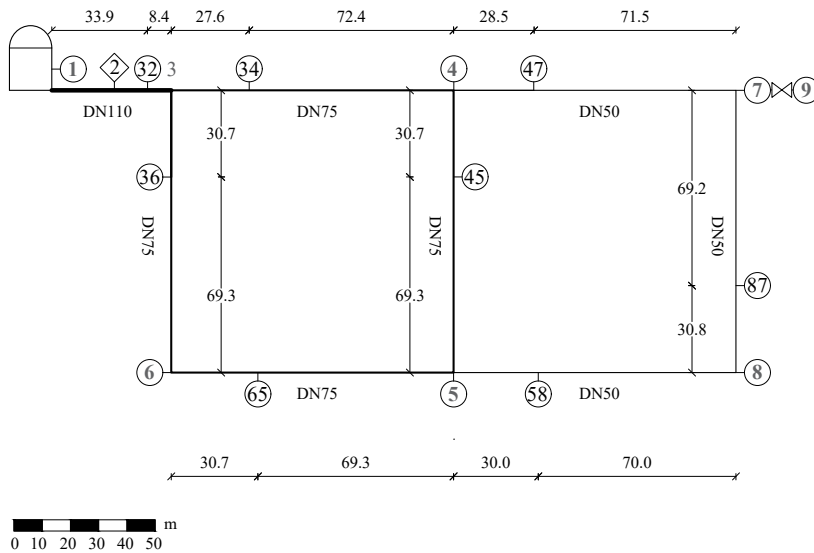


**Fig. 7.1:** Schematic representation of the pipe rig for Test series #7.

initial  $Re < 2000$ ; otherwise, it is considered turbulent in a smooth-walled pipe. In the latter case, the Blasius formula is used for the calculation of steady-state friction.

The initial flow rate regime is established in all pipes (Figure 7.2): 63% of the flow rate follows the shortest path (nodes 3-4-7), which has ca. 200 m, whereas 37% follows the longest way (nodes 3-6-5-8-7), with ca. 400 m. The results show that mean velocities and Reynolds numbers are very low in this network and for the analysed set of tests (Table 7.2).

**Table 7.2:** Initial values of Darcy.

Pipe	$\lambda_s$	$Q(L/s)$	$V(m/s)$	$Re$
1-2	0.039	0.027	0.039	3682
2-32	0.039	0.027	0.039	3682
32-3	0.039	0.027	0.039	3682
3-34	0.038	0.169	0.053	3373
34-4	0.038	0.169	0.053	3374
4-45	0.040	0.001	0.000	20
45-5	0.040	0.001	0.000	22
5-65	0.032	-0.101	-0.031	-2009

65-6	0.032	-0.101	-0.031	-2008
6-36	0.032	-0.101	-0.031	-2009
36-3	0.032	-0.101	-0.032	-2012
4-47	0.038	0.168	0.118	5031
47-7	0.038	0.168	0.118	5033
7-87	0.036	-0.102	-0.071	-3045
87-8	0.036	-0.102	-0.072	-3047
8-58	0.036	-0.102	-0.072	-3048
58-5	0.036	-0.102	-0.072	-3050
7-9	0.036	0.270	0.039	3682

The manouvre is described by the percentage of valve opening with time. Knowing the valve discharge head law and the pressure-head at the upstream end of the valve end, the valve opening is determined. Results are presented in Figure 7.3.

The manouvre is described by a tri-linear manoeuvre. Note that a fitted valve law could be incorporated in the FTS, however, the input data file only allows the definition of pairs of points opening-time, which are sufficient for calibration.

#### 7.3.4. Calculation of the elastic wave speed

The estimation of the elastic wave speed values,  $a_0$ , is carried out experimentally, by measuring the travel time of the pressure wave generated by the maneuver. The preliminary tests performed to determine the wave speed are described in Chapter 4. Estimated values are 398.82, 387.89 and 379.81 m/s for pipes DN110, DN75 and DN50, respectively.

The obtained values are compatible with the geometrical and mechanical characteristics of the pipes.

#### 7.3.5. Calibration of the viscoelastic pipe behaviour and model validation

For the experimental layout, consisting of high-density polyethylene (HDPE) pipes, the effects of unstable friction are neglected. Therefore, as observed in previous research (Covas et al., 2005, Meniconi et al., 2012a, Meniconi et al., 2012b, Pezzinga et al., 2014, Pezzinga et al., 2016) the pipe wall viscoelastic effect is predominant over friction effects.

Before proceeding with the calibration of the pipe wall viscoelasticity, two simulations are carried out. The first simulation uses only a classic transient solver without unsteady friction and viscoelasticity. The second one uses the creep function determined by (Covas et al., 2004b; Covas et al., 2004c). Obtained numerical results are compared with collected data at three different nodes –

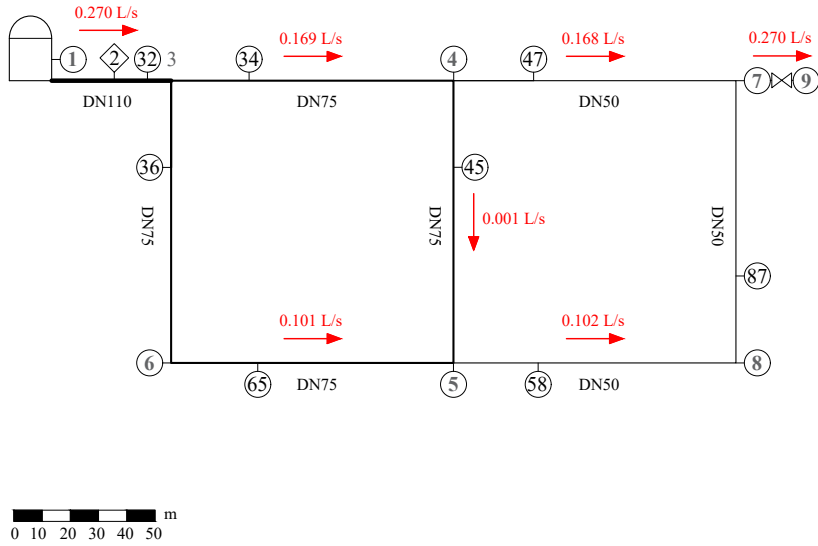


Fig. 7.2: Distribution of the initial flow rate values in the looped pipe system.

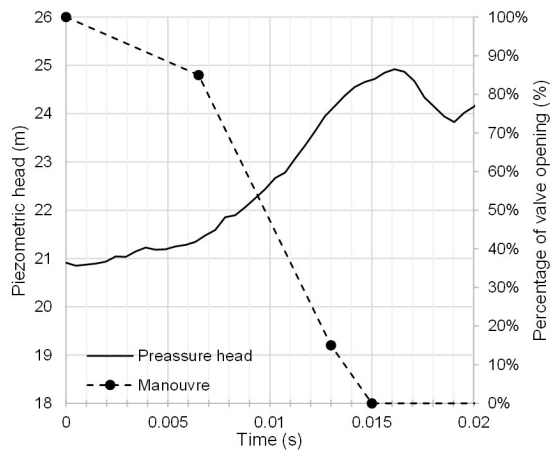


Fig. 7.3: Test series #7 – Calibrated valve manoeuvre.

immediately upstream of the valve, at an intermediate section of the network and at the upstream end (node 32). Later, the inverse transient solver is used for the calibration of the Kelvin-Voigt parameters (step v) associated with the pipe wall viscoelastic creep function. The Levenberg-Marquardt technique is used for driving the optimization and then, once the K-V parameters are obtained, the numerical simulations are carried out using the wave speed values determined experimentally.

Finally, the calibrated valve manoeuvre and creep function parameters are then validated.

The results of the calibration of the viscoelastic pipe behavior and model validation for the cases considered in this chapter are shown separately in the following sections.

### 7.4. Hydraulic model calibration and validation for test series #6

The calibration of the pipe wall viscoelasticity for test series #6 is carried out considering two simulations. Firstly, without considering unsteady friction and viscoelasticity, and later using the creep function determined by (Covas et al., 2004b; Covas et al., 2004c).

A comparison of the numerical results with collected data at three different nodes (node 7, immediately upstream of the valve; node 5, intermediate section; node 32, upstream end) is shown in Figure 7.4 and Figure 7.5. Simulation results obtained by the classic transient solver (Figure 7.4), highlight a major disagreement both in terms of pressure-head amplitude and phase. On the other hand, simulation results before calibration of viscoelasticity and the wave speed (Figure 7.5) highlight a reasonable agreement when the creep function of the HDPE of the Imperial College pipes is used, though with some discrepancies since the used creep function was obtained for a different pipe system. Finally, the inverse transient solver is used for the calibration of the Kelvin-Voigt parameters (step v) associated with the pipe wall viscoelastic creep function. For this purpose, several initial numerical simulations run and several assumptions are considered: (i) the elastic wave speed in all pipes is set equal to 400 m/s; (ii) the viscoelastic behaviour of the pipes is described by three K-V elements in series, plus the elastic spring; (iii) the retarded strains are set to 0.002, 0.20 and 1.50 s, following the recommendations of (Covas et al., 2004b). The optimal values obtained for the viscoelastic parameters are  $5.19\text{E-}11$ ,  $1.05\text{E-}10$ , and  $1.41\text{E-}13$ .

The Levenberg-Marquardt technique is used for driving the optimization and then, once the K-V parameters are obtained, the numerical simulations are carried out using the wave speed values determined.

Obtained results are presented in Figure 7.6. An excellent agreement is observed between experimental data and numerical results. This highlights the

utmost importance of using the calibrated creep function in viscoelastic pipes, in particular when carrying out the diagnosis of existing problems in this kind of pipe systems. Finally, the calibrated valve manoeuvre and creep function parameters are then validated for Test series #7 (Table 7.1). In this case, the valve is located at node 6 and the initial flow rate is 0.15 l/s, whereas the valve manoeuvre and the remaining parameters are the same used for Test series #6. Results, presented in Figure 7.7, show an excellent agreement which demonstrates the robustness of the calibrated parameters (the valve manoeuvre and the creep function).

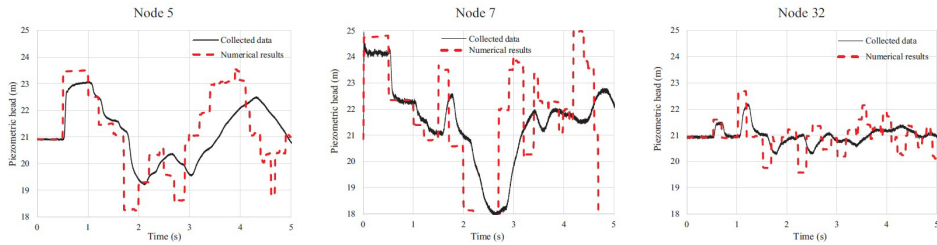


Fig. 7.4: Test series #6 – Simulation results obtained by the classic transient solver.

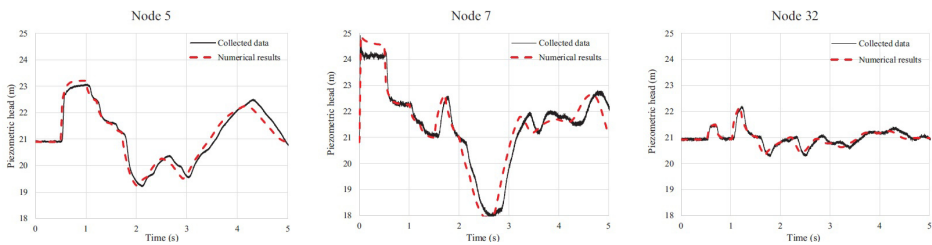


Fig. 7.5: Test series #6 – Simulation results before calibration of viscoelasticity and the wave speed.

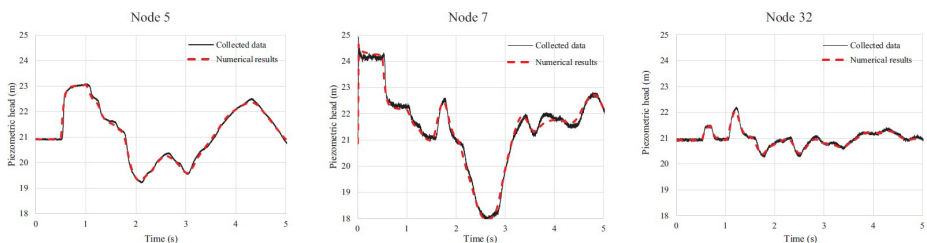
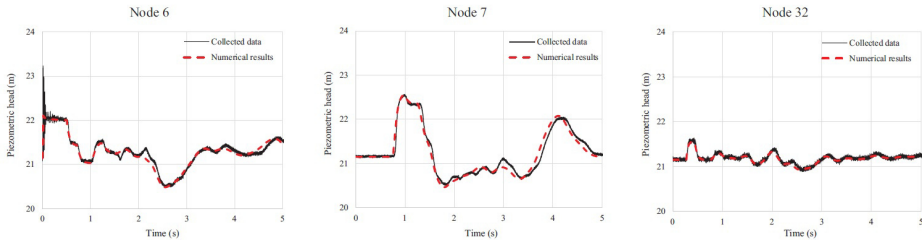


Fig. 7.6: Test series #6 – Simulation results after calibration of viscoelasticity and the wave speed.



**Fig. 7.7:** Test series #7 – Model validation. Simulation results for a different transient test.

### 7.5. Hydraulic model validation for test series #8

For the leak case (Test series #8), simulated by a discharge pipe with an opened valve, the system is calibrated by running the transient solver with the optimal coefficients values obtained for the non-leak case.

The pressure wave propagation was assumed equal to 400 m/s and transient pressure data for the initial flow rate of 0.27 L/s and leaking flow of 0.329 L/s at node 47 were used.

The effective leak area ( $C_{SV}A_{SV}$ ) was determined using leak discharges and pressure heads at node 47 for steady state flow, as shown in Chapter 4.

Results from numerical simulations have shown that the creep coefficient of the discharge pipe for the leak case was the same as the one for the non-leak case (as verified Soares et al., 2011).

Numerical results for transient pressures with the observed data at three different nodes (node 7, node 5, node 32) are presented in Figure 7.8. The viscoelastic transient solver fits extremely well with the collected pressure data, satisfactorily describing the transient pressure wave and its shape.

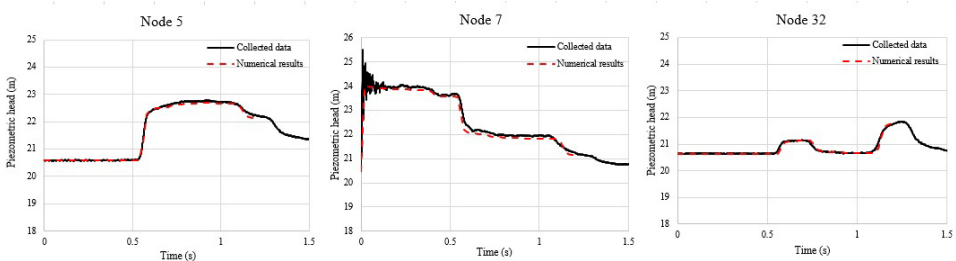


**Fig. 7.8:** Test series #8 – Simulation results after calibration of viscoelasticity and the wave speed.

### 7.6. Hydraulic model validation for test series #1

The calibrated model was validated for another configuration of the network (Test series #1), where a service line is connected to node 5. The transient solver was initially run considering the elastic wave speed of the service line (400 m/s) similar that of the main pipes (370-380 m/s) and the same K-V coefficients calibrated for the no-leak case. However, discrepancies in the numerical results and collected data were observed and it was necessary to calibrate the creep function of the service line.

Several numerical simulations were run to better describe the creep compliance function of the service line. Three Kelvin–Voigt elements were considered. The wave speed of service line was calculated (455 m/s) and considered in the simulations. Accordingly, the best combination of  $J_k$  parameters for the service line was  $1.2E-10$ ,  $5E-10$  and  $7.2E-12$  GPa $\cdot$ s, respectively, for the retardation times equal to 0.002, 0.20 and 1.50 s. This fitting was obtained considering different creep functions of the polyethylene pipes: one for the main pipes of the network and the second one for the service line. The calibrated K-V coefficients of the service line are different from those of the network pipes due to several main reasons discussed as follows.

The creep compliance function of polyethylene pipes is dependent on the polymeric material, temperature and axial and circumferential constraints of the pipes, whereas the calibrated K-V parameters rely on these characteristics as well as on the elastic wave speed, the number of K-V elements and the retardation times (Covas et al., 2004b; Covas et al., 2005). Thus, it is expectable that the calibrated K-V coefficients of the service line are different from those of the network pipes. Firstly, despite the main network pipes and the service line being made of polyethylene, the polymer may not be exactly the same and, thus, slight differences may be expected in the creep function and in respective K-V parameters. Secondly, the constraints of the pipes are different: the main pipes are installed in coils with 100 m each and the service line is a straight pipe with 23.6 m fixed at the upstream end. Finally, the calibrated K-V parameters depend on the considered elastic wave speed; since the ratios of wall thickness and inner diameter of the main pipes are different from those of the service line, the elastic wave speed and the calibrated K-V parameters are also different.

The numerical results at three different nodes (node 5u, immediately upstream of the valve; node 4, intermediate section; and node 32, upstream end) are presented in Figure 7.9. A reasonable agreement is observed when numerical results are compared with collected data, though with some discrepancies. This highlights again the importance of using the calibrated creep function in viscoelastic pipes.

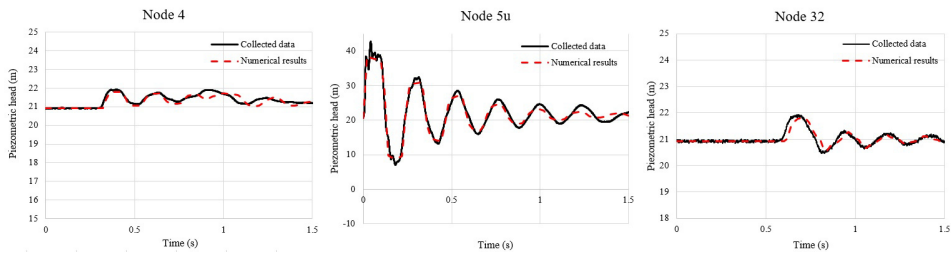


**Fig. 7.9:** Test series #1 – Simulation results after calibration of viscoelasticity and the wave speed.

### 7.7. Conclusions

A hydraulic transient solver is used for simulating transient events in a looped experimental facility assembled at the University of Perugia. Pressure data collected at three different locations are used for the calibration of the transient solver parameters, namely, the valve initial opening and time-manoevre, the elastic wave speed of the pipes and the Kelvin-Voigt parameters associated with the pipe wall viscoelastic behaviour function. The calibration of the Kelvin-Voigt parameters is carried out by an inverse transient solver.

Calibrated parameters are used to validate model results for a different transient test being obtained an excellent fitting. Additionally, they are used to validate the model for the leak case and another experimental system setup.

Main results from this calibration procedure are the following:

- (i) The first parameter to be calibrated is the valve initial opening (or the valve diameter) that, combined with the pipe friction losses, determines the initial flow rate. Though this value can be theoretically calculated based on the valve discharge law and measured pressure-head at the upstream section of the valve, it must be calibrated when using a transient solver whose valve law is not exactly the one considered or is unknown;
- (ii) The valve manoeuvre can be estimated, once again, by using the valve law and the pressure head signal. Usually, transient solvers define the valve manoeuvre as a set of points opening – time, thus, this manoeuvre has to be specified as pairs of points in the transient solver;
- (iii) The elastic wave speeds are typically obtained by the travelling time between transducers and compared with values by theoretical formulae. In elastic pipes, these correspond exactly to the pipe elastic wave speeds, whereas in viscoelastic pipes, the elastic wave speed values tend to be slightly higher than those experimentally obtained;
- (iv) The most adequate unsteady friction model should be chosen depending on the initial flow regime. For laminar flows, (Zielke, 1968) formulation

should be used; for smooth-wall flows, (Vardy and Brown, 1995) formula can be used; for turbulent flows, the acceleration-based formulas are recommendable (Brunone et al., 1991; Vítkovský et al., 2000a). For viscoelastic pipes, this component tends to be significantly lower than the viscoelastic effect and can be neglected (Duan et al., 2010);

- (v) The K-V parameters of the viscoelastic mechanical model can be calibrated by inverse engineering. This can be carried out by an inverse trial-and-error procedure or by using an optimization algorithm as illustrated herein. Three K-V elements are usually sufficient for attaining a good fitting, though the more elements are considered, the better the agreement between experimental and numerical results is;
- (vi) In the presence of a service line, which has a diameter smaller than the diameters of the pipes of the network, it is convenient to use the solver for the service line separately from the network.

Overall, results show that the most relevant parameters in hydraulic transient solvers in viscoelastic pipes are the valve manoeuvre and the viscoelastic pipe behaviour described by the elastic wave speed and K-V parameters, whereas the unsteady friction effect can be neglected and described by the calibrated creep function.

## 8. Conclusions

### 8.1. Research overview

The dynamic response of a pressure pipe network to transients caused by a change in water consumption was investigated, in both intact and damaged conditions.

A comprehensive state-of-the-art is presented in [Chapter 2](#). This review highlights the need to carry out further physical experiments on the hydraulic transients in the water pipe networks. In more detail, very few tests were executed to analyze the effect of water consumption variations in both the service line and the main pipes. Such tests also do not highlight the role of the network topology or the location of the transient generation point.

To fill this gap, an extensive experimental programme has been carried out in a polymeric pipe network with two loops assembled at the Water Engineering Laboratory (WEL) of the University of Perugia, Italy. The laboratory tests allow for isolating and understanding the nature of the transients. Instead, due to the uncontrolled changes in boundary conditions, repeatability of tests in real systems is very hard to achieve and then it is arduous to observe the effect of each cause of transients.

To point out the dynamic response of the system, transients are generated by the fast and total closure of end-users, located at the downstream end of a service line. A description of the experimental set-up, the list of the laboratory transient tests, and the key quantities that characterize the network transient response are presented in [Chapter 4](#).

A detailed analysis of the transient behaviour of the network is described in [Chapters 5 and 6](#). Specifically, the possible occurrence of cavitation in the service line, the acquired pressure signals for no-cavitating flows, the effect of the end-user discharge variations, and the combined effect of simultaneous consumers — with consumption varied both deterministically and stochastically — are highlighted in [Chapter 5](#). Moreover, the mechanism of propagation of a pressure wave in the network with one active service line but in different lo-

cations is analyzed in [Chapter 6](#). In addition, the Lagrangian Model, able to capture the extreme values of pressure in the first phases of the transient tests, is then used to create a map of the most excited parts of the network. Finally, in [Chapter 7](#) numerical simulations of pressurized pipe systems in unsteady-state conditions have been carried out, by considering both unsteady friction and pipe wall viscoelasticity, and the pipes with and without leaks. A calibration procedure has been established and an excellent agreement has been obtained.

### 8.2. Main scientific contributions

The thesis has several important scientific outcomes that will be described in the following.

In WNDs, transients can differ in the entity of the water consumption variation, location, and number of active end-users.

First, in the case of an inactive WDN (i.e., during the night), the service lines are overexcited and cavitation can occur in the service line for large outflow and severe maneuver. However, experiments show that, for a given discharge, cavitation does not occur when the difference in diameter between the service connection and nearby piping is small.

Second, the larger the water consumption at the end-users is, the larger the pressure variations and the more stressed both the service line and the main pipes are.

Third, the location of active users is not irrelevant. In fact, for a given consumption, the largest transient pressure damping occurs when consumers are located in the part of the network with the smallest diameter pipes. Moreover, tests demonstrated that the most stressed part of the WDN is the one with the smaller diameters regardless of where the transient is generated, both in the case of a WDN inactive and a WDN active.

Fourth, the most severe transients occur when there are no further end-users consuming water beyond the one where the maneuver is carried out. In fact, the active end-users behave like pressure relief valves that dampen the transient events.

The results obtained in this research work may help the water utility managers to better understand the WDNs' transient behavior and to identify the possible reasons for the higher frequency of occurrence and severity of faults in some specific parts of WDNs apparently "similar" to other parts where damages are less. The first reason could be the occurrence of severe consumption change due to the activity of important users during the night when large parts of the network are almost inactive. The second reason could be the repetitive and fast maneuvers (not necessarily severe) especially when they are carried out at night. The third reason could be the percentage of small-diameter pipes.

## Chapter 8. Conclusions

Moreover, the results of numerical simulations show that the most relevant parameters in hydraulic transient solvers in viscoelastic pipes are the valve maneuver, the elastic wave speed and K-V parameters, whereas the unsteady friction effect can be neglected.

### 8.3. Research perspectives

The research on the transient response of water distribution networks is still an ongoing topic.

Based on the work carried out, several future goals can be identified.

The main objective of future research is to make the laboratory setup at the WEL closer to a real WDN. The first upgrade option could be the installation of a device (a PRV or a variable speed pump) to verify its role during transients due to the variation of water consumption. Second, the transient response of service lines to maneuvers carried out in the main pipes (e.g., due to a pump trip) could be explored. Third, the complexity of the network could be enhanced by increasing the number of loops, or change the pipe materials. Fourth, different types of anomaly (e.g., leaks with a fixed area, as well as cracks) and constraint could be also included.

## References

- Abbasi, T. and Abbasi, S. A. (2011). Small hydro and the environmental implications of its extensive utilization. *Renewable and Sustainable Energy Reviews*, 15(4):2134–2143.
- Abdulshaheed, A., Mustapha, F., and Ghavamian, A. (2017). A pressure-based method for monitoring leaks in a pipe distribution system: A review. *Renewable and Sustainable Energy Reviews*, 69:902–911.
- Al-Khomairi, A. (2008). Leak detection in long pipelines using the least squares method. *Journal of Hydraulic Research*, 46(3):392–401.
- Alexander, J. M., Lee, P. J., Davidson, M., Li, Z., Murch, R., Duan, H.-F., Meniconi, S., and Brunone, B. (2020). Experimental investigation of the interaction of fluid transients with an in-line air pocket. *Journal of Hydraulic Engineering*, 146(3):04019067.
- Alnaimat, F. and Ziauddin, M. (2020). Wax deposition and prediction in petroleum pipelines. *Journal of Petroleum Science and Engineering*, 184.
- Amin, M. M., Hadi, A., and Ghazali, M. F. (2014). Leakage detection in pipeline using synchrosqueeze wavelet transform. *Applied Mechanics and Materials*, 465:467–471.
- Asada, Y., Kimura, M., Azechi, I., Iida, T., and Kubo, N. (2020). Transient damping method for narrowing down leak location in pressurized pipelines. *Hydrological Research Letters*, 14(1):41–47.
- Axworthy, D. and Karney, B. (1997). Efficient valve closure for slow transient pipe network models. In *BHR Group Conference Series*, pages 261–269.
- Axworthy, D. and Karney, B. (2000). Valve closure in graph-theoretical models for slow transient network analysis. *Journal of Hydraulic Engineering*, 126(4):304–309.

## References

- Ayati, A. H., Haghghi, A., and Ghafouri, H. R. (2022). Machine learning-assisted model for leak detection in water distribution networks using hydraulic transient flows. *Journal of Water Resources Planning and Management*, 148(2):04021104.
- Ayati, A. H., Haghghi, A., and Lee, P. J. (2019). Statistical review of major standpoints in hydraulic transient-based leak detection. *Journal of Hydraulic Structures*, 5(1):1–26.
- Ayed, L., Hafsi, Z., Elaoud, S., Meniconi, S., and Brunone, B. (2023). A transient-based analysis of a leak in a junction of a series pipe system: Mathematical development and numerical modeling. *Journal of Pipeline Systems Engineering and Practice*, 14(2):04023009.
- Beck, S., Curren, M., Sims, N., and Stanway, R. (2005). Pipeline network features and leak detection by cross-correlation analysis of reflected waves. *Journal of Hydraulic Engineering*, 131(8):715–723.
- Beck, S., Foong, J., and Staszewski, W. (2006). Wavelet and cepstrum analyses of leaks in pipe networks. In *Progress in Industrial Mathematics at ECMI 2004*, pages 559–563. Springer.
- Bergant, A., Ross Simpson, A., and Vitkovsk, J. (2001). Developments in unsteady pipe flow friction modelling. *Journal of Hydraulic Research*, 39(3):249–257.
- Blocher, C., Pecci, F., and Stoianov, I. (2020). Localizing leakage hotspots in water distribution networks via the regularization of an inverse problem. *Journal of Hydraulic Engineering*, 146(4):04020025.
- Blokker, E., Vreeburg, J., and Dijk, J. (2010). Simulating residential water demand with a stochastic end-use model. *Journal of Water Resources Planning and Management*, 136(1):19–26.
- Bohorquez, J., Alexander, B., Simpson, A. R., and Lambert, M. F. (2020a). Leak detection and topology identification in pipelines using fluid transients and artificial neural networks. *Journal of Water Resources Planning and Management*, 146(6):04020040.
- Bohorquez, J., Lambert, M. F., and Simpson, A. R. (2020b). Identifying head accumulation due to transient wave superposition in pipelines. *Journal of Hydraulic Engineering*, 146(1):04019044.
- Brunone, B. (1999). Transient test-based technique for leak detection in outfall pipes. *Journal of Water Resources Planning and Management*, 125(5):302–306.

## References

- Brunone, B., Capponi, C., and Meniconi, S. (2021). Design criteria and performance analysis of a smart portable device for leak detection in water transmission mains. *Measurement*, 183:109844.
- Brunone, B. and Ferrante, M. (2001). Detecting leaks in pressurised pipes by means of transients. *Journal of Hydraulic Research*, 39(5):539–547.
- Brunone, B. and Ferrante, M. (2004). Pressure waves as a tool for leak detection in closed conduits. *Urban Water Journal*, 1(2):145–155.
- Brunone, B., Ferrante, M., and Meniconi, S. (2008a). Discussion of “detection of partial blockage in single pipelines” by P. K. Mohapatra, M. H. Chaudhry, A. A. Kassem, and J. Moloo. *Journal of Hydraulic Engineering*, 134(6):872–874.
- Brunone, B., Ferrante, M., and Meniconi, S. (2008b). Portable pressure wave-maker for leak detection and pipe system characterization. *Journal American Water Works Association*, 100(4):108–116.
- Brunone, B., Golia, U., and Greco, M. (1991). Some remarks on the momentum equation for fast transients. In *Proceedings of the International Meeting on Hydraulic Transients with Column Separation*, pages 201–209.
- Brunone, B., Golia, U. M., and Greco, M. (1995). Effects of two-dimensionality on pipe transients modeling. *Journal of Hydraulic Engineering*, 121(12):906–912.
- Brunone, B., Maietta, F., Capponi, C., Keramat, A., and Meniconi, S. (2022). A review of physical experiments for leak detection in water pipes through transient tests for addressing future research. *Journal of Hydraulic Research*, 60(6):894–906.
- Brunone, B., Meniconi, S., and Capponi, C. (2018). Numerical analysis of the transient pressure damping in a single polymeric pipe with a leak. *Urban Water Journal*, 15(8):760–768.
- Brunone, B., Meniconi, S., Capponi, C., and Ferrante, M. (2015). Leak-induced pressure decay during transients in viscoelastic pipes. preliminary results. *Procedia Engineering*, 119:243–252.
- Cannizzaro, D. and Pezzinga, G. (2005). Energy dissipation in transient gaseous cavitation. *Journal of Hydraulic Engineering*, 131(8):724–732.
- Capelo, M., Brentan, B., Monteiro, L., and Covas, D. (2021). Near-real time burst location and sizing in water distribution systems using artificial neural networks. *Water*, 13(13):1841.

## References

- Capponi, C., Ferrante, M., Zecchin, A. C., and Gong, J. (2017). Leak detection in a branched system by inverse transient analysis with the admittance matrix method. *Water Resources Management*, 31(13):4075–4089.
- Capponi, C., Meniconi, S., Lee, P. J., Brunone, B., and Cifrodelli, M. (2020). Time-domain analysis of laboratory experiments on the transient pressure damping in a leaky polymeric pipe. *Water Resources Management*, 34(2):501–514.
- Carriço, N. J., Soares, A. K., and Covas, D. I. (2016). Uncertainties of inverse transient modelling with unsteady friction and pipe-wall viscoelasticity. *Journal of Water Supply: Research and Technology—AQUA*, 65(4):342–353.
- Chaudhry, M. H. (2014). *Applied hydraulic transients* (3rd edition).
- Che, T., Duan, H., Pan, B., Lee, P. J., and Ghidaoui, M. (2019). Energy analysis of the resonant frequency shift pattern induced by nonuniform blockages in pressurized water pipes. *Journal of Hydraulic Engineering*, 145(7):04019027.
- Che, T.-C., Duan, H.-F., and Lee, P. J. (2021). Transient wave-based methods for anomaly detection in fluid pipes: A review. *Mechanical Systems and Signal Processing*, 160:107874.
- Che, T.-C., Wang, X., and Ghidaoui, M. S. (2022). Leak localization in looped pipe networks based on a factorized transient wave model: Theoretical framework. *Water Resources Research*, 58(4):e2021WR031364.
- Choura, O., Capponi, C., Meniconi, S., Elaoud, S., and Brunone, B. (2021). A nelder–mead algorithm-based inverse transient analysis for leak detection and sizing in a single pipe. *Water Supply*, 21(4):1580–1593.
- Collins, R. P., Boxall, J. B., Karney, B. W., Brunone, B., and Meniconi, S. (2012). How severe can transients be after a sudden depressurization? *Journal American Water Works Association*, 104(4):E243–E251.
- Colombo, A., Lee, P., and Karney, B. W. (2009). A selective literature review of transient-based leak detection methods. *Journal of Hydro-environment Research*, 2(4):212–227.
- Colombo, A. F. and Karney, B. W. (2002). Energy and costs of leaky pipes: toward comprehensive picture. *Journal of Water Resources Planning and Management*, 128(6):441–450.
- Contractor, D. N. (1965). The reflection of water hammer pressure waves from minor losses. *Journal of Basic Engineering*, 87(2):445–451.
- Covas, D. and Ramos, H. (1999). Practical methods for leakage control, detection, and location in pressurized systems. In *BHR group conference series*

## References

publication, volume 37, pages 135–152. Bury St. Edmunds; Professional Engineering Publishing; 1998.

Covas, D. and Ramos, H. (2010). Case studies of leak detection and location in water pipe systems by inverse transient analysis. *Journal of Water Resources Planning and Management*, 136(2):248–257.

Covas, D., Ramos, H., Graham, N., and Maksimovic, C. (2004a). Application of hydraulic transients for leak detection in water supply systems. *Water Science and Technology: Water Supply*, 4(5-6):365–374.

Covas, D., Stoianov, I., Mano, J. F., Ramos, H., Graham, N., and Maksimovic, C. (2005). The dynamic effect of pipe-wall viscoelasticity in hydraulic transients. part ii—model development, calibration and verification. *Journal of Hydraulic Research*, 43(1):56–70.

Covas, D., Stoianov, I., Ramos, H., Graham, N., and Maksimovic, C. (2004b). The dynamic effect of pipe-wall viscoelasticity in hydraulic transients. part i—experimental analysis and creep characterization. *Journal of Hydraulic Research*, 42(5):517–532.

Covas, D., Stoianov, I., Ramos, H., Graham, N., Maksimović, Č., and Butler, D. (2004c). Water hammer in pressurized polyethylene pipes: conceptual model and experimental analysis. *Urban Water Journal*, 1(2):177–197.

Covas, D. I. C. (2003). *Inverse Transient Analysis for Leak Detection and Calibration of Water Pipe Systems - Modelling Special Dynamic Effects*.

Creaco, E., Campisano, A., Fontana, N., Marini, G., Page, P., and Walski, T. (2019). Real time control of water distribution networks: A state-of-the-art review. *Water Research*, 161:517–530.

Creaco, E., Pezzinga, G., and Savic, D. (2017). On the choice of the demand and hydraulic modelling approach to WDN real-time simulation. *Water Resources Research*, 53(7):6159–6177.

Duan, H., Lee, P., Che, T., Ghidaoui, M., Karney, B., and Kolyshkin, A. (2017). The influence of non-uniform blockages on transient wave behavior and blockage detection in pressurized water pipelines. *Journal of Hydro-Environment Research*, 17:1–7.

Duan, H., Pan, B., Wang, M., Chen, L., Zheng, F., and Zhang, Y. (2020). State-of-the-art review on the transient flow modeling and utilization for urban water supply system (uwss) management. *Journal of Water Supply: Research and Technology-Aqua*, 69(8):858–893.

## References

- Duan, H.-F., Ghidaoui, M. S., Lee, P. J., and Tung, Y. K. (2010). Unsteady friction and visco-elasticity in pipe fluid transients. *Journal of Hydraulic Research*, 48(3):354–362.
- Duan, H. F., Lee, P. J., Ghidaoui, M. S., and Tuck, J. (2014). Transient wave-blockage interaction and extended blockage detection in elastic water pipelines. *Journal of Fluids and Structures*, 46:2–16.
- Duan, H.-F., Lee, P. J., Kashima, A., Lu, J., Ghidaoui, M. S., and Tung, Y.-K. (2013). Extended blockage detection in pipes using the system frequency response: analytical analysis and experimental verification. *Journal of Hydraulic Engineering*, 139(7):763–771.
- Duan, W., Kirby, R., Prisutova, J., and Horoshenkov, K. V. (2015). On the use of power reflection ratio and phase change to determine the geometry of a blockage in a pipe. *Applied Acoustics*, 87:190–197.
- Edwards, J. and Collins, R. (2014). The effect of demand uncertainty on transient propagation in water distribution systems. *Procedia Engineering*, 70:592–601.
- Eldayih, Y., Cetin, M., and Vasconcelos, J. G. (2020). Air-pocket entrapment caused by shear flow instabilities in rapid-filling pipes. *Journal of Hydraulic Engineering*, 146(4):04020016.
- Fathi-Moghadam, M. and Kiani, S. (2020). Simulation of transient flow in viscoelastic pipe networks. *Journal of Hydraulics Research*, 58(3):531–540.
- Ferrante, M. and Brunone, B. (2003). Pipe system diagnosis and leak detection by unsteady-state tests. 2. wavelet analysis. *Advances in Water Resources*, 26(1):107–116.
- Ferrante, M., Brunone, B., and Meniconi, S. (2007). Wavelets for the analysis of transient pressure signals for leak detection. *Journal of Hydraulic Engineering*, 133(11):1274–1282.
- Ferrante, M., Brunone, B., and Meniconi, S. (2009a). Leak detection in branched pipe systems coupling wavelet analysis and a lagrangian model. *Journal of Water Supply: Research and Technology—AQUA*, 58(2):95–106.
- Ferrante, M., Brunone, B., and Meniconi, S. (2009b). Leak-edge detection. *Journal of Hydraulic Research*, 47(2):233–241.
- Ferrante, M., Brunone, B., Meniconi, S., Karney, B. W., and Massari, C. (2014). Leak size, detectability and test conditions in pressurized pipe systems. *Water Resources Management*, 28(13):4583–4598.

## References

- Ferreira, J. P., Buttarazzi, N., Ferras, D., and Covas, D. I. (2021). Effect of an entrapped air pocket on hydraulic transients in pressurized pipes. *Journal of Hydraulic Research*, 59(6):1018–1030.
- Filion, Y. R. and Karney, B. W. (2002). Extended-period analysis with a transient model. *Journal of Hydraulic Engineering*, 128(6):616–624.
- Filion, Y. R., MacLean, H. L., and Karney, B. W. (2004). Life-cycle energy analysis of a water distribution system. *Journal of Infrastructure Systems*, 10(3):120–130.
- Ghazali, M., Beck, S., Shucksmith, J., Boxall, J., and Staszewski, W. (2012). Comparative study of instantaneous frequency based methods for leak detection in pipeline networks. *Mechanical Systems and Signal Processing*, 29:187–200.
- Ghazali, M., Staszewski, W., Shucksmith, J., Boxall, J., and Beck, S. (2011). Instantaneous phase and frequency for the detection of leaks and features in a pipeline system. *Structural Health Monitoring*, 10(4):351–360.
- Ghorbanian, V., Karney, B., and Guo, Y. (2017). Intrinsic relationship between energy consumption, pressure, and leakage in water distribution systems. *Urban Water Journal*, 14(5):515–521.
- Gong, J., Lambert, M. F., Nguyen, S. T., Zecchin, A. C., and Simpson, A. R. (2018a). Detecting thinner-walled pipe sections using a spark transient pressure wave generator. *Journal of Hydraulic Engineering*, 144(2):06017027.
- Gong, J., Lambert, M. F., Zecchin, A. C., and Simpson, A. R. (2016). Experimental verification of pipeline frequency response extraction and leak detection using the inverse repeat signal. *Journal of Hydraulic Research*, 54(2):210–219.
- Gong, J., Stephens, M. L., Lambert, M. F., Zecchin, A. C., and Simpson, A. R. (2018b). Pressure surge suppression using a metallic-plastic-metallic pipe configuration. *Journal of Hydraulic Engineering*, 144(6):04018025.
- Guo, G., Yu, X., Liu, S., Ma, Z., Wu, Y., Xu, X., Wang, X., Smith, K., and Wu, X. (2021). Leakage detection in water distribution systems based on time–frequency convolutional neural network. *Journal of Water Resources Planning and Management*, 147(2):04020101.
- Guo, X., Yang, K., and Guo, Y. (2012). Leak detection in pipelines by exclusively frequency domain method. *Science China Technological Sciences*, 55(3):743–752.
- Haghighi, A. (2015). Analysis of transient flow caused by fluctuating consumptions in pipe networks: A many-objective genetic algorithm approach. *Water Resources Management*, 29(7):2233–2248.

## References

- Haghighi, A., Covas, D., and Ramos, H. (2012). Direct backward transient analysis for leak detection in pressurized pipelines: from theory to real application. *Journal of Water Supply: Research and Technology—AQUA*, 61(3):189–200.
- Haghighi, A. and Ramos, H. M. (2012). Detection of leakage freshwater and friction factor calibration in drinking networks using central force optimization. *Water Resources Management*, 26(8):2347–2363.
- Hampson, W., Collins, R., Beck, S., and Boxall, J. (2014). Transient source localization methodology and laboratory validation. *Procedia Engineering*, 70:781–790.
- Holmboe, E. L. and Rouleau, W. T. (1967). The effect of viscous shear on transients in liquid lines. *Journal of Basic Engineering*, 89(1):174–180.
- Hu, X., Han, Y., Yu, B., Geng, Z., and Fan, J. (2021). Novel leakage detection and water loss management of urban water supply network using multiscale neural networks. *Journal of Cleaner Production*, 278:123611.
- Huang, Y., Duan, H.-F., Zhao, M., Zhang, Q., Zhao, H., and Zhang, K. (2017). Probabilistic analysis and evaluation of nodal demand effect on transient analysis in urban water distribution systems. *Journal of Water Resources Planning and Management*, 143(8):04017041.
- Huang, Y., Zheng, F., Duan, H.-F., and Zhang, Q. (2020a). Multi-objective optimal design of water distribution networks accounting for transient impacts. *Water Resources Management*, 34(4):1517–1534.
- Huang, Y., Zheng, F., Duan, H.-F., Zhang, Q., and Shen, Y. (2020b). Impacts of nodal demand allocations on transient-based skeletonization of water distribution systems. *Journal of Hydraulic Engineering*, 146(9):04020058.
- Idel'cik, I. E. (1986). *Handbook of Hydraulic Resistance*. Hemisphere publishing corp, New York.
- Jing, L., Li, Z., Wang, W., Dubey, A., Lee, P., Meniconi, S., Brunone, B., and Murch, R. D. (2018). An approximate inverse scattering technique for reconstructing blockage profiles in water pipelines using acoustic transients. *The Journal of the Acoustical Society of America*, 143(5):EL322–EL327.
- Jönsson, L. (1994). Leak detection in pipelines using hydraulic transients - laboratory measurements. In *Department of Water Resources Engineering, Univ. of Lund., Sweden, Report to the Carl Trygger Foundation*.
- Jönsson, L. (1999). Hydraulic transients as a monitoring device. In *Proc. XXVIII Congress of Intl. Assoc. of Hydraulic Engrg. & Res., Delft, the Netherlands*.

## References

- Jönsson, L. (2001a). Experimental studies of leak detection using hydraulic transients. In *Proc. of IAHR Congress*, pages 559–565.
- Jönsson, L. (2001b). Interaction of a hydraulic transient with a leak in a pipe flow. In *14th Australasian Fluid Mechanics Conference, University of Adelaide*.
- Jung, B. S., Boulos, P. F., and Wood, D. J. (2007). Pitfalls of water distribution model skeletonization for surge analysis. *Journal-American Water Works Association*, 99(12):87–98.
- Jung, B. S. and Karney, B. W. (2006). Hydraulic optimization of transient protection devices using GA and PSO approaches. *Journal of Water Resources Planning and Management*, 132(1):44–52.
- Karney, B. W. and McInnis, D. (1992). Efficient calculation of transient flow in simple pipe networks. *Journal of Hydraulic Engineering*, 118(7):1014–1030.
- Kazemi, E. and Collins, R. (2018a). Comparison of probabilistic modelling techniques for transients in water distribution networks. In *13th International Conference on Pressure Surges*, pages 805–817.
- Kazemi, E. and Collins, R. (2018b). Propagating uncertainties in hydraulic transient modelling using a non-intrusive polynomial chaos methods. In *WDSA/CCWI Joint Conference Proceedings*, volume 1.
- Keramat, A., Wang, X., Louati, M., Meniconi, S., Brunone, B., and Ghidaoui, M. S. (2019). Objective functions for transient-based pipeline leakage detection in a noisy environment: least square and matched-filter. *Journal of Water Resources Planning and Management*, 145(10):04019042.
- Koelle, E. and Almeida, A. (1991). Fluid transients in pipe networks.
- Kwon, H. J. and Lee, C.-E. (2008). Reliability analysis of pipe network regarding transient flow. *KSCE Journal of Civil Engineering*, 12(6):409–416.
- Lee, J. (2015). Hydraulic transients in service lines. *International Journal of Hydraulic Engineering*, 4(2):31–36.
- Lee, J., Lohani, V. K., Dietrich, A. M., and Loganathan, G. (2012). Hydraulic transients in plumbing systems. *Water Science and Technology: Water Supply*, 12(5):619–629.
- Lee, P., Lambert, M., Simpson, A., Vítkovsky, J., and Misiunas, D. (2007a). Leak location in single pipelines using transient reflections. *Australasian Journal of Water Resources*, 11(1):53–65.

## References

- Lee, P. J., Duan, H.-F., Tuck, J., and Ghidaoui, M. (2015). Numerical and experimental study on the effect of signal bandwidth on pipe assessment using fluid transients. *Journal of Hydraulic Engineering*, 141(2):04014074.
- Lee, P. J., Lambert, M. F., Simpson, A. R., Vítkovský, J. P., and Liggett, J. (2006). Experimental verification of the frequency response method for pipeline leak detection. *Journal of Hydraulic research*, 44(5):693–707.
- Lee, P. J., Vítkovsky, J. P., Lambert, M. F., Simpson, A. R., and Liggett, J. (2007b). Leak location in pipelines using the impulse response function. *Journal of Hydraulic Research*, 45(5):643–652.
- Lile, N. L. T., Jaafar, M. H. M., Roslan, M. R., and Azmi, M. S. M. (2012). Blockage detection in circular pipe using vibration analysis. *International Journal on Advanced Science, Engineering and Information Technology*, 2(3):54–57.
- Liou, C. (1998). Pipeline leak detection by impulse response extraction. *Journal of Fluids Engineering*, 120(4):833–838.
- Liou, J. and Wylie, E. B. (2016). *WaterHammer. Handbook of Fluid Dynamics (ch. 25)*. CRC Press – Taylor & Francis Group, Boca Raton, FL.
- Liou, J. C. and Tian, J. (1995). Leak detection–transient flow simulation approaches. *Journal of Energy Resources Technology*, 117(3):243–248.
- Liu, Z. and Kleiner, Y. (2013). State of the art review of inspection technologies for condition assessment of water pipes. *Measurement*, 46:1–15.
- Loganathan, G. V. and Lee, J. (2005). Decision tool for optimal replacement of plumbing systems. *Civil Engineering and Environmental Systems*, 22(4):189–204.
- Louati, M., Ghidaoui, M. S., Meniconi, S., and Brunone, B. (2018). Bragg-type resonance in blocked pipe system and its effect on the eigenfrequency shift. *Journal of Hydraulic Engineering*, 144(1):04017056.
- Louati, M., Meniconi, S., Ghidaoui, M. S., and Brunone, B. (2017). Experimental study of the eigenfrequency shift mechanism in a blocked pipe system. *Journal of Hydraulic Engineering*, 143(10):04017044.
- Machell, J., Mounce, S., Farley, B., and Boxall, J. (2014). Online data processing for proactive UK water distribution network operation. *Drinking Water Engineering and Science*, 7(1):23–33.
- Marsili, V., Meniconi, S., Alvisi, S., Brunone, B., and Franchini, M. (2020). Experimental analysis of the water consumption effect on the dynamic behaviour of a real pipe network. *Journal of Hydraulic Research*, 59(3):477–487.

## References

- Marsili, V., Meniconi, S., Alvisi, S., Brunone, B., and Franchini, M. (2022). Stochastic approach for the analysis of demand induced transients in real water distribution systems. *Journal of Water Resources Planning and Management*, 141(1):04021093.
- Martínez García, D., Lee, J., Keck, J., Kooy, J., Yang, P., and Wilfley, B. (2020). Pressure-based analysis of water main failures in California. *Journal of Water Resources Planning and Management*, 146(9):05020016.
- Martins, N. C., Brunone, B., Meniconi, S., Ramos, H. M., and Covas, I. D. (2018). Efficient CFD model for transient laminar flow modeling: pressure wave propagation and velocity profile changes. *J. of Fluids Engineering*, 140(1):011102.
- Martins, N. M. C., Brunone, B., Meniconi, S., Ramos, H. M., and Covas, D. I. C. (2017). CFD and 1D approaches for the unsteady friction analysis of low Reynolds number turbulent flows. *J. of Hydraulic Engineering*, 143(12):04017050.
- Martins, N. M. C., Covas, D. I. C., Meniconi, S., Capponi, C., and Brunone, B. (2021). Characterization of low-Reynolds number flow through an orifice: CFD results vs. laboratory data. *Journal of Hydroinformatics*, 23(4):709–723.
- Massari, C., Yeh, T.-C., Ferrante, M., Brunone, B., and Meniconi, S. (2015). A stochastic approach for extended partial blockage detection in viscoelastic pipelines: numerical and laboratory experiments. *Journal of Water Supply: Research and Technology—AQUA*, 64(5):583–595.
- McInnis, D. and Karney, B. W. (1995). Transients in distribution networks: Field tests and demand models. *Journal of Hydraulic Engineering*, 121(3):218–231.
- Meniconi, S., Brunone, B., and Ferrante, M. (2011a). In-line pipe device checking by short-period analysis of transient tests. *Journal of Hydraulic Engineering*, 137(7):713–722.
- Meniconi, S., Brunone, B., and Ferrante, M. (2012a). Water-hammer pressure waves interaction at cross-section changes in series in viscoelastic pipes. *Journal of Fluids and Structures*, 33:44–58.
- Meniconi, S., Brunone, B., Ferrante, M., and Capponi, C. (2016). Mechanism of interaction of pressure waves at a discrete partial blockage. *Journal of Fluids and Structures*, 62:33–45.
- Meniconi, S., Brunone, B., Ferrante, M., Capponi, C., Carrettini, C., Chiesa, C., Segalini, D., and Lanfranchi, E. (2015). Anomaly pre-localization in

## References

distribution–transmission mains by pump trip: preliminary field tests in the milan pipe system. *Journal of Hydroinformatics*, 17(3):377–389.

Meniconi, S., Brunone, B., Ferrante, M., and Massari, C. (2011b). Potential of transient tests to diagnose real supply pipe systems: What can be done with a single extemporaneous test. *Journal of Water Resources Planning and Management*, 137(2):238–241.

Meniconi, S., Brunone, B., Ferrante, M., and Massari, C. (2011c). Small amplitude sharp pressure waves to diagnose pipe systems. *Water Resources Management*, 25(1):79–96.

Meniconi, S., Brunone, B., Ferrante, M., and Massari, C. (2011d). Transient tests for locating and sizing illegal branches in pipe systems. *Journal of Hydroinformatics*, 13(3):334–345.

Meniconi, S., Brunone, B., Ferrante, M., and Massari, C. (2012b). Transient hydrodynamics of in-line valves in viscoelastic pressurized pipes: long-period analysis. *Experiments in fluids*, 53(1):265–275.

Meniconi, S., Brunone, B., Ferrante, M., and Massari, C. (2013a). Numerical and experimental investigation of leaks in viscoelastic pressurized pipe flow. *Drinking Water Engineering and Science*, 6(1):11–16.

Meniconi, S., Brunone, B., and Frisinghelli, M. (2018). On the role of minor branches, energy dissipation, and small defects in the transient response of transmission mains. *Water*, 10(2):187.

Meniconi, S., Brunone, B., Mazzetti, E., Laucelli, D., and G., B. (2017). Hydraulic characterization and transient response of pressure reducing valves. Laboratory experiments. *Journal of Hydroinformatics*, 19(6):798–810.

Meniconi, S., Capponi, C., Frisinghelli, M., and Brunone, B. (2021a). Leak detection in a real transmission main through transient tests: Deeds and misdeeds. *Water Resources Research*, 57(3):e2020WR027838.

Meniconi, S., Cifrodelli, M., Capponi, C., Duan, H.-F., and Brunone, B. (2021b). Transient response analysis of branched pipe systems toward a reliable skeletonization. *Journal of Water Resources Planning and Management*, 147(2):04020109.

Meniconi, S., Duan, H. F., Lee, P. J., Brunone, B., Ghidaoui, M. S., and Ferrante, M. (2013b). Experimental investigation of coupled frequency and time-domain transient test–based techniques for partial blockage detection in pipelines. *Journal of Hydraulic Engineering*, 139(10):1033–1040.

## References

- Meniconi, S., Maietta, F., Alvisi, S., Capponi, C., Marsili, V., Franchini, M., and Brunone, B. (2022). Consumption change-induced transients in a water distribution network: laboratory tests in a looped system. *Water Resources Research*, 58(10):e2021WR031343.
- Misiunas, D., Vítkovský, J., Olsson, G., Lambert, M., and Simpson, A. (2006). Failure monitoring in water distribution networks. *Water Science and Technology*, 53(4-5):503–511.
- Misiunas, D., Vítkovský, J., Olsson, G., Simpson, A., and Lambert, M. (2005). Pipeline break detection using pressure transient monitoring. *Journal of Water Resources Planning and Management*, 131(4):316–325.
- Mitosek, M. and Chorzelski, M. (2003). Influence of visco-elasticity on pressure wave velocity in polyethylene MDPE pipe. *Archit. Hydro. Eng. Environ. Mech.*, 50(2):127–140.
- Mounce, S., Mounce, R., and Boxall, J. (2012). Identifying sampling interval for event detection in water distribution networks. *Journal of Water Resources Planning and Management*, 138(2):187–191.
- Mounce, S., Pedraza, C., Jackson, T., Linford, P., and Boxall, J. (2015). Cloud based machine learning approaches for leakage assessment and management in smart water networks. *Procedia Engineering*, 119:43–52.
- Nault, J. and Karney, B. (2016). Improved rigid water column formulation for simulating slow transients and controlled operations. *Journal of Hydraulic Engineering*, 142(9):04016025.
- Nault, J., Karney, B., and Jung, B.-S. (2018). Generalized flexible method for simulating transient pipe network hydraulics. *Journal of Hydraulic Engineering*, 144(7):04018031.
- Nogueira Vilanova, M. R. and Perrella Balestrieri, J. A. (2014). Energy and hydraulic efficiency in conventional water supply systems. *Renewable and Sustainable Energy Reviews*, 30:701–714.
- Nogueira Vilanova, M. R. and Perrella Balestrieri, J. A. (2015). Modeling of hydraulic and energy efficiency indicators for water supply systems. *Renewable and Sustainable Energy Reviews*, 48:540–557.
- Pal, S., Hanmaiahgari, P. R., and Karney, B. W. (2021). An overview of the numerical approaches to water hammer modelling: The ongoing quest for practical and accurate numerical approaches. *Water*, 13(11):1597.
- Pan, B., Capponi, C., Meniconi, S., Brunone, B., and Duan, H.-F. (2022). Efficient leak detection in single and branched polymeric pipeline systems by transient wave analysis. *Mechanical Systems and Signal Processing*, 162:108084.

## References

- Papadopoulou, K. A., Shamout, M. N., Lennox, B., Mackay, D., Taylor, A. R., Turner, J. T., and Wang, X. (2008). An evaluation of acoustic reflectometry for leakage and blockage detection. *Proceedings of the Institution of Mechanical Engineers, Part C: Journal of Mechanical Engineering Science*, 222(6):959–966.
- Pezzinga, G. (2000). Evaluation of unsteady flow resistances by quasi-2d or 1d models. *Journal of Hydraulic Engineering*, 126(10):778–785.
- Pezzinga, G., Brunone, B., Cannizzaro, D., Ferrante, M., Meniconi, S., and Berni, A. (2014). Two-dimensional features of viscoelastic models of pipe transients. *Journal of Hydraulic Engineering*, 140(8):0401403.
- Pezzinga, G., Brunone, B., and Meniconi, S. (2016). The relevance of pipe period on kelvin-voigt viscoelastic parameters: 1-d and 2-d inverse transient analysis. *J. of Hydraulic Engineering*, 142(12):04016063.
- Prescott, S. L. and Ulanicki, B. (2008). Improved control of pressure reducing valves in water distribution networks. *Journal of Hydraulic Engineering*, 134(1):56–65.
- Pudar, R. S. and Liggett, J. A. (1992). Leaks in pipe networks. *Journal of Hydraulic Engineering*, 118(7):1031–1046.
- Puust, R., Kapelan, Z., Savic, D., and Koppel, T. (2010). A review of methods for leakage management in pipe networks. *Urban Water Journal*, 7(1):25–45.
- Rezaei, H., Ryan, B., and Stoianov, I. (2015). Pipe failure analysis and impact of dynamic hydraulic conditions in water supply networks. *Procedia Engineering*, 119:253–262.
- Sattar, A. M., Chaudhry, M. H., and Kassem, A. A. (2008). Partial blockage detection in pipelines by frequency response method. *Journal of Hydraulic Engineering*, 134(1):76–89.
- Sharp, W. W. and Walski, T. M. (1988). Predicting internal roughness in water mains. *Journal American Water Works Association*, 80(11):34–40.
- Shi, H., Gong, J., Simpson, A. R., Zecchin, A. C., and Lambert, M. F. (2020). Leak detection in virtually isolated pipe sections within a complex pipe system using a two-source-four-sensor transient testing configuration. *Journal of Hydroinformatics*, 22(5):1306–1320.
- Shucksmith, J. D., Boxall, J. B., Staszewski, W. J., Seth, A., and Beck, S. B. (2012). Onsite leak location in a pipe network by cepstrum analysis of pressure transients. *Journal American Water Works Association*, 104(8):E457–E465.

## References

- Soares, A. K., Covas, D. I., and Reis, L. F. R. (2011). Leak detection by inverse transient analysis in an experimental pvc pipe system. *Journal of Hydroinformatics*, 13(2):153–166.
- Souza, A., Cruz, S., and Pereira, J. (2000). Leak detection in pipelines through spectral analysis of pressure signals. *Brazilian Journal of Chemical Engineering*, 17(4-7):557–564.
- Srirangarajan, S., Allen, M., Preis, A., Iqbal, M., Lim, H. B., and Whittle, A. J. (2013). Wavelet-based burst event detection and localization in water distribution systems. *Journal of Signal Processing Systems*, 72(1):1–16.
- Starczewska, D., Boxall, J., and Collins, R. (2015a). A method to characterise transients from pressure signals recorded in real water distribution networks. In *12th International Conference on Pressure Surges*, pages 609–623. BHR Group.
- Starczewska, D., Collins, R., and Boxall, J. (2014). Transient behavior in complex distribution network: A case study. *Procedia Engineering*, 70:1582–1591.
- Starczewska, D., Collins, R., and Boxall, J. (2015b). Occurrence of transients in water distribution networks. *Procedia Engineering*, 119:1473–1482.
- Stephens, M. L., Lambert, M. F., Simpson, A. R., and Vitkovsky, J. (2011). Calibrating the water-hammer response of a field pipe network by using a mechanical damping model. *Journal of Hydraulic Engineering*, 137(10):1225–1237.
- Sun, J., Wang, R., and Duan, H.-F. (2016). Multiple-fault detection in water pipelines using transient-based time-frequency analysis. *Journal of Hydroinformatics*, 18(6):975–989.
- Swaffield, J. and Boldy, A. (1993). *Pressure surges in pipe and duct systems*. Ashgate Publishing Group.
- Taghvaei, M., Beck, S., and Boxall, J. (2010). Leak detection in pipes using induced water hammer pulses and cepstrum analysis. *Int. Journal of COMADEM*, 13(1):19.
- Taghvaei, M., Beck, S., and Staszewski, W. (2006). Leak detection in pipelines using cepstrum analysis. *Measurement Science and Technology*, 17(2):367.
- Taghvaei, M., Beck, S., and Staszewski, W. (2007). Leak detection in pipeline networks using low-profile piezoceramic transducers. *Structural Control and Health Monitoring*, 14(8):1063–1082.
- Tuck, J. and Lee, P. (2013). Inverse transient analysis for classification of wall thickness variations in pipelines. *Sensors*, 13(12):17057–17066.

## References

- Tuck, J., Lee, P. J., Davidson, M., and Ghidaoui, M. S. (2013). Analysis of transient signals in simple pipeline systems with an extended blockage. *Journal of Hydraulic Research*, 51(6):623–633.
- Ulanicki, B. and Beaujean, P. (2021). Modeling dynamic behavior of water distribution systems for control purposes. *Journal of Water Resources Planning and Management*, 147(8):04021043.
- Vardy, A. E. and Brown, J. M. (1995). Transient, turbulent, smooth pipe friction. *Journal of hydraulic research*, 33(4):435–456.
- Vítkovský, J., Lambert, M., Simpson, A., and Bergant, A. (2000a). Advances in unsteady friction modelling in transient pipe flow. In *Proc., 8th Int. Conf. on Pressure Surges*, pages 471–482. BHR Group Bedford, UK.
- Vítkovský, J. P., Lambert, M. F., Simpson, A. R., and Liggett, J. A. (2007). Experimental observation and analysis of inverse transients for pipeline leak detection. *Journal of Water Resources Planning and Management*, 133(6):519–530.
- Vítkovský, J. P., Lee, P. J., Zecchin, A. C., Simpson, A. R., and Lambert, M. F. (2011). Head- and flow-based formulations for frequency domain analysis of fluid transients in arbitrary pipe networks. *Journal of Hydraulic Engineering*, 137(5):556–568.
- Vítkovský, J. P., Liggett, J. A., Simpson, A. R., and Lambert, M. F. (2003). Optimal measurement site locations for inverse transient analysis in pipe networks. *Journal of Water Resources Planning and Management*, 129(6):480–492.
- Vítkovský, J. P., Simpson, A. R., and Lambert, M. F. (2000b). Leak detection and calibration using transients and genetic algorithms. *Journal of Water Resources Planning and Management*, 126(4):262–265.
- Wang, W., Mao, X., Liang, H., Yang, D., Zhang, J., and Liu, S. (2021). Experimental research on in-pipe leaks detection of acoustic signature in gas pipelines based on the artificial neural network. *Measurement*, 183:109875.
- Wang, X., Ghidaoui, M. S., and Lin, J. (2019a). Identification of multiple leaks in pipeline. iii: Experimental results. *Mechanical Systems and Signal Processing*, 130:395–408.
- Wang, X., Lin, J., Keramat, A., Ghidaoui, M. S., Meniconi, S., and Brunone, B. (2019b). Matched-field processing for leak localization in a viscoelastic pipe: An experimental study. *Mechanical Systems and Signal Processing*, 124:459–478.

## References

- Wang, X., Simpson, A., Lambert, M., and Vítkovský, J. (2001). Leak detection in pipeline systems using hydraulic methods: A review. In *Conference on Hydraulics in Civil Engineering, The Institution of Engineers, Australia, Hobart*, pages 23–30.
- Wang, X.-J., Lambert, M. F., and Simpson, A. R. (2005). Detection and location of a partial blockage in a pipeline using damping of fluid transients. *Journal of Water Resources Planning and Management*, 131(3):244–249.
- Wang, X.-J., Lambert, M. F., Simpson, A. R., Liggett, J. A., and Vítkovský, J. P. (2002). Leak detection in pipelines using the damping of fluid transients. *Journal of Hydraulic Engineering*, 128(7):697–711.
- Wood, D. J., Lingireddy, S., Boulos, P. F., Karney, B. W., and McPherson, D. L. (2005). Numerical methods for modeling transient flow in distribution systems. *Journal American Water Works Association*, 97(7):104–115.
- Wylie, E. B. and Streeter, V. L. (1993). *Fluid transients in systems*. Prentice Hall Englewood Cliffs, NJ.
- Xing, L. and Sela, L. (2020). Transient simulations in water distribution networks: Tsnet python package. *Advances in Engineering Software*, 149:102884.
- Xu, X. and Karney, B. (2017). An overview of transient fault detection techniques. In *Modeling and Monitoring of Pipelines and Networks*, pages 13–37. Springer.
- Yang, L., Fu, H., Liang, H., Wang, Y., Han, G., and Ling, K. (2019). Detection of pipeline blockage using lab experiment and computational fluid dynamic simulation. *Journal of Petroleum Science and Engineering*, 183.
- Yusop, M. H., Ghazali, M. F., Yusof, M. F. M., and Hamat, W. S. W. (2019). Improvement of cepstrum analysis for the purpose to detect leak, feature and its location in water distribution system based on pressure transient analysis. *Journal of Mechanical Engineering (JMEchE)*, SI 4(4):103–122.
- Zecchin, A., Do, N., Gong, J., Leonard, M., Lambert, M., and Stephens, M. (2022). Optimal pipe network sensor layout design for hydraulic transient event detection and localization. *Journal of Water Resources Planning and Management*, 148(8):04022041.
- Zecchin, A., Lambert, M., Simpson, A., and White, L. (2014). Parameter identification in pipeline networks: transient-based expectation-maximization approach for systems containing unknown boundary conditions. *Journal of Hydraulic Engineering*, 140(6):04014020.

## References

Zeidan, M. and Ostfeld, A. (2022). Using hydraulic transients for biofilm detachment in water distribution systems: Approximated model. *Journal of Water Resources Planning and Management*, 148(4):04022008.

Zeng, W., Zecchin, A. C., Cazzolato, B. S., Simpson, A. R., Gong, J., and Lambert, M. F. (2021). Extremely sensitive anomaly detection in pipe networks using a higher-order paired-impulse response function with a correlator. *Journal of Water Resources Planning and Management*, 147(10):04021068.

Zielke, W. (1968). Frequency-dependent friction in transient pipe flow.

Zouari, F., Louati, M., Meniconi, S., Blåsten, E., Ghidaoui, M. S., and Brunone, B. (2020). Experimental verification of the accuracy and robustness of area reconstruction method for pressurized water pipe system. *Journal of Hydraulic Engineering*, 146(3):04020004.